ABSTRACT

PHASE-LOCKED LOOP, DELAY-LOCKED LOOP, AND LINEAR DECORRELATING DETECTOR FOR ASYNCHRONOUS MULTIRATE DS-CDMA SYSTEM

by
Sok-kyu Lee

The performance of phase synchronization and code tracking of a digital phase-locked loop (PLL) and delay-locked loop (DLL), respectively, is investigated in wideband asynchronous multirate DS-CDMA system. Dynamic Partial Correlation (DPC) method is proposed to evaluate the autocorrelation and its power spectrum density (PSD) of the cross-correlated terms in the presence of multirate multiple access interference (MMAI) under additive white gaussian noise (AWGN) and fading channel environments. The steady-state probability density function (PDF) and variance of the phase estimator error and code tracking jitter is evaluated by solving the first-order Fokker-Planck equation.

Among many linear multiuser detectors which decouple the multiple access interference from each of the interfering users, one-shot window linear decorrelating detector (LDD) based on a one bit period to reduce the complexity of the LDD has attracted wide attention as an implementation scheme. Therefore, we propose Hybrid Selection Diversity/Maximal Ratio Combining (Hybrid SD/MRC) one-shot window linear decorrelating detector (LDD) for asynchronous DS-CDMA systems. The selection diversity scheme at the input of the Hybrid SD/MRC LDD is based on choosing the branch with the maximum signal-to-noise ratio (SNR) of all filter outputs. The MR Combining scheme at the output of the Hybrid SD/MRC LDD adopts to maximize the output SNR and thus compensates for the enhanced output noise. The Hybrid SD/MRC one-shot LDD with PLL is introduced to track its phase error and to improve the demodulation performance. The probability density

functions of the maximum SNR of the SD combiner , the near-far resistance (NFR) of one-shot LDD by Gaussian approximation, and the maximum SNR of the MR combiner for Hybrid SD/MRC LDD are evaluated, and the bit error probability is obtained from these pdfs. The performance of Hybrid SD/MRC one-shot LDD is assessed in a Rayleigh fading channel.

PHASE-LOCKED LOOP, DELAY-LOCKED LOOP, AND LINEAR DECORRELATING DETECTOR FOR ASYNCHRONOUS MULTIRATE DS-CDMA SYSTEM

by
Sok-kyu Lee

A Dissertation
Submitted to the Faculty of
New Jersey Institute of Technology
in Partial Fulfillment of the Requirements for the Degree of
Doctor of Philosophy in Electrical Engineering

Department of Electrical and Computer Engineering

January 2001

APPROVAL PAGE

Phase-Locked Loop, Delay-Locked Loop, and Linear Decorrelaing Detector for Asynchronous Multirate DS-CDMA System

Sok-Kyu Lee

Dr. Jacob Klapper, Dissertation Advisor Professor, Department of Electrical and Computer Engineering, NJIT	Date
Dr. Nirwan Ansari, Committee Member Professor, Department of Electrical and Computer Engineering, NJIT	Date
Dr. Joseph Frank, Committee Member Associate Professor, Department of Electrical and Computer Engineering, NJIT	Date
Dr. Yun-Qing Shi, Committee Member Associate Professor, Department of Electrical and Computer Engineering, NJIT	Date
Dr.Eliza(Z.-H.) Michalopoulou , Committee Member Associate Professor, Department of Mathematical Sciences, NJIT	Date

BIOGRAPHICAL SKETCH

Author : Sok-kyu Lee

Degree : Doctor of Philosophy

Date : January 2001

Undergraduate and Graduate Education :

- Doctor of Philosophy in Electrical Engineering,
  New Jersey Institute of Technology (NJIT), Newark, NJ, USA, 2001

- Master of Science in Electrical Engineering,
  Polytechnic University, Brooklyn, New York, USA, 1996

- Bachelor of Science in Electronics Engineering,
  Kwangwoon University, Seoul, Korea, 1985

Major : Electrical Engineering

To my father and mother

To my father-in-law and mother-in-law

To my wife, Eunhwa Roh

To my son, Brian Taehyun Lee

ACKNOWLEDGMENT

I would like to express my deepest gratitude to my advisor, Dr. Jacob Klapper. His advice, guidance and insight helped me enormously throughout this research.

My gratitude is extended to Dr. Nirwan Ansari, Dr. Joseph Frank, Dr. Yun-Qing Shi, and Dr. Eliza Michalopoulou for serving as members on the dissertation committee and for their comments.

I had the pleasure of working with my colleagues at Department of Electrical Engineering, New Jersey Institute of Technology. Their help and suggestions are appreciated and acknowledged.

Finally, I would like to sincerely thank my father, mother, brother, and sisters for always being there when I most needed them. Also, I would like to thank my father-in-law, mother-in-law, brothers-in-law, and my son, Brian Taehyun Lee for their love and support.

I dedicate this thesis with my love to my wife, Eunhwa Roh.

TABLE OF CONTENTS

TABLE OF CONTENTS
(Continued)

Chapter **Page**

LIST OF FIGURES

Figure **Page**

LIST OF FIGURES
(Continued)

Figure **Page**

LIST OF FIGURES
(Continued)

Figure **Page**

CHAPTER 1

INTRODUCTION

1.1 Wideband CDMA

The origins of spread spectrum are in the military field and navigation systems. Techniques developed to counteract intentional jamming have also proved suitable for communication through dispersive channels in cellular applications. In this section we highlight the milestones for CDMA development starting from the 1950s after the invention of the Shannon theorem.

In 1949, John Pierce wrote a technical memorandum where he described a multiplexing system in which a common medium carries coded signals that need not be synchronized. This system can be classified as a time hopping spread spectrum multiple access system. Claude Shannon and Robert Pierce introduced the basic ideas of CDMA in 1949 by describing the interference averaging effect and the graceful degradation of CDMA. In 1959, De Rosa-Rogoff proposed a direct sequence spread spectrum system and introduced the processing gain equation and noise multiplexing ideas. In 1956, Price and Green filed for the antimultipath 'RAKE' patent. Signals arriving over different propagation paths can be resolved by a wideband spread spectrum signal and combined by the RAKE receiver. The near-far problem (i.e, a high interference overwhelming a weaker spread spectrum signal) was first mentioned in 1961 by Magnuski.

For cellular applications spread spectrum was suggested by Cooper and Nettleton in 1978. During the 1980s Qualcomm investigated DS-CDMA techniques, which finally led to the commercialization of cellular spread spectrum communications in the form of the narrowband CDMA IS-95 standard in July 1993. Commercial operation of IS-95 systems started in 1996. Multiuser detection (MUD) has been subject of extensive research since 1986 when Verdu formulated an optimum

multiuser detection scheme for the additive white gaussian noise (AWGN) channel, maximum likelihood sequence estimator (MLSE).

During the 1990s wideband CDMA techniques with a bandwidth of 5 MHz or more have been studied intensively throughout the world, and several trial systems have been built and tested. These include FRAMES Multiple Access (FRAMES FMA2) in Europe, Core-A in Japan, the European/Japanese harmonized WCDMA scheme, cdma2000 in the United States, and the Telecommunication Technology Association I and II (TTA I and TTA II) schemes in Korea. Introduction of third-generation wireless communication systems using wideband CDMA is expected around the year 2000.

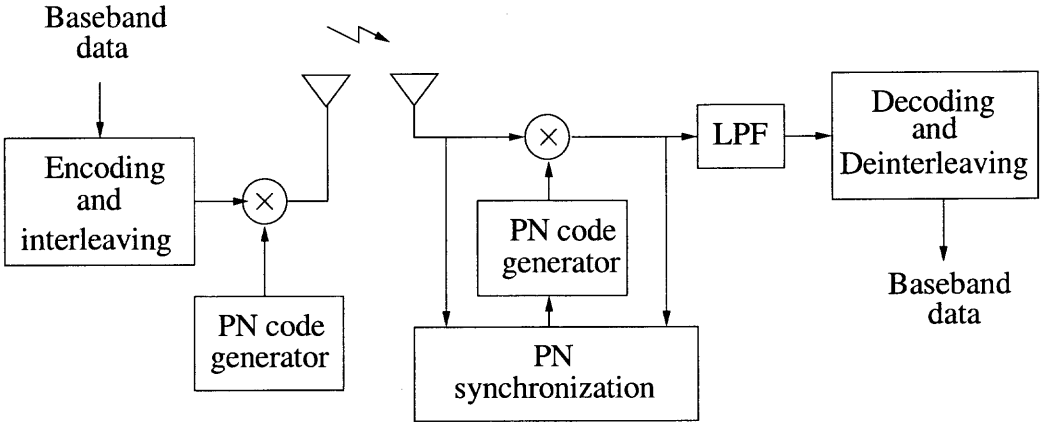

Figure 1.1 The baseband model of a DS-CDMA transceiver

A spread spectrum CDMA scheme is one in which the transmitted signal is spread over a wide frequency band, much wider than the minimum bandwidth required to transmit the information being sent. It employs a waveform that for all purposes appears random to anyone but the intended receiver of the transmitter waveform. Actually, for ease of both generation and synchronization by the receiver, the waveform is pseudorandom, meaning that it can be generated by mathematically

precise rules, but statistically it nearly satisfies the requirements of a truly random sequence. In spread spectrum CDMA all users use the same bandwidth, but each transmitter is assigned a distinct code. A block diagram of the baseband model of a DS-CDMA modulator and demodulator is shown in Fig.1.1.

For more than a decade, research has been ongoing to find enabling techniques to introduce multimedia capabilites into mobile communications. Research efforts have been aligned with efforts in the International Telecommunication Union (ITU) and other bodies to find standards and recommendations which ensure that mobile communications of the future have access to multimedia capabilities and service quality similar to the fixed network.

Compared to the second-generation CDMA, the following new main capabilities characterize the third-generation CDMA:

· Wider bandwidth and chip rate

· Provision of multirate services

· Packet data

· Complex spreading

· A coherent Uplink using a user-dedicated pilot

· Multiuser detection

The third-generation mobile communication systems, called International Mobile Telecommunications 2000 (IMT-2000) in the International Telecommunication Union (ITU) have been under intense research and development recently. One of the main objectives for the IMT-2000 air interface is that the system will be designed to support the multimedia services at data rates as high as 2Mb/s [5]. The most promising candidate is the code division multiple access (CDMA) system. As is well known, each user in a CDMA system is assigned a unique code, called pseudo-random (PN) codes. The PN codes must be generated at the receiver as well

and must be synchronized to coincide perfectly with the timing of the received transmission. The tracking process, which should be refined after synchronization, is the focus and thus, we approach the code jitter tracking process with the delay-locked loop (DLL) in this paper.

1.2 Phase and Code Synchronization

CDMA based on spread spectrum communication is an access method where all the users are permitted to transmit simultaneously, operate at the same nominal frequency, and use the entire system bandwidth. Recently, extensive investigations for effective operation of multirate signals have been carried out into the application of a code division multiple access (CDMA) system as an air interface multiple access scheme for IMT-2000.

Wideband CDMA systems are designed to accommodate a higher data rate for better multimedia service. Since the spreaded signal bandwidth is the same for all users, the transmitter needs multiple spreading factors (SF) to support a variable rate code in the physical channel. Variable Length Orthogonality (VLO) presented in [8] is necessary for channelization and the Gold code is used as a PN code for scrambling in the asynchronous system.

Fine synchronization is becoming increasingly important for the development of advanced receivers for wideband DS-CDMA systems in which multiuser interference cancellation is employed to overcome the reduction of system capacity due to this fundamental source of interference. Carrier phase synchronization of wireless communication systems is an already well-developed technique after the considerable research efforts provided in the past[3] [4]. It is evident that the performance of the PLL is degraded in the presence of MMAI and AWGN. Performance is dependent on the signal-to-noise and interference power ratio (SNIR) and the frequency difference between the desired signal and the interference signal. Among the many behaviors

which can explain the performance of the PLL, our main concern is the steady-state PDF of the phase estimate error as a function of the number of the simultaneous users.

Although various aspects of Multirate CDMA communication were discussed in a number of publications, there were few analytical results on asynchronous PLL systems and their applications. The need for considering the aperiodic crosscorrelation properties of the code sequence is shown in papers [10] [11] [12]. However, they did not treat asynchronous multirate code sequences nor evaluate the autocorrelations of cross-correlations and PSDs of the MMAI terms.

Our approach is first to derive the carrier phase estimate of the pilot signal that allows the receiver to extract and to synchronize its local oscillator to the carrier frequency and phase of the received signal. Therefore, we configure an integrated structure of DLL and PLL for receiving the desired signal effectively and simply since noncoherent code tracking performance will not be influenced directly by the performance of the carrier phase synchronization. After receiving, we evaluate gaussian noise and MMAI components using the Dynamic Partial Correlation (DPC) method to solve the cross-correlation terms and the corresponding power spectral densities of various interference terms in detail in an asynchronous multirate DS-CDMA communications environment.

Since a linear analysis yields a large deviation between the analytical results and actual performance in a low SNR environment [1], [2], here the effect of these sources of noise on the PLL performance is performed based on a nonlinear model. We also adopt a pilot signal for coherent demodulation. Thus, the steady-state PDF and variance of the phase estimator error of the PLL under various fading environments is performed by solving the first-order Fokker-Planck equation[4]. Finally, we will compare the performance in faded environment with the performance in unfaded environment.

Delay lock tracking of PN codes for CDMA systems is an already well-developed technique after the considerable research efforts provided in the past[3] [4]. The general DLL process is performed by the so-called early-late gate(ELG) device. Although its output S-curve is very useful to track the PN code phase of the desired user, it is not perfect since several noise factors distort it. The noncoherent DLL is the most popular technique. It suffers from tracking jitter due to the noise enhancement arising from the square-law detector (squaring loss). The coherent DLL overcomes this problem and improves the transmission performance. However, it requires accurate channel estimation in the receiver, which is generally difficult to do in fast fading. Fortunately, the chip synchronization process can take advantage of the pilot channel in both the forward and the reverse link of the third-generation systems.

In this paper we model the system that can be characterized by new capabilities such as asynchronous operation, multirate service and pilot aided operation. In the asynchronous system each user or cell site is assigned to a distinct Gold or Kasami code for scrambling. To meet the requirment of multimedia services, variable length orthogonal (VLO) code is necessary for channelization [7]. For coherent operation, the channel estimator supports DLL. Therefore, various effects of noise and interference in our system will be distinguished from the result shown in publications as [6], [10]-[12]. The scrambing PN code of different users or cell sites occurs to the DLL as an interference. The amount of interference is represented by the cross-correlation of codes. Since Pursley and Sarwate showed the cross-correlation properties of PN codes for CDMA in [12], the result was extended to multirate CDMA [34]. As they examined only the mean and the variance, we can't extend to evaluate the performance of DLL and it will be mentioned in detail later. The interferences of the output of the ELG device are the time function consisting of the cross-correlations.

After we determine the autocorrelation and its PSD of the time functions, we evaluate the performance via the PDF of the jitter.

1.2.1 Phase-locked Loop

Phase-Locked Loops are used widely in modern communication systems. There are several kinds of phase-locked receivers on the market for a variety of applications. These applications include demodulation of information carrying signals, synchronization, tracking, and ranging. Its application is more useful in low SNR environments because of the improved performance in the threshold region. Because of the importance of the application of the phase-locked loop (PLL), there has been a tremendous amount of work done in this area. There are several books [1],[2] which look into the analysis and design of the PLL in one way or the other.

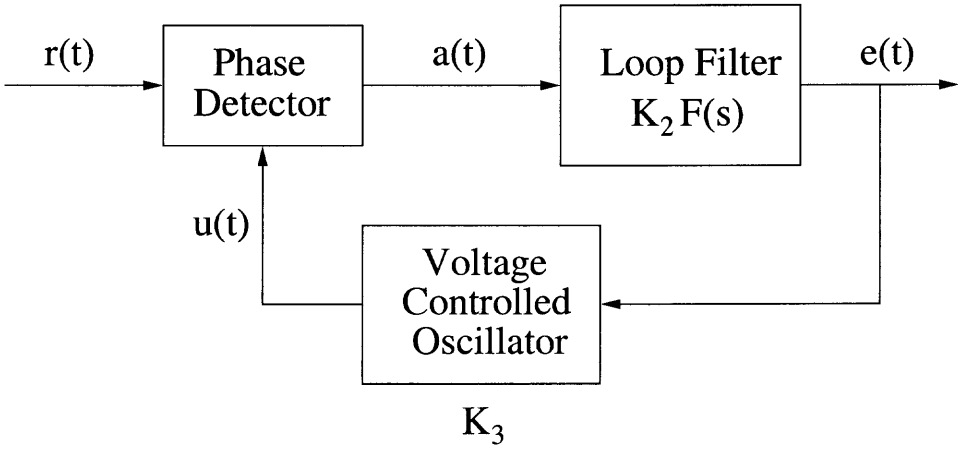

Figure 1.2 Block Diagram of Conceptual Phase Locked Loop

A PLL is a device which continuously tries to track the phase of the incoming signal. It is realized by a phase detector, a loop filter, and a voltage-controlled oscillator (VCO). The conceptual configuration is shown in Fig.1.2.

The basic operation requirement for the loop is to track the phase of the input signal. This is accomplished by forming in the phase detector a voltage proportional to the phase difference between the input signal and VCO signal. This error signal is then amplified, filtered to remove excess noise and other undesirable components, and applied to the VCO to effect input signal phase tracking. Consider an input signal of form

$$r(t) = Acos[\omega_i t + \phi_i(t)] \tag{1.1}$$

where A is the peak signal amplitude (a constant), ω_i is the input signal center frequency, and ϕ_i is the input signal phase. Assume that the VCO output signal is of the form

$$u(t) = -(2/A)sin[\omega_i t + \hat{\phi}(t)] \tag{1.2}$$

where $\hat{\phi}(t)$ is the VCO phase estimate. A particular form of VCO signal is chosen, with the main feature being the quadrature relationship between the input and the VCO output. A secondary feature is the 2/A amplitude, chosen solely as a matter of convenience. Both characteristics stem from the multiplier form of the phase detector, as will be apparent presently.

Let the phase detector be characterized as an ideal multiplier which, in turn, is an idealization of the doubly-balanced mixer often used as a phase detector in practice. The result is an output of

$$\begin{aligned} a(t) &= r(t)u(t) \\ &= -sin[2\omega_i t + \phi_i(t) + \hat{\phi}(t)] + sin[\phi_i(t) - \hat{\phi}(t)]. \end{aligned} \tag{1.3}$$

If we neglect the upper sideband component (the first term in (1.3)), or assume that it is subsquently rejected by the loop filter, the filter output becomes

$$e(t) = K_2 f(t) \otimes sin\theta(t) \tag{1.4}$$

where K_2 is the baseband amplifier gain, f(t) is the impulsive response of the filter,

$$\theta(t) = \phi_i(t) - \hat{\phi}(t) \tag{1.5}$$

and $\otimes$ denotes convolution. This baseband voltage is applied to the VCO, and results in an FM signal whose frequency deviation is directly propotional to the control voltage,

$$d\hat{\phi}(t)/dt = Kf(t) \otimes sin\theta(t) \tag{1.6}$$

with $K = K_2K_3$, and K_3 being the VCO sensitivity.

1.2.2 Delay-Locked Loop

Once receiver timing has been synchronized to within a fraction of a chip time, the estimate should be further refined to approach zero. Furthermore, because of the relative motion of transmitter and receiver and the instability of clocks, corrections must be made continuously. This process, which is called tracking, is performed by the so-called "early-late" gate device[15]. It is an elabolation of the basic demodulator and acquisition device.

The function of a baseband DLL is to track the time-varying phase of the received spreading waveform $C(t-\tau)$. The function $\hat{\tau}(t)$ will denote the receiver estimate of $\tau(t)$, and $\tau(t)$ and $\tau\hat{(t)}$ are always functions of time, whether or not this dependence is written explicity. The received signal consists of the spreading waveform $C(t-\tau)$ and additive white gaussian noise. That is,

$$r(t) = C(t-\tau) + n(t). \tag{1.7}$$

Fig.1.3 is a conceptual block diagram of the tracking loop. It consists of a phase discriminator, a loop filter, a voltage controlled oscillator, and a code waveform generator

Input signal r(t) is cross-correlated with the advanced version $C(t-\hat{\tau}+(\Delta/2)T_c)$ and retarded version $C(t-\hat{\tau}-(\Delta/2)T_c)$ of the local PN code generator sequence. Parameter Δ is the total normalized time difference between the advanced and retarded discriminator channels.

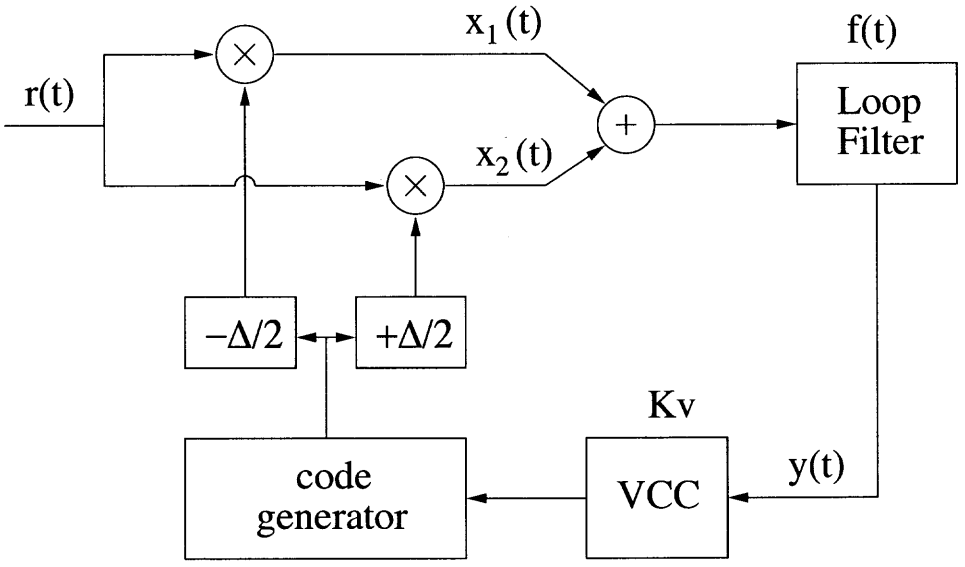

Figure 1.3 Block Diagram of Conceptual Delay Locked Loop

Consider the operation of the delay-lock discriminator as a static phase-measuring device in a noiseless environment. That is, let τ and $\hat{\tau}$ be fixed and determine the output of the discriminator. This output will contain a component which is a function of $\delta = (\tau - \hat{\tau})/T_c$ and is suitable for driving the VCC just as the phase-locked-loop multiplier output contained a component $sin(\phi - \phi_0)$. In the static case, it is convenient to write x_1, x_2, and $\varepsilon(t, \delta)$ as explicit functions of τ, $\hat{\tau}$, and t. Thus, the advanced-correlator output is

$$x_1(t, \tau, \hat{\tau}) = C(t - \tau)C(t - \hat{\tau} + (\Delta/2)T_c) \tag{1.8}$$

and the retarded-correlator output is

$$x_2(t, \tau, \hat{\tau}) = C(t - \tau)C(t - \hat{\tau} - (\Delta/2)T_c). \tag{1.9}$$

The delay-locked discriminator output is the difference of $x_1(t)$ and $x_2(t)$ and is

$$\begin{aligned}\varepsilon(t,\tau,\hat{\tau}) &= x_2(t,\tau,\hat{\tau}) - x_1(t,\tau,\hat{\tau}) \\ &= C(t-\tau)[C(t-\tau)C(t-\hat{\tau}-(\Delta/2)T_c) - C(t-\hat{\tau}+(\Delta/2)T_c)]. \quad (1.10)\end{aligned}$$

The dc component of this signal is used for code tracking. The dc component of $\varepsilon(t,\tau,\hat{\tau})$ is denoted $D_\Delta(\tau,\hat{\tau})$ and the time average of $\varepsilon(t,\tau,\hat{\tau})$. Thus

$$\begin{aligned}D_\Delta(\tau,\hat{\tau}) &= \frac{1}{NT_c}\int_{-NT_c/2}^{NT_c/2} C(t-\tau)[C(t-\tau)C(t-\hat{\tau}-(\Delta/2)T_c) \\ &\quad -C(t-\hat{\tau}+(\Delta/2)T_c)]dt \quad (1.11)\end{aligned}$$

where NT_c is the period of C(t). The autocorrelation function of C(t) is

$$\begin{aligned}D_\Delta(\tau,\hat{\tau}) &= R(\tau-\hat{\tau}-\frac{\Delta}{2}T_c) - R(\tau-\hat{\tau}+\frac{\Delta}{2}T_c) \\ &= R[(\delta-\frac{\Delta}{2})T_c] - R[(\delta+\frac{\Delta}{2})T_c] \\ &= D_\Delta(\delta). \quad (1.12)\end{aligned}$$

Assuming that code self-noise can be ignored, discriminator output can be written

$$\varepsilon(t,\tau,\hat{\tau}) = D_\Delta(\delta) + n'(t) \quad (1.13)$$

where

$$n'(t) = n(t)[C(t-\tau)C(t-\hat{\tau}-(\Delta/2)T_c) - C(t-\hat{\tau}+(\Delta/2)T_c)] \quad (1.14)$$

The filter output is the convolution of the input signal and the impulse response. That is,

$$y(t) = \int_{-\infty}^{t} \varepsilon(\lambda,\delta)f(t-\lambda)d\lambda. \quad (1.15)$$

Finally, considering the VCC, the nonlinear integral equation representing the operation of the tracking loop of Fig.1.3 is

$$\begin{aligned}\frac{\hat{\tau}(t)}{T_c} &= K_v \int_0^t y(\lambda) d\lambda \\ &= K_v \int_0^t \int_{-\infty}^{\lambda} \Big[D_\Delta(\delta(\alpha)) + n'(\alpha) \Big] f(t-\alpha) d\alpha d\lambda. \end{aligned} \tag{1.16}$$

1.3 One-shot Linear Decorrelating Detector

There has been great interest in improving DS-CDMA detection through the use of multiuser detectors. In multiuser detection, code amplitude and phase information of multiple users are jointly used to better detect each indivisual user. The important assumption is that the codes of multiple users are known to the receiver a priori.

Verdú's seminal work [30] proposed and analyzed the optimum multiuser detector, otherwise known as the maximum likelihood sequence detector. Unfortunately, this detector is much too complex for practical DS-CDMA systems. Therefore, over the last decade or so, most of the research has focused on finding suboptimal multiuser detector solutions which are more feasible to implement.

Most of the proposed detectors can be classified in one of two categories: linear multiuser detectors and subtractive interference cancellation detectors. In linear multiuser detection, a linear mapping (transformation) is applied to the soft outputs, which hopefully provides better performance.

Among many suboptimal detectors proposed, Lupas and Verdu's linear decorrelating detector (LDD) [28],[29] has attracted wide attention. The LDD achieves the same near-far resistance as the optimum detector while its complexity is linear in the number of users. Although the LDD is much simpler than Verdu's optimum detector, it is still too complicated and will lead to unacceptable detection delay while dealing with asynchronous CDMA. Therefore, another scheme, also proposed by Lupas [33], called one-shot LDD, where the detection of data is based on the signal observed in

one bit length period, the detection of an asynchronous CDMA is transformed into that of synchronous CDMA. One-shot LDD is synchronized with one of the users, so for a U-user asynchronous CDMA, a (2U-1)-user synchronous CDMA problem must be solved for the detection of one user, and a total of U different (2U-1)-user synchronous CDMA problems must be solved for the detection of the total U users.

1.4 Fading Channel

The mobile radio channel places fundamental limitations on the performance of wireless communication systems. The transmission path between the transmitter and the receiver can vary from simple line-of-sight to one that is severely obstructed by building, mountains, and foliage.

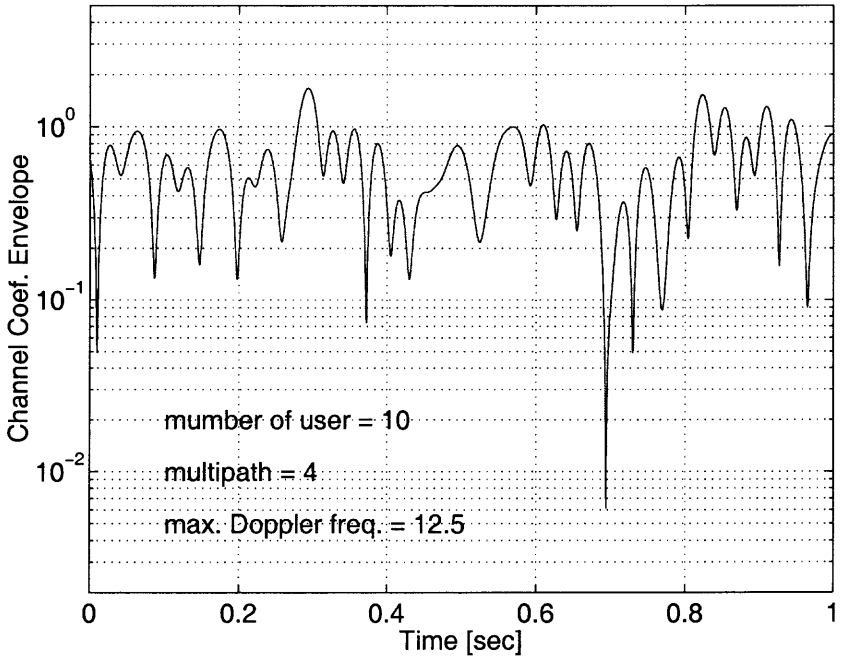

Figure 1.4 Signal envelope of Rayleigh fading

Unlike wired channels that are stationary and predictable, radio channels are extremely random and do not offer easy analysis. Even the speed of motion impacts

how rapidly the signal level fades as a mobile terminal moves in space. Modeling the radio channel has historically been one of the most difficult parts on measurements made specifically for an intended communication system.

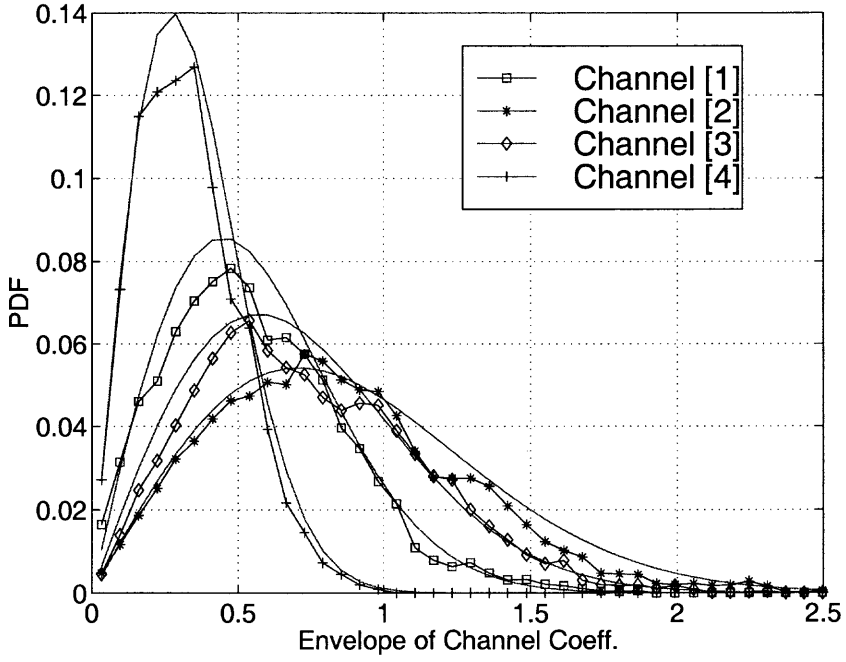

Figure 1.5 PDF (Histogram) of envelope of Rayleigh fading

Propagation models that predict the mean signal strength for an arbitrary transmitter-receiver separation distance are useful in estimating the radio coverage area of a transmitter and are called large-scale propagation models, since they characterize signal strength over large Tx-Rx separation distances (several hundreds or thousands of meters). On the other hand, propagation models that characterize the rapid fluctuations of the received signal strength over very short travel distances (a few wavelengths) or short time durations (on the order of seconds) are called small-scale or fading models.

From now on, we will consider only small-scale fading models ignoring the distance. In the fading model, depending on how rapidly the transmitted baseband

signal changes as compared to the rate of change of the channel, a channel may be classified either as a fast fading or slow fading channel. In the fast fading channel, the channel impulse response changes rapidly within the symbol duration. That is, the coherence time of the channel is smaller than the symbol period of the transmitted signal. On the other hand, a slow fading channel is one whose impulse response changes at a rate much slower than the transmitted baseband signal.

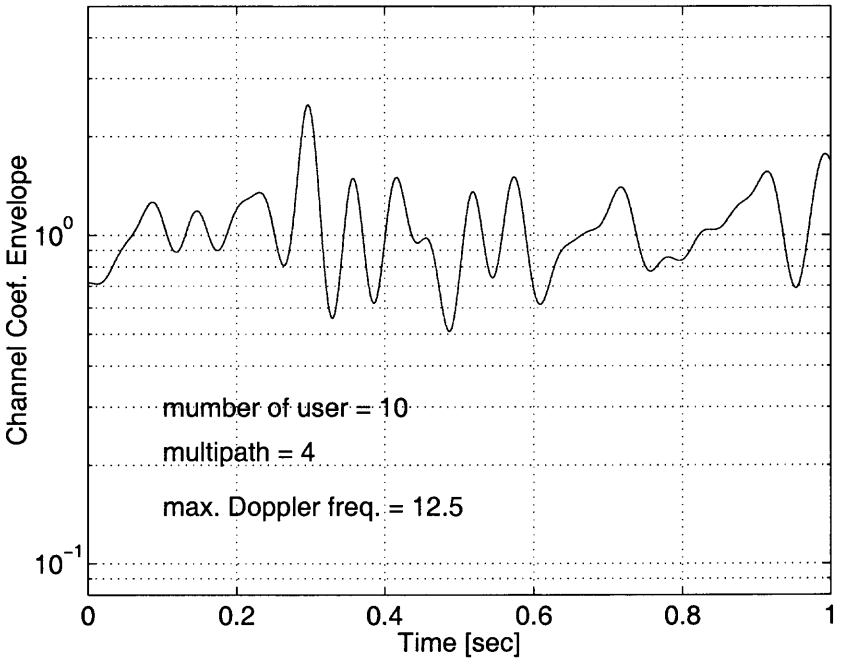

Figure 1.6 Signal envelope of Lognormal fading

In mobile radio channels, the Rayleigh distribution is commonly used to describe the statistical time varying nature of the received envelope of a flat fading signal, or the envelope of an individual multipath component. When the received signal is made up of multiple reflective rays plus a significant line-of-sight (no faded) component, the envelope amplitude due to small-scale fading has a Rician pdf containing a specular component. As the amplitude of the specular component approaches zero, the Rician pdf approaches a Rayleigh pdf, expressed as

$$p(r) = \begin{cases} \frac{r}{\sigma^2} exp\Big[- \frac{r^2}{2\sigma^2} \Big] & \text{for r} \geq 0 \\ 0 & \text{otherwise} \end{cases} \tag{1.17}$$

where r is the envelope amplitude of the received signal, and σ^2 is the predetection mean power of the multipath signal. The Rayleigh faded component is sometimes called the random, or scatter, or diffuse component. The Rayleigh pdf results from having no specular component of the signal; thus, for a single link it represents the pdf associated with the worst case of fading per mean received signal power.

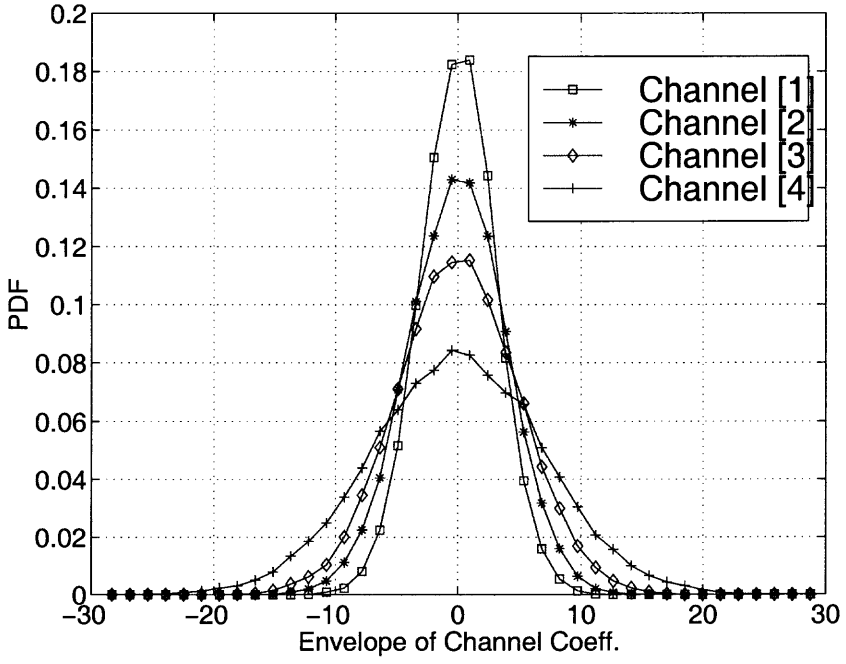

Figure 1.7 PDF (Histogram) of envelope of Lognormal fading with zero mean

Clarke developed a model where the statistical characteristics of the electromagnetic fields of the received signal at the mobile are deduced from scattering [9]. Fig.1.4 shows the envelope of Rayleigh faded signal as a function of time from the Clarke simulation method.

Fig.1.5 illustrates the probability density function (PDF) of the Rayleigh faded envelope as a function of the envelopes in multipath channel environment.

In power control environment, if the received signals are imperfectly power controlled, the signal powers are log-normally distributed [3]. Fig.1.6 shows the envelope of Lognormal faded signal as a function of time and Fig.1.7 shows the pdf of the Lognormal faded envelope as a function of the envelopes.

1.5 Contribution of Dissertation

- Dynamic Partial Correlation (DPC)
  - Evaluation of autocorrelation and its power spectrum density function of cross-correlated terms in asynchronous multirate DS-CDMA systems.
  - Application for asynchronous multirate multiple access interference.
- Phase-Locked Loop (PLL)
  - Integration of PLL and DLL to operate efficiently.
  - Performance analysis via the PDF and variance of phase estimator error using DPC method in asynchronous multirate DS-CDMA system under AWGN, Log-Normal, and Rayleigh fading channel environments.
  - Combination of PLL and one-shot CLDD to improve the performance of multiuser detection.
- Delay-Locked Loop (DLL)
  - Integration of PLL and DLL to operate efficiently.
  - Performance analysis by the PDF and variance of the delay jitter of PN code signature waveform using DPC method in asynchronous multirate DS-CDMA system under AWGN and Rayleigh fading channel environments.

- Linear Decorrelating Detector (LDD)

  - Propose the Hybrid SD/MRC one-shot linear decorrelating detector.
  - Adopt the selection diversity (SD) combining scheme to compensate the deep faded signal by the selection of the largest instantaneous SNR from the SD combiner.
  - Adopt the maximal ratio (MR) Combining scheme to maximize the output SNR for compensating the reduction of signature waveform energy of conventional LDD.
  - Apply the Phase-Locked Loop to the Hybrid SD/MRC one-shot LDD for fine synchronization of carrier phase error in asynchronous DS-CDMA system.
  - Evaluate the pdfs of the maximum SNR at the SD combiner output, the near-far resistance (NFR) of LDD, and the maximum SNR at the Hybrid SD/MRC one-shot LDD output.
  - Obtain the bit error probability by using the pdfs, analyze the performance of Hybrid SD/MRC LDD, and compare with conventional LDD in Rayleigh fading channel.

CHAPTER 2

PHASE-LOCKED LOOP

2.1 Transmitter Channel Modelling

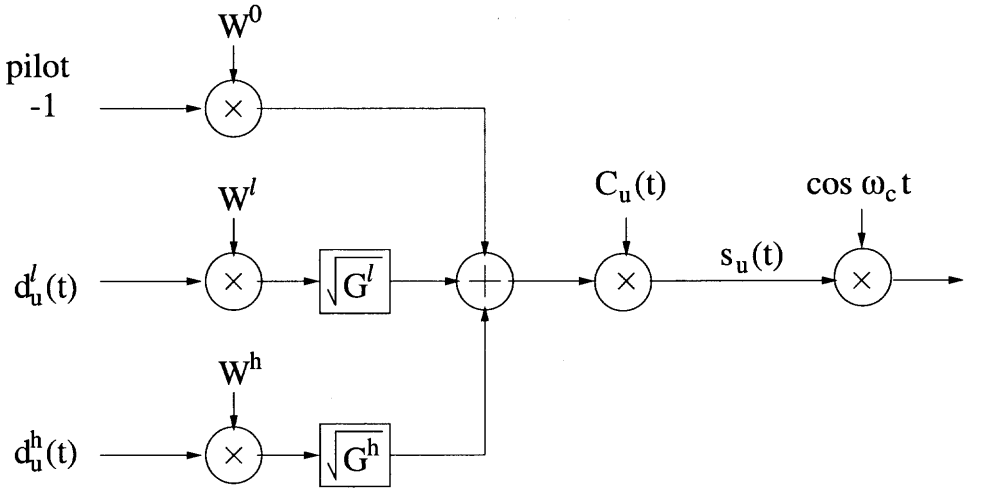

Figure 2.1 Transmitter Structure for u^{th} user

The transmitted signal of the u^{th} user is modelled by multiplying $s_u(t)$ with a carrier $\cos\omega_c t$. The signal $s_u(t)$ with the pilot and multirate data is expressed by

$$s_u(t) = \left[1 + \sqrt{G^l} d_u^l(t) W^l(t) + \sqrt{G^h} d_u^h(t) W^h(t)\right] C_u(t) \tag{2.1}$$

where the pilot signal and its channelization code sequence W^0 is assumed to be all -1 [5] and G^r is the power gain and $r = \ell$, h denote low-rate and high-rate signals, respectively. Defining a rectangular pulse by $h_T(t) = 1$ for $0 \leq t \leq T$ and $h_T(t) = 0$, otherwise, the data sequence with r rate, $d_u^r(t)$, can be written as

$$d_u^r(t) = \sum_{n=-\infty}^{\infty} d_u^r(n) h_T(t - nT_r) \tag{2.2}$$

with consecutive data bits $\{d_u^r(n)\}$ taking on values of ± 1 with equal probability. Since the two different data channels should share the same channel bandwidth, multiple spreading factors (SF) are required [13].

For variable sequence length synchronization, we shall denote the bit interval of the low-rate data as T_l and the number of bits of channelization code corresponding to T_l as N_l . The high-rate data will be transmitted data with bit intervals of duration T_h and channelization code length N_h. The channelization code waveform, $W^r(t)$, for the r channel can be written as

$$W^r(t) = \sum_{n=-\infty}^{\infty} W^r(n) h_{T_w}(t - nT_w) \tag{2.3}$$

where $T_w = T_l/N_l = T_h/N_h$ and $W^r(n)$ is a periodic sequence with length N_r chosen in VLO code set.

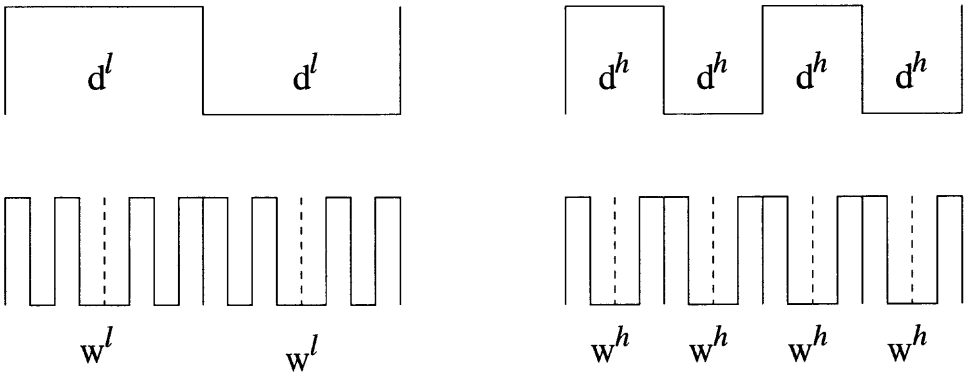

(a) Low-rate, $N_l = 8$ (b) High-rate, $N_h = 4$

Figure 2.2 Variable sequence length multirate spreading

As shown, for example, in Fig.2.2, each bit of the low rate data d_u^l is spread by a code of length $N_l = 2^n$, where n is an abitrary integer. Since the bit duration of high rate data T_h is half the duration of a bit in the low rate T_l, we need a spreading code of length $N_h = N_l/2 = 2^{n-1}$ for spreading. Orthogonality between different rates and SFs is necessary for multirate multiuser detection to be accomplished. Thus the channelization code waveform $W^l(t)$ should be orthogonal to

$$W^l(t) \perp \sum_{\omega=1}^{\Omega} W^h(t - (\omega - 1)T_h) \tag{2.4}$$

where the ratio $\Omega = T_l/T_h = N_l/N_h$ is an integer.

The scrambling PN code waveform, $C_u(t)$, for u^{th} user can be written as

$$C_u(t) = \sum_{n=-\infty}^{\infty} C_u(n) h_{T_c}(t - nT_c) \tag{2.5}$$

where $C_u(n)$ is a periodic sequence with length N chosen in Gold or Kasami code set. If we assume that the length of the PN code is the same as T_l, then $T_l = NT_c$. Notice that $T_h = NT_c/\Omega$, $T_w = NT_c/N_l = NT_c/N_h\Omega$. From now on, we assume that the ratios N/N_l and $N/N_h\Omega$ are integers.

2.2 Phase-Locked Loop Receiver

Fig.2.3 illustrates a receiver configuration for reception of the pilot signal in asynchronous multirate DS-CDMA systems.

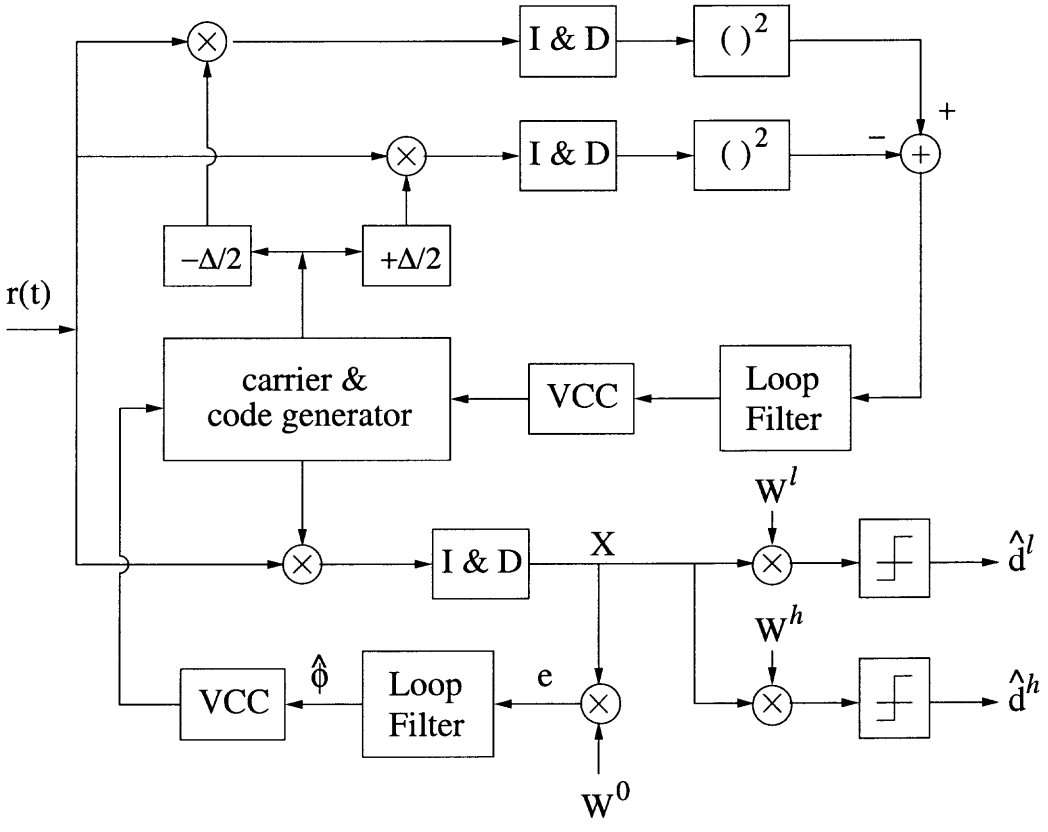

Figure 2.3 Block Diagram of Phase-Locked Loop

We assume that a channel delays the signals transmitted through it and corrupts them by adding gaussian noise. Hence, the incoming signal r(t) to the integrated receiver of DLL and PLL in Fig.2.3 can be expressed as

$$r(t) = \sum_{u=1}^{U} A_u(t) s_u(t - \tau_u) \cos(\omega_c t - \phi_u(t)) + n(t) \tag{2.6}$$

where A(t) and $\phi_u(t)$ are the received envelope and the carrier phase delay due to the channel, respectively, U indicates the number of users, τ_u is the code phase delay, and n(t) is additive white gaussian noise having a zero mean and a one-sided PSD N_0.

Without loss of generality, we will assume that the signal to be tracked belongs to the pilot signal of the first user. The locally generated code and phase sequence of user one with pilot signal is represented by

$$V_{LO}(t) = C_1(t - \hat{\tau}_1) \cos(\omega_c t + \hat{\phi}_1(t)) \tag{2.7}$$

where $\hat{\tau}_1$ and $\hat{\phi}_1(t)$ are the estimates of the code and phase delay of the local oscillator for user one determined by the DLL and PLL estimator signal, respectively. When the one-sided loop bandwidth B_L is much less than the PN code chip rate $1/T_c$, the effect of the PN code self-noise on the loop performance can be neglected [15].

Assuming that the PN code of the desired user was tracked well, $\tau_1 = 0$ and the output of the Integrate-and-Dump operations after multiplying the input r(t) by the estimate of the local oscillator, $V_{LO}(t)$, X can be evaluated as

$$\begin{aligned} X &= \int_0^{T_l} r(t) V_{LO}(t) dt \\ &= N T_c A_1 \cos\theta_1(t) + I_P(t) + I_d^l(t) + I_d^h(t) + I_n(t). \end{aligned} \tag{2.8}$$

Letting $\theta_u(t) = \phi_u(t) - \hat{\phi}_u(t)$ and defining $\xi_u = (\hat{\tau}_1 - \tau_u)/T_l$, AWGN and MAI terms are as follows :

$$I_P(t) = \sum_{u=2}^{U} A_u \Phi_p(t, \xi_u) \cos\theta_u(t) \tag{2.9}$$

$$I_d^l(t) = \sum_{u=1}^{U} A_u \sqrt{G^l} \Phi_u^l(t, \xi_u) \cos\theta_u(t) \tag{2.10}$$

$$I_d^h(t) = \sum_{u=1}^{U} A_u \sqrt{G^h} \Phi_u^h(t, \xi_u) \cos\theta_u(t) \tag{2.11}$$

$$I_n(t) = \int_0^{T_l} n(t) C_1(t - \hat{\tau}_1) \cos(\omega_c t + \hat{\phi}_1(t)) dt \tag{2.12}$$

with

$$\Phi_p(t, \xi_u) = \int_0^{T_l} C_u(t - \xi_u) C_1(t) dt \tag{2.13}$$

$$\Phi_u^r(t, \xi_u) = \int_0^{T_l} d_u^r(t - \xi_u) W^r(t - \xi_u) C_u(t - \xi_u) C_1(t) dt. \tag{2.14}$$

The error signal to the loop filter is multiplied by the term of the estimated pilot envelope with all 1's as follows:

$$e(\theta) = W^0 X. \tag{2.15}$$

From Fig.2.3, the instantaneous phase delay estimate of the PN code generator output, $\hat{\phi}_1$, is related to $e(\theta)$ by

$$\hat{\phi}_1 = \frac{K_p F(p)}{p} e(\theta) \tag{2.16}$$

where K_p is an overall closed loop gain including the gain of the voltage controlled clock which drives the carrier generator. The coherent integro-differential equation of the operation of Fig.2.3 with p = d/dt becomes

$$p\theta_1 = p\phi_1 - K_p p F(p) \Big[A_1 \sin\theta_1 + \frac{N(t)}{p} \Big] \tag{2.17}$$

where

$$N(t) = I_P(t) + I_d^l(t) + I_d^h(t) + I_n(t). \tag{2.18}$$

2.3 Dynamic Partial Correlation (DPC)

We will now find the probability density function (PDF) as a function of the number of simultaneous users for investigating the behavior of the phase estimate error. We have to evaluate the power spectrum density (PSD) of the corresponding MMAI and AWGN terms prior to finding the PDF, $p(\theta)$.

However, the conventional continuous partial correlation method cannot evaluate the autocorrelations and corresponding PSDs of the cross-correlation terms with asynchronous multirate signals clearly since the method cannot treat with a multirate signal. Therefore, we will introduce a new method called Dynamic Partial Correlation (DPC) to solve the autocorrelations and corresponding PSDs of cross-correlation terms in any specific time duration in NT_c for asynchronous multirate signals.[1]

The crosscorrelation between two codes in a specific interval $[\alpha, \beta]$ is defined as

$$M_u^r(\alpha, \beta, \gamma) = \int_\alpha^\beta W^r(t-\gamma) C_u(t-\gamma) C_1(t) dt \tag{2.19}$$

where $\alpha = iT_c + \delta_\alpha$ and $\beta = jT_c + \delta_\beta$ for $0 < i < j < N$, and $\gamma = kT_c + \delta_\gamma$ for $0 < k < N$. As shown in Figure 2.4, the wave form $W^r(t-\gamma)C_u(t-\gamma)C_1(t)$ is represented by two rectangular pulse trains as

$$p_u^r(t, \gamma) = \sum_{l=0}^{N-1} p_u^r(l)\ \Pi(lT_c, lT_c + \delta_\gamma) \tag{2.20}$$

$$q_u^r(t, \gamma) = \sum_{l=0}^{N-1} q_u^r(l)\ \Pi(lT_c + \delta_\gamma, (l+1)T_c) \tag{2.21}$$

where the magnitudes $p_u^r(l)$ and $q_u^r(l)$ taking on values of ± 1 can be found by multiplying a code bit of the desired user and a delayed code bit of the u^{th} user and the channelization code as $p_u^r(l) = C_1(l)C_u(N-1-l-k)W^r(z^r)$ and $q_u^r(l) = C_1(l)C_u(N-l-k)W^r(z^r)$ where z^r is an integer which satisfies the equation $(N-1-$

[1]Sections 2 and 3 with DPC method did with Hunkee Kim and D. S. Phatak at Dept. of Electrical Engineerong of Binghamton, SUNY.

$l - k) = z^r(N/N_r)$+residue of (N/N_r) and rectangular pulse defined as $\Pi(a, b) = 1$ for $a < t < b$ and $\Pi(a, b) = 0$, otherwise.

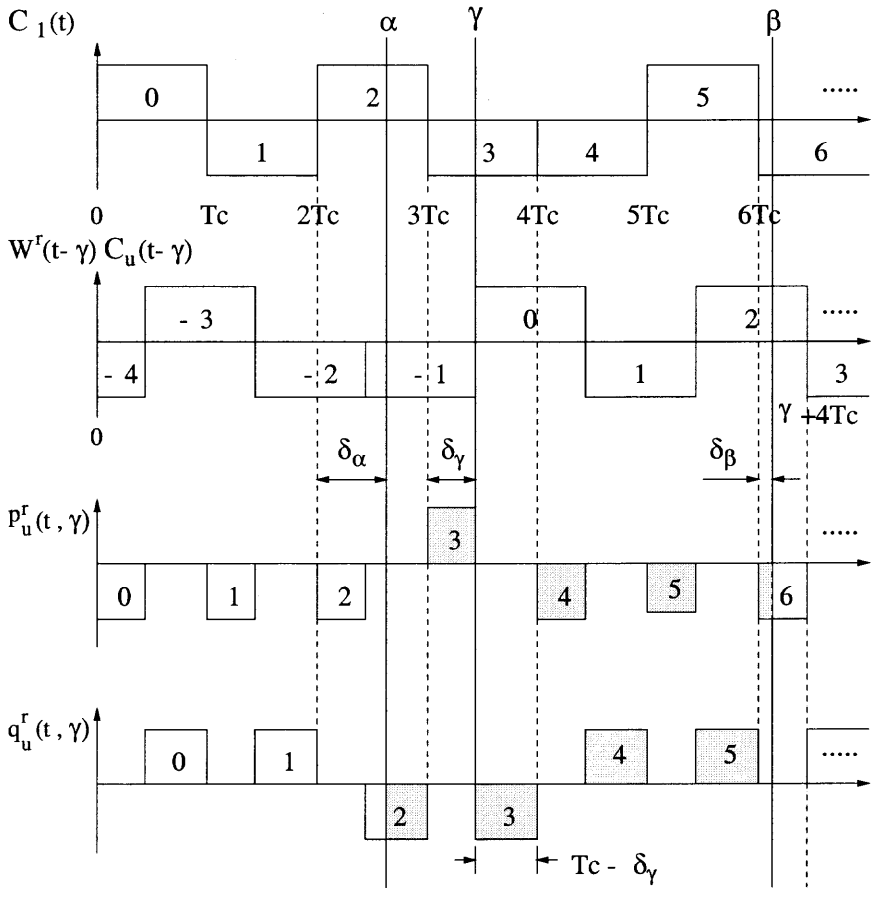

Figure 2.4 An example of the DPC method in $[\alpha, \beta]$: i = 2, j = 6, k = 3

Thus, the summations of $p_u^r(t,\gamma)$ and $q_u^r(t,\gamma)$ in $[\alpha,\beta]$ are

$$\begin{aligned}\int_\alpha^\beta p_u^r(t,\gamma)dt &= \sum_{l=i}^{j} p_u^r(l)\delta_\gamma - p_u^r(i)B(\delta_\alpha,\delta_\gamma)\delta_\gamma \\ &\quad -p_u^r(j)B(\delta_\gamma,\delta_\beta)(\delta_\gamma-\delta_\beta) - p_u^r(i)B(\delta_\gamma,\delta_\alpha)\delta_\alpha \qquad (2.22)\end{aligned}$$

$$\begin{aligned}\int_\alpha^\beta q_u^r(t,\gamma)dt &= \sum_{l=i}^{j} q_u^r(l)(T_c-\delta_\gamma) - q_u^r(j)B(\delta_\gamma,\delta_\beta)(T_c-\delta_\gamma) \\ &- q_u^r(i)B(\delta_\alpha,\delta_\gamma)(\delta_\alpha-\delta_\gamma) - q_u^r(j)B(\delta_\beta,\delta_\gamma)(T_c-\delta_\beta) \qquad (2.23)\end{aligned}$$

where B(a,b) = 1 for a> b and B(a,b) = 0, otherwise. Therefore, equation (2.19) can be solved in terms of α and β as

$$\begin{aligned}M_u^r(\alpha,\beta,\gamma) &= \int_\alpha^\beta p_u^r(t,\gamma)dt + \int_\alpha^\beta q_u^r(t,\gamma)dt \\ &= \mathcal{F}_u^r(\alpha,\gamma)\alpha + \mathcal{G}_u^r(\beta,\gamma)\beta + \mathcal{H}_u^r(\alpha,\beta,\gamma) \qquad (2.24)\end{aligned}$$

where the three constant terms are as follows :

$$\mathcal{F}_u^r(\alpha,\gamma) = -p^r(i)B(\delta_\gamma,\delta_\alpha) - q^r(i)B(\delta_\alpha,\delta_\gamma) \qquad (2.25)$$

$$\mathcal{G}_u^r(\beta,\gamma) = p^r(j)B(\delta_\gamma,\delta_\beta) - q^r(j)B(\delta_\beta,\delta_\gamma) \qquad (2.26)$$

$$\begin{aligned}\mathcal{H}_u^r(\alpha,\beta,\gamma) &= \sum_{l=i}^{j}\left[p^r(l)\delta_\gamma + q^r(l)(T_c-\delta_\gamma)\right] \\ &\quad -p^r(i)B(\delta_\alpha,\delta_\gamma)\delta_\gamma \\ &\quad -p^r(j)B(\delta_\gamma,\delta_\beta)(\delta_\gamma+jT_c) \\ &\quad +p^r(i)B(\delta_\gamma,\delta_\alpha)iT_c \\ &\quad -q^r(j)B(\delta_\gamma,\delta_\beta)(T_c-\delta_\gamma) \\ &\quad +q^r(i)B(\delta_\alpha,\delta_\gamma)(iT_c+\delta_\gamma) \\ &\quad -q^r(j)B(\delta_\beta,\delta_\gamma)(T_c+jT_c). \qquad (2.27)\end{aligned}$$

Eqns. (2.25)-(2.27) have the constant terms and first order terms for α and β. Therefore, the PSD is simplified by using the definition of $S_m(a,b,f) = \int_a^b me^{-j2\pi fm}dm$ for first order and $S_1(a,b,f) = \int_a^b e^{-j2\pi fm}dm$ for constant.

2.3.1 Case of Pilot Interference

The sequences of the channelization code with pilot signal are all 1's. Therefore, $\mathcal{R}_{I_P}(m)$ with $\alpha = 0, \beta = T_l$, and $W(t) = 1$ from DPC method can be expressed by

$$\begin{aligned}\mathcal{R}_{I_P}(m) &= \sum_{u=2}^{U} P_u E\{\Phi_u(t,\xi_u)\Phi_u(t+m,\xi_u)\} \\ &= \sum_{u=2}^{U} P_u M_u(0,T_l,\xi_u) M_u(m,T_l+m,\xi_u)\end{aligned} \tag{2.28}$$

where $P_u = E\{A_u^2\}$ is the average received signal power.

The PSD of $\mathcal{R}_{I_P}(m)$ can be evaluated as

$$\begin{aligned}S_{I_P}(f) &= \sum_{u=2}^{U} \int_{-\infty}^{\infty} \mathcal{R}_{I_P}(m) e^{-j2\pi fm} dm \\ &= \sum_{u=2}^{U} P_u \Big[K_{P1} S_m(0,T_l,f) + K_{P2} S_1(0,T_l,f)\Big]\end{aligned} \tag{2.29}$$

where

$$K_{P1} = J_P[\mathcal{F}_u(m,T_l+m) + \mathcal{G}_u(T_l+m,m)] \tag{2.30}$$

$$K_{P2} = J_P[\mathcal{G}_u(T_l+m,\xi_u)T_l + \mathcal{H}_u(m,T_l+m,\xi_u)] \tag{2.31}$$

with the constant term $J_P = M_u(0,T_l,\xi_u)$.

2.3.2 Case of Low-Rate Data Interference

Next, we will find the PSD of $\mathcal{R}_{I_d^r}(m)$ due to multiple access interferences with different data rate. The autocorrelation function of the low-rate MAI is represented by DPC terms as

$$\mathcal{R}_{I_d^l}(m) = \sum_{u=1}^{U_l} A_u G^l \mathcal{R}_{\Phi_u^l}(m) \tag{2.32}$$

where

$$\begin{aligned}\mathcal{R}_{\Phi_u^l}(m) &= E\{A_u^2\} E\{\Phi_u^l(t,\xi_u)\Phi_u^l(t+m,\xi_u)\} \\ &= \begin{cases} P_u\Big[J_1 M_u^l(m,\xi_u,\xi_u) + P_u J_2 M_u^l(\xi_u,T_l+m,\xi_u)\Big], & 0 \le m < \xi_u \\ J_2 M_u^l(m,T_l+\xi_u,\xi_u), & m \ge \xi_u \end{cases}\end{aligned} \tag{2.33}$$

with $J_1 = M_u^l(0, \xi_u, \xi_u)$ and $J_2 = M_u^l(0, T_l, \xi_u)$. The low-rate continuous partial cross-correlation can be represented as

$$\begin{aligned}
&\Phi_u^l(t+m, \xi_u) \\
&= \int_m^{T_l+m} d_u^l(t-\tau_u) W^l(t-\tau_u) C_u(t-\tau_u) C_1(t-\hat{\tau_u}) dt \\
&= \begin{cases} d_u^l(-1) M_u^l(m, \xi_u, \xi_u) + d_u^l(0) M_u^l(\xi_u, T_l+m, \xi_u), & 0 \le m < \xi_u \\ d_u^l(0) M_u^l(m, T_l+\xi_u, \xi_u) + d_u^l(1) M_u^l(T_l+\xi_u, T_l+m, \xi_u), & m \ge \xi_u \end{cases}
\end{aligned} \tag{2.34}$$

where $E\{d_u^l(p) d_u^l(q)\} = 1$ for p=q and $E\{d_u^l(p) d_u^l(q)\} = 0$, otherwise, and the subscript, -1,0, and 1 denote the last previous data bit, the present data bit, and the first next data bit, respectively.

Therefore, the PSD of $\mathcal{R}_{I_d^l}(m)$, $\mathcal{S}_{I_d^l}(f)$ can be evaluated as

$$\begin{aligned}
S_{I_d^l}(f) &= \sum_{u=1}^{U_l} P_u G^l \int_{-\infty}^{\infty} \mathcal{R}_{\Phi_u^l}(m) e^{-j\omega m} dm \\
&= \sum_{u=1}^{U_l} P_u G^l S_{\phi_u^l}(f)
\end{aligned} \tag{2.35}$$

where

$$S_{\phi_u^l}(f) = \begin{cases} K_{11} S_m(0, \xi_u, f) + K_{12}^l S_1(0, \xi_u, f), & 0 \le m < \xi_u \\ K_{21}^l(n) S_m(\xi_u, T_l, f) + K_{22}^l(n) S_1(\xi_u, T_l, f), & m \ge \xi_u \end{cases} \tag{2.36}$$

with

$$K_{11} = J_1 \mathcal{F}_u^l(m, \xi_u) + J_2 \mathcal{G}_u^l(T_l+m, \xi_u) T_l \tag{2.37}$$

$$\begin{aligned}
K_{12} = {} & J_1 \mathcal{G}_u^l(\xi_u, \xi_u) \xi_u + J_1 \mathcal{H}_u^l(m, \xi_u, \xi_u) \\
& + J_2 \mathcal{G}_u^l(T_l+m, \xi_u) T_l + J_2 \mathcal{H}_u^l(\xi_u, T_l+m, \xi_u)
\end{aligned} \tag{2.38}$$

$$K_{21} = J_2 \mathcal{F}_u^l(m, \xi_u^l) \tag{2.39}$$

$$K_{22} = J_2 \mathcal{G}_u^l(T_l+\xi_u, \xi_u) T_l + J_2 \mathcal{G}_u^l(T_l+\xi_u, \xi_u) \xi_u + J_2 \mathcal{H}_u^l(m, T_l+\xi_u, \xi_u). \tag{2.40}$$

2.3.3 Case of High-Rate Data Interference

The autocorrelation function of the high-rate MAI is represented by DPC terms as

$$\mathcal{R}_{I_d^h}(m) = \sum_{u=1}^{U_h} A_u G^h \mathcal{R}_{\Phi_u^h}(m) \tag{2.41}$$

where

$$\begin{aligned}
&\mathcal{R}_{\Phi_u^h}(m) = E\{\Phi_u^h(t,\xi_u)\Phi_u^h(t+m,\xi_u)\} \\
&= \begin{cases}
J_{11}^h M_u^h(m, \xi_u - aT_h) + J_{12}^h + J_{13}^h M_u^h(\xi_u + (\Omega - a - 1)T_h, m + T_l), \\
for \quad 0 \le m < \xi_u \\
J_{21}^h M_u^h(m, \xi_u + (b-a+1)T_h) + J_{22}^h + J_{23}^h M_u^h(\xi_u + (\Omega - a + b)T_h, m + T_l), \\
for \quad \xi_u + (\Omega - a - 1)T_h \le m < T_h \\
J_{31}^h M_u^h(m, \xi_u(\Omega - a) + T_h) + J_{32}^h + J_{33}^h M_u^h(\xi_u + (2\Omega - a - 1)T_h, m + T_l), \\
for \quad \xi_u + T_h \le m < T_l
\end{cases}
\end{aligned} \tag{2.42}$$

where 6 constant terms, Js, not depending on m are following with $n = 1, 2, 3$ and $N(1) = -a$, $N(2) = b - a + 1$, $N(3) = \Omega - a$.

Then the high-rate continuous partial cross-correlation is

$$\begin{aligned}
&\Phi_u^h(t+m, \xi_u) \\
&= \int_m^{T_l+m} d_u^h(t-\tau_u) W^h(t-\tau_u) C_u(t-\tau_u) C_1(t-\tau_u) dt \\
&= \begin{cases}
d_u^h(-a-1) M_u^h(m, \xi_u - aT_h) \\
+ \sum_{i=0}^{\Omega-2} d_u^h(i-a) M_u^h(\xi_u + (i-a)T_h, \xi_u + (i-a+1)T_h, \xi_u) \\
+ d_u^h(\Omega - 1 - a) M_u^h(\xi_u + (\Omega - 1 - a)T_h, m + T_l), \xi_u \\
for \quad 0 \le m < \xi_u - aT_h
\end{cases} \\
&\quad \begin{cases}
d_u^h(b-a) M_u^h(m, \xi_u + (b-a+1)T_h, \xi_u) \\
+ \sum_{i=0}^{\Omega-2} d_u^h(i-a+b+1) M_u^h(\xi_u + (i-a+b+1)T_h, \xi_u + (i-a+b+2)T_h, \xi_u) \\
+ d_u^h(\Omega - a - b) M_u^h(\xi_u + (\Omega - a + b)T_h, m + T_l), \xi_u \\
for \ \xi_u + (b-a)T_h \le m < \xi_u + (b-a+1)T_h
\end{cases}
\end{aligned}$$

$$\begin{cases} d_u^h(\Omega-1-a)M_u^h(m,\xi_u+(\Omega-a)T_h,\xi_u) \\ +\sum_{i=0}^{\Omega-2} d_u^h(\Omega-a+i)M_u^h(\xi_u+(\Omega-a+i)T_h,\xi_u+(\Omega-a+i+1)T_h,\xi_u) \\ +d_u^h(2\Omega-a-1)M_u^h(\xi_u+((2\Omega-a-1)T_h,m+T_l,\xi_u) \\ for\ \xi_u+(\Omega-a-1)T_h \le m < T_l \end{cases} \tag{2.43}$$

The PSD of the high-rate term can be represented as

$$\begin{aligned} S_{I_d^h}(f) &= \sum_{u=1}^{U_h} P_u G^h \int_{-\infty}^{\infty} \mathcal{R}_{\Phi_u^h}(m) e^{-j\omega m} dm \\ &= \sum_{u=1}^{U_h} P_u G^h S_{\Phi_u^h}(f) \end{aligned} \tag{2.44}$$

where

$$S_{\Phi_u^h}(f) = \begin{cases} K_{11}^h S_m(0,\xi_u-aT_h,f)+K_{12}^h S_1(0,\xi_u-aT_h,f)], \\ for \quad 0 \le m < \xi_u - aT_h \\ \\ K_{21}^h(n) S_m(\xi_u+(b-a)T_h,\xi_u+(b-a+1)T_h+,f) \\ +K_{22}^h S_1(\xi_u+(b-a)T_h,\xi_u+(b-a+1)T_h+,f)], \\ for \quad \xi_u+(b-a)T_h \le m < \xi_u+(b-a+1)T_h \\ \\ K_{31}^h(n) S_m(\xi_u+(\Omega-a-1)T_h,T_l,f)+K_{32}^h(n) S_1(\xi_u,(\Omega-a-1)T_h,T_l,f)], \\ for \quad (\Omega-a-1)T_h \le m < T_l \end{cases} \tag{2.45}$$

with

$$K_{n1}^h = J_{n1}^h \mathcal{F}^h(m,\xi_u,\xi_u) + J_{n3}^h \mathcal{G}^h(m+T_l,\xi_u,\xi_u)) \tag{2.46}$$

$$\begin{aligned} K_{n2}^h &= J_{n1}^h[\mathcal{G}^h(\xi_u+N(n)T_h,\xi_u,\xi_u)(\xi_u+N(n)T_h) \\ &\quad +\mathcal{H}^h(m,\xi_u+N(n)T_h,\xi_u)] + J_{n2}^h \end{aligned}$$

$$+J_{n3}^{h}[\ \mathcal{F}^{h}(\xi_u + (N(n)+\Omega-1)T_h, \xi_u, \xi_u)$$
$$\times(\xi_u+(N(n)+\Omega-1)T_h)+\mathcal{G}^{h}(m+T_l, \xi_u, \xi_u)T_l$$
$$+\mathcal{H}^{h}(\xi_u + (N(n)+\Omega-1)T_h, m+T_l, \xi_u)\ ]. \tag{2.47}$$

2.3.4 Case of AWGN

Assuming that the AWGN has zero mean and that the in-phase term and quadrature-terms are independent, and ignoring parameters(ℓ, k, u), the autocorrelation of AWGN is represented by

$$\begin{aligned}
&\mathcal{R}_n(m) \\
&= E\{A_1^2\}E\{n(t)n(t+m)\} \\
&= P_1\int_0^{T_l}\int_m^{T_l+m} E\{n_e(t)n_e(t+m)\}C_1(t-\tau)C_1(t+m-\tau) \\
&\quad \times \cos\omega_c t\cos\omega_c(t+m)dtd(t+m) \\
&= P_1\int_0^{T_l}\int_m^{T_l+m}\frac{N_0}{2}\delta(m)C_1(t-\tau)C_1(t+m-\tau)\cos\omega_c t\cos\omega_c(t+m)dtd(t+m) \\
&= \frac{N_0}{2}P_1\int_0^{T_l} C_1^2(t-\tau)\cos^2\omega_c t dt \\
&\approx \frac{N_0}{4}P_1T_l\delta(m).
\end{aligned} \tag{2.48}$$

The PSD of the noise is

$$S_{R_n} = \frac{N_0}{4}P_1T_l. \tag{2.49}$$

2.4 System Analysis

The solution of a nonlinear stochastic differential equations such as (2.17) for the steady-state probability density function (PDF), $p(\theta)$, may be accomplished via the Fokker-Planck method [4], [11], [14], [17]. From here on, we will use $\theta = \theta_1$ for convenience and simplicity. To illustrate the theory, we shall consider the case of a first-order loop (i.e., F(s) = 1) and also assume $d(\phi_1)/dt = 0$. The PDF, $p(\theta)$,

satisfies the stationary equation :

$$\frac{d}{d\theta}[A(\theta)p(\theta)] = \frac{1}{2}\frac{d^2}{d\theta^2}[B(\theta)p(\theta)] \tag{2.50}$$

where

$$A(\theta) = -K_p P_1 T_l \sin\theta \tag{2.51}$$

$$B(\theta) = \frac{1}{2}K_p^2 S_N. \tag{2.52}$$

From (4.28), using the well-known method of [1],[4], [22], we get the PDF of the phase estimator error as

$$p(\theta) = \frac{exp(\nu\cos\theta)}{2\pi I_0(\nu)} \tag{2.53}$$

where $I_0(\cdot)$ is the modified Bessel function of 0th-order. For ν, it can be shown by using the aymptotic formula $I_0(\nu) \approx exp(\nu)/\sqrt{2\pi\nu}$ that $p(\theta)$ approaches a Gaussian density function with zero mean and variance $\sigma^2_{\hat{\phi}}$. Parameter ν represents the loop signal-to-noise and interference power ratio (SNIR), defined by

$$\nu = \frac{T_l^2}{S_{I_p} + S_{d_u^l} + S_{d_u^h} + \frac{N_0}{4}P_1 T_l} B_L \tag{2.54}$$

where the loop bandwidth $B_L = K_p T_l/4$ for the loop transfer function H(s) = K/(s+K) with K = $K_p T_l/4$.

By using the PDF of the phase estimator error given by expression (3.42), the variance of the phase estimator error can be evaluated using

$$\sigma_\theta^2 = E^2\{\theta\} = \int_{-\pi}^{\pi} \theta^2 p(\theta) d\theta. \tag{2.55}$$

The PDF of the phase estimator error can be approximated by a Gaussian distribution for a large equivalent loop SNIR, and the variance becomes

$$\sigma_\theta^2 = \frac{K_p(S_{I_P} + S_{d_u^l} + S_{d_u^h} + \frac{N_0}{4}P_1 T_l)}{4NT_c}. \tag{2.56}$$

2.5 Numerical Analysis

We have evaluated in detail the PDF of the steady-state phase estimator error of a phase-locked loop in a multirate multiple access interference (MMAI) and AWGN environment. The transmitter has three different channels which can be separated by channelization codes. The transmitter signal for each user is despreaded by Gold code with length N=128. At first, the PDF of the steady-state phase estimator error of a phase-locked loop in a multirate multiple access interference (MMAI) and AWGN environment without fading channel is investigated. Next, the PDF and variance under no power controlled slow fading channel environment is shown in various aspects.

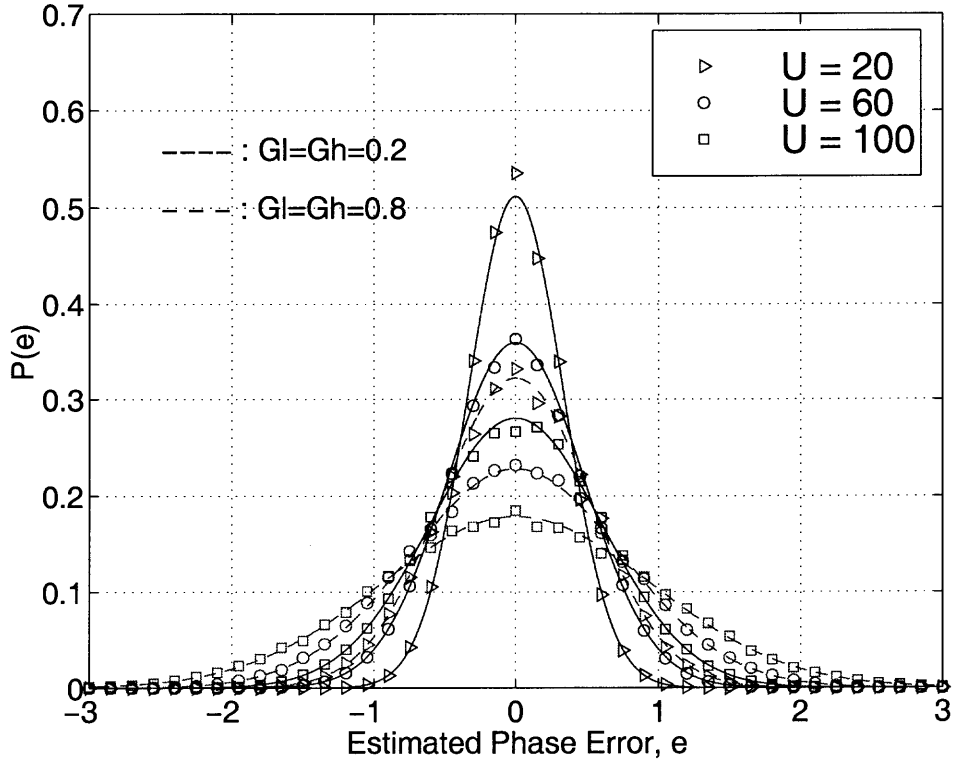

Figure 2.5 PDF of Phase Estimator Error under no fading channel

Fig.2.5 illustrates the behavior of the phase estimator error PDF, $p(\theta)$, as a function of the number of simultaneous users U, power gain of low-rate data, and power gain of high-rate data. The peak height of the PDF clearly increases with a reduction of the power gain of low-rate and high-rate data (in other words, the tracking ability of the phase-locked loop is degraded), and decreases as the number of simutaneous users increases. As shown in Fig.2.5, if the power gain of the multirate data signal increases by approximately the power of the pilot signal, the variance of the phase estimator error decreases rapidly; therefore, a tradeoff exists between the power limitations imposed by the pilot signal, low-rate data signal, and high-rate data signal.

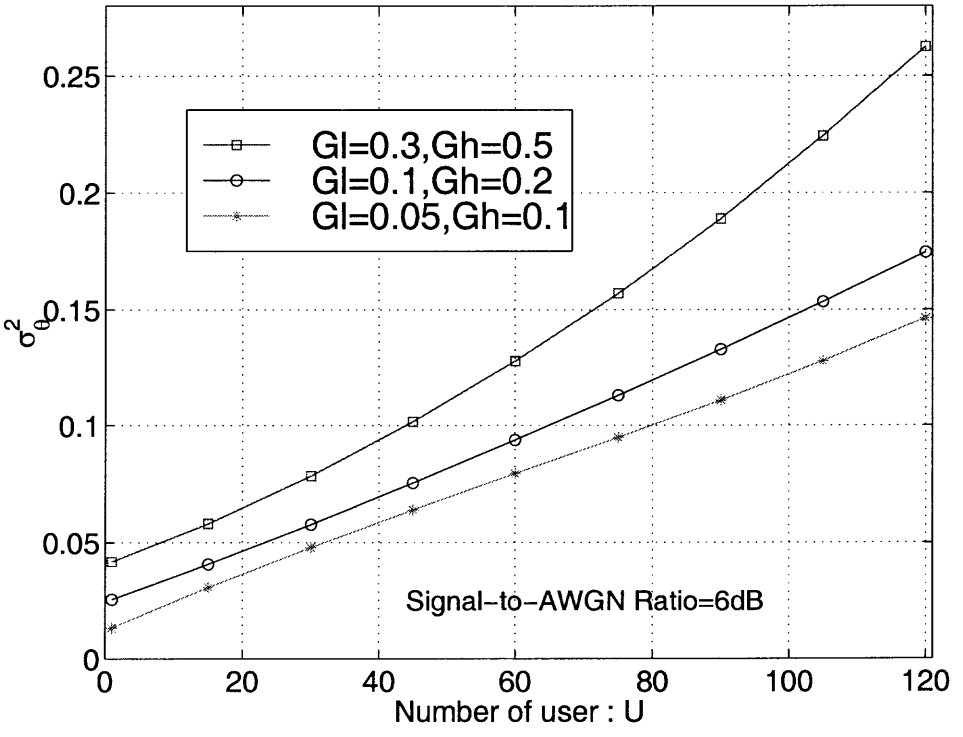

Figure 2.6 Variance of Phase Estimator Error under no fading channel

Fig.2.6 shows the variance of the phase estimator error as a function of the number of simultaneous users with the power gain of multirate signals as a parameter. Note that the variance increases with a reduction of the power gain of multirate data signals. The signal-to-AWGN ratio is fixed at 6dB. For example, when the number of users is U = 60, the variance of phase tracking error for $G_l = 0.3$ and $G_h = 0.5$ is required about 0.125 while the variance for $G_l = 0.1$ and $G_h = 0.2$ is required 0.09. This means that the larger the power of multirate signal, the larger the variance and thus the PLL can not track the phase error of the pilot signal exactly.

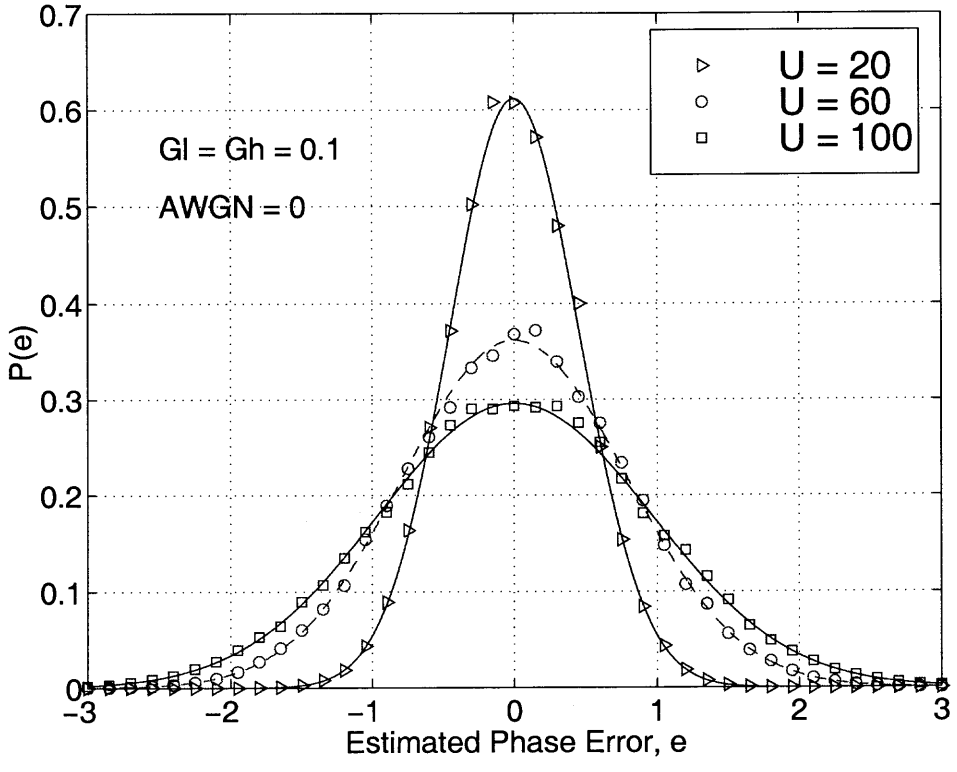

Figure 2.7 PDF of Phase Estimator Error without AWGN

Fig.2.7 shows the behavior of the phase estimator error PDF, $p(\theta)$, as a function of the number of simutaneous users U under no power controlled fading environment.

The peak height of pdf decreases as the number of users increases. For example, the peak height for 20 active users is around o.6 much higher than that for 60 active users at the fixed multirate signal powers $G_l = G_h = 0.1$. The tracking ability of PLL may be degraded quickly with the increase of the number of active users.

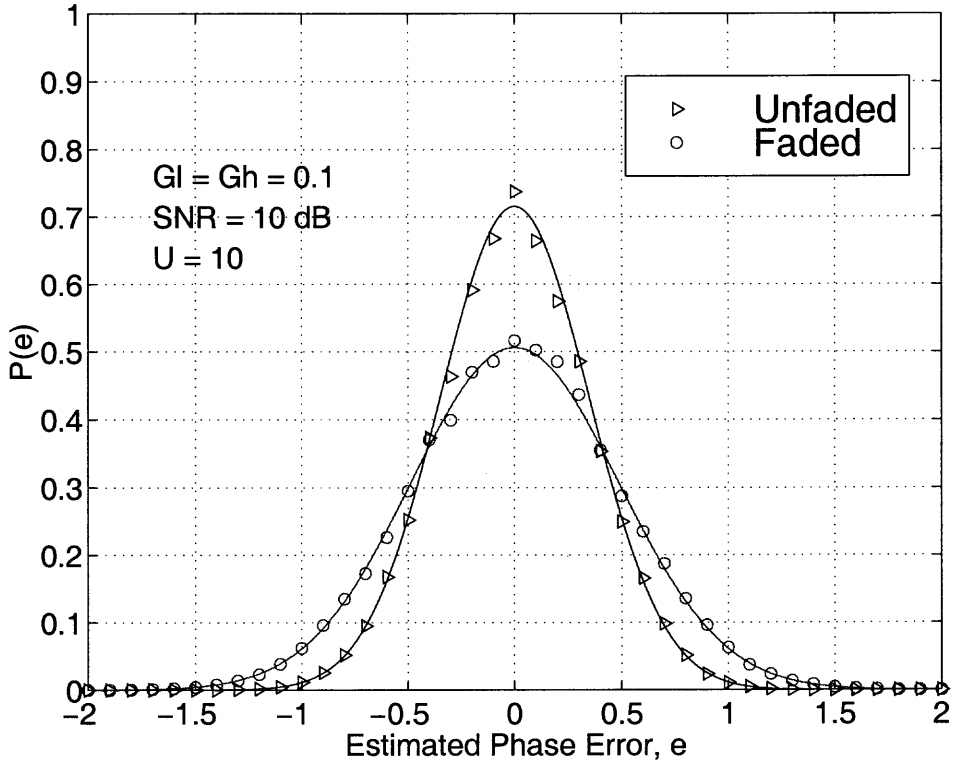

Figure 2.8 PDF of Phase Estimator Error with Comparison of Unfaded and Faded Channel Environment

Fig.2.8 shows the PDFs of phase estimator error in unfaded channel and faded channel environments. As expected, it shows that the tracking performance of the phase-locked loop in faded channel is worse than that in no fading channel for no power controlled environment.

Fig.2.9 illustrates the variance of phase estimator error as a function of number of simultaneous users and AWGN. The variance increases as the number of the users increases, but is not influenced greatly by AWGN. When the variance for 5 active

users is 0.035 at SNR 10 dB, the variance for 80 active users is 0.35 at the same SNR and for 40 active users is 0.75. The number of users effects the tracking ability of PLL since the multiple access interference increases as the number of users increases.

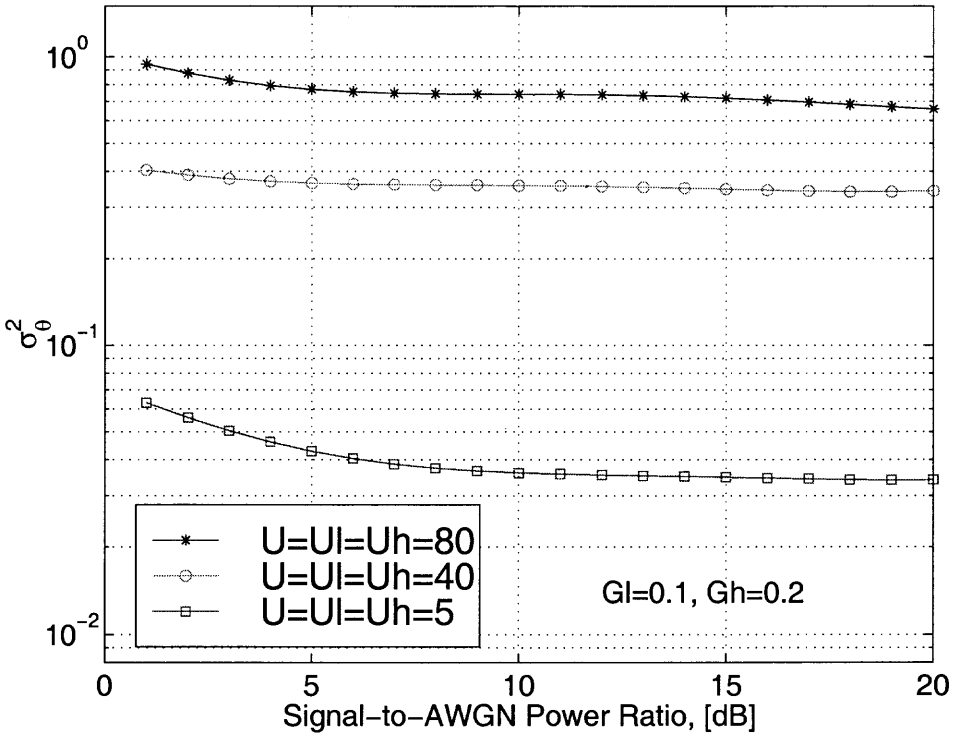

Figure 2.9 Variance of Phase Estimator Error as a function of various users

Fig.2.10 shows that the difference of the tracking performance of phase estimator error between fading and unfading channel environment increases with an increase of the number of simultaneous users. And the variance of phase estimator error decreases as signal-to-AWGN+MAI ratio(SNIR) increases with a fixed power gain of multi-rate signal.

Since the performance of Rayleigh faded received signals are degraded rapidly, adaptation of power control system can mitigate near-far effect and improve the SNIR performance. Assuming the power control of real system is imperfect, the power controlled received signal with fading channel has log-normally distributed envelope

under the variance 2-3[dB] in log scale. As see in the Fig.2.10, the variances of all the channels do not change above the SNR of 6 dB. This means that the multiple access interference and faded signal effect much more than the AWGN channel. For example, the variances for all the cases are 0.77, 0.38, 0.16, and 0.09, respectively, at the SNR 6 dB, the variances did not more decrease with the reduction of SNR.

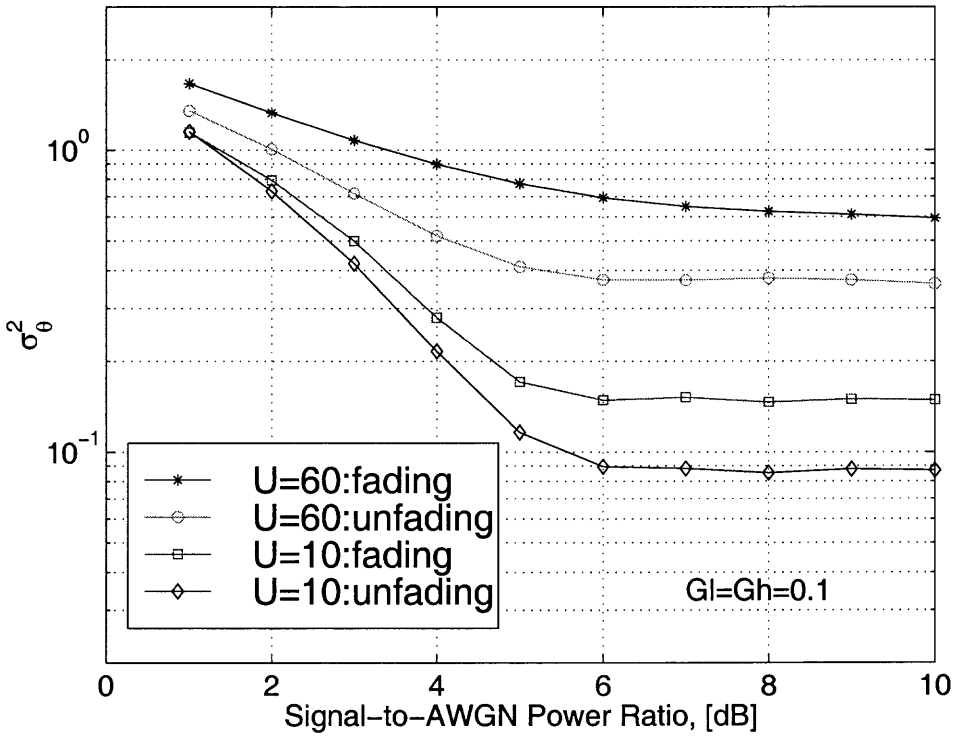

Figure 2.10 Variance of Phase Estimator Error with comparison of unfaded and faded channel environments

Fig.2.11 illustrates the behavior of the phase estimator error PDF, $p(\theta)$, as a function of the number of simultaneous users U. The performances of PDFs for Rayleigh and Log-normal faded environment cannot be compared directly. But, as seen in the simulated results, the Log-normal faded environment with variance 2-3 [dB] almost equals to Rayleigh faded environment while the received signal average powers are same. If the power of multirate data increases, the peak height of pdf will

be decreases deeply since the multirate data channels are also invoking the multiple access interference with othe user.

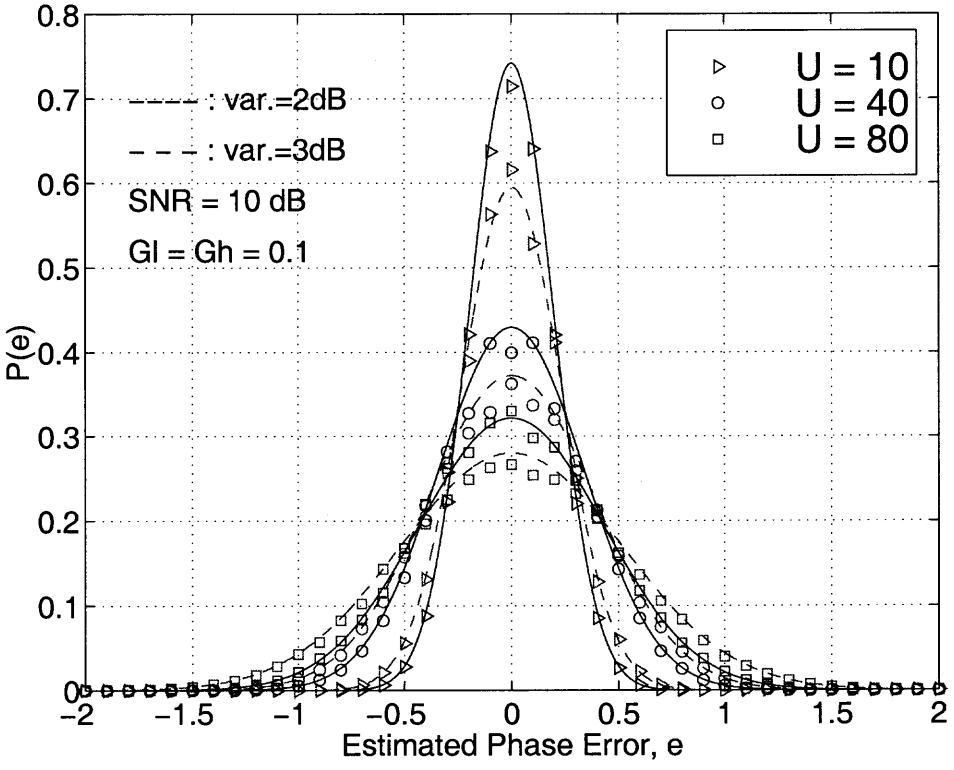

Figure 2.11 PDF of Phase Estimator Error in imperfect power control (Log-Normal fading) environment

Finally, Fig.2.12 shows the variance of phase estimator error in imperfect power controlled environment as a function of the number of simultaneous users and the variance of the imperfect power controlled received envelope. The performance of variance does not effect greatly the performance, especially, for a lot of active users. For example, when the variances for 10 active users with the variance of the fading envelopes of 2 and 3 dB at an SNR 10 dB, are 0.22 and 0.35, respectively, the variances for 40 active users with the fading envelopes 2 and 3 dB, are 0.16 and 0.17, respectively. These results are almost the same for 80 active users.

Fine synchronization is becoming increasingly important for the development of advanced receivers for wideband DS-CDMA systems in which multiuser interference cancellation is employed to overcome the reduction of system capacity due to this fundamental source of interference. In the numerical analysis, the performance was, as expected, degraded when there is a phase delay error of the received signal in wideband CDMA systems, the PLL was used to mitigate the degradation of performance of receiver in AWGN and Rayleigh fading channels, and we confirmed that the performance of receiver with PLL improved the pdf and variance of phase estimator error.

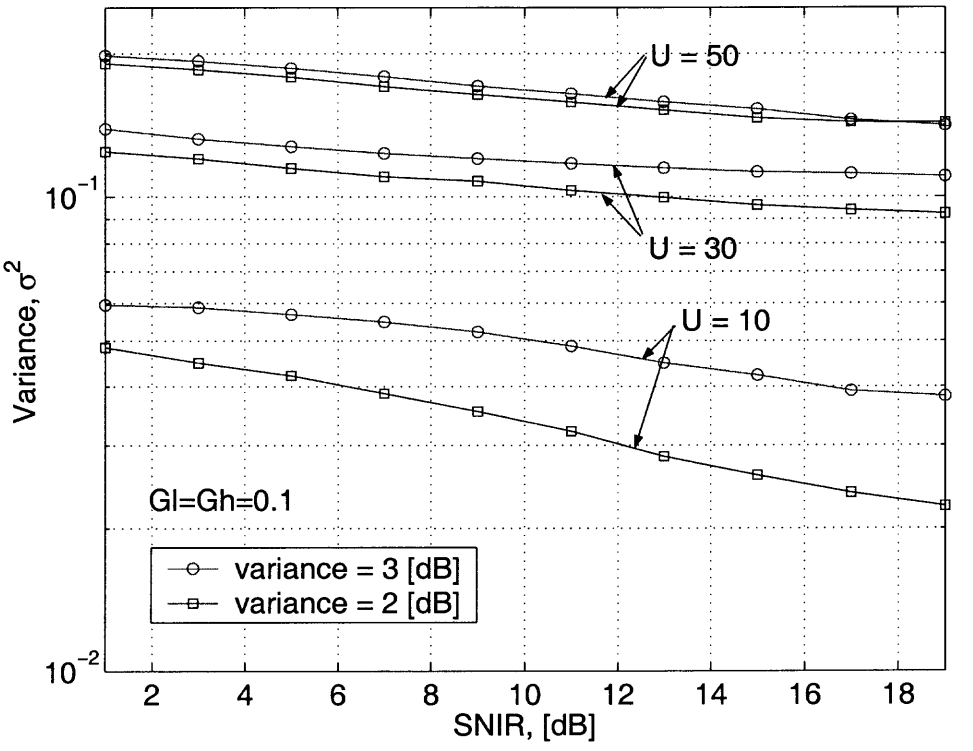

Figure 2.12 Variance of Phase Estimator Error in imperfect power control environment

CHAPTER 3

DELAY-LOCKED LOOP

3.1 Coherent Delay-Locked Loop Receiver

The coherent DLL receiver consists of the ELG for spread PN code tracking and the channel estimator for coherent tracking and several filters [5]. The block diagram of the coherent delay locked loop is shown in Fig.3.1.

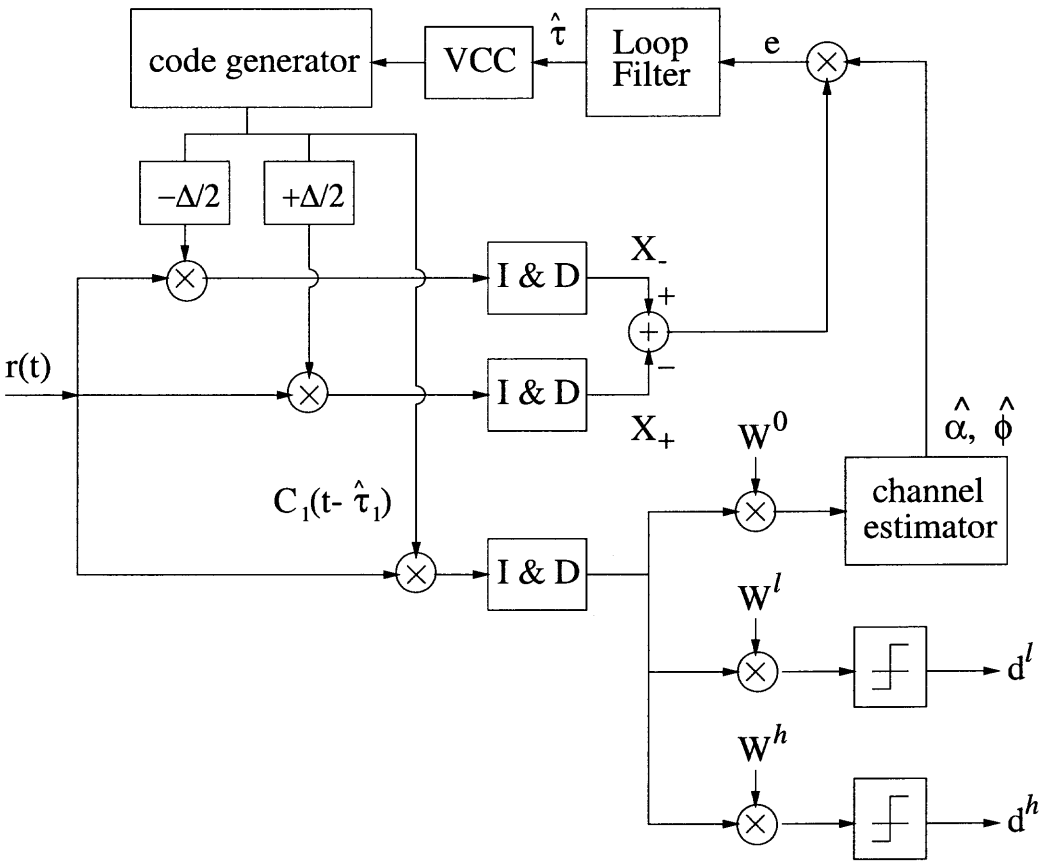

Figure 3.1 Block diagram of coherent delay locked loop

Without loss of generality, we will assume that the signal to be tracked belongs to the first user, represented as $u = 1$. Therefore the function of a baseband DLL is to track the time-varying delay of the untracked PN sequence $C_1(t - \tau_1)$ of a desired

user. Since the tracking begins after successful code acquisition, the code delay of a desired user is assumed as $-T_c/2 \leq \tau_1 \leq T_c/2$.

The incoming baseband signal r(t) to the coherent DLL in Fig.3.1, can be modelled as

$$r(t) = \sum_{u=1}^{U} \alpha_u s_u(t - \tau_u) e^{j\phi_u} + n(t) \tag{3.1}$$

where α_u is the attenuation factor due to the fading, τ_u is the overall time delay, and ϕ_u is the path phase delay of the u^{th} user received signal. Because of the asynchronous system, u^{th} user's time delays τ_u except $u = 1$ can be assumed as $0 \leq \tau_u \leq NT_c$. We now assume n(t) in (3.1) as a white Gaussian process with one sided PSD $N_0/2$.

We consider a slow Rayleigh fading channel. If the channel impulse response changes at a rate much slower than the transmitted baseband signal, the channel may be assumed to be static over one or several reciprocal bandwidth intervals. In a slow fading channel, the factor α and corresponding phase delay ϕ can be considered as zero-mean complex gaussian random variables having a variance σ^2 each so that the α is rayleigh distributed with the variance $\sigma_r^2 = (2 - \pi/2)\sigma^2$ and ϕ is uniformly distributed. Channel estimator estimates α and ϕ by using the demodulated pilot sequence.

The locally generated scrambling PN code waveform of user one is $C_1(t - \hat{\tau}_1)$, where $\hat{\tau}_1$ is the estimate of the code delay for user one. The received signal is the input to the ELG where it is correlated with an early code waveform $C_1(t - \hat{\tau}_1 + \Delta)$ and a late code waveform $C_1(t - \hat{\tau}_1 - \Delta)$. When the single-sided loop bandwidth B_L is much less than the PN code chip rate $1/T_c$, then the effect of the PN code self-noise on loop performance can be neglected [15]. The output of the Integrate-and-Dump operations, $X_\pm$ can be expressed as

$$X_\pm = \frac{1}{2} \int_0^{T_l} r(t) C_1(t - \hat{\tau}_1 \pm \Delta) dt \tag{3.2}$$

where $\pm\Delta$ denotes one half of the length (in seconds) of a PN code chip, T_c.

The error signal to the loop filter is multiplied by the estimated fading envelope $\hat{\alpha}_1$ and the estimated conjugate phase $e^{-j\hat{\phi}_1}$ in the following way:

$$\begin{aligned} e(t) &= \frac{1}{2}\hat{\alpha}_1 e^{-j\hat{\phi}_1}(X_- - X_+) \\ &= \frac{1}{2}\xi_1 D_1^P(0,\gamma_1) + N(t) \end{aligned} \tag{3.3}$$

where $D_1^P(0,\gamma_1)$ is the normalized desired output of the ELG S-curve and it is multiplied by $\xi_1 = \alpha_u\hat{\alpha}_1$ and it also distorted by the total interference $I(t)$, and we assume perfect channel estimation. Total interference $N(t)$ is

$$N(t) = I^P(t) + I^l(t) + I^h(t) + n_e(t) \tag{3.4}$$

where the interference terms are introduced in detail in (3.5)-(3.11).

The term due to the pilot channel interference is

$$I^P(t) = \frac{1}{2}\sum_{u=2}^{U} \xi_u D_u^P(0,\gamma_u) e^{j(\phi_u - \hat{\phi}_1)} \tag{3.5}$$

where U is the number of total active users and

$$D_u^P(0,\gamma_u) = \Phi_u^P(0,\gamma_u^-) - \Phi_u^P(0,\gamma_u^+) \tag{3.6}$$

with $\gamma_u^{\pm} = \tau_u - \hat{\tau}_1 \pm \Delta$ and the code cross-correlation

$$\Phi_u^P(0,\gamma_u^{\pm}) = \int_0^{T_l} C_u(t-\tau_u) C_1(t-\hat{\tau}_1 \pm \Delta)dt. \tag{3.7}$$

Next $I^l(t)$ and $I^h(t)$, terms due to the data channels, are expressed by

$$I^r(t) = \frac{1}{2}\sum_{u=1}^{U^r} \xi_u G^r D_u^r(0,\gamma_u) e^{j(\theta_u - \hat{\theta}_1)} \tag{3.8}$$

where U^r is the number of the active users of the r rate data channel in total users and

$$D_u^r(0,\gamma_u) = \Phi_u^r(0,\gamma_u^-) - \Phi_u^r(0,\gamma_u^+) \tag{3.9}$$

with the multirate code cross-correlation having the data and channelization waveforms as

$$\Phi_u^r(0,\gamma_u^{\pm}) = \int_0^{T_l} d_u(t-\tau_u)W^r(t-\tau_u)C_u(t-\tau_u)C_1(t-\hat{\tau}_1 \pm \Delta)dt \tag{3.10}$$

and last noise term from AWGN is

$$n_e(t) = \frac{1}{2}\hat{\alpha}_1 e^{-j\hat{\phi}_1}\int_0^{T_l} n(t)[C_1(t-\hat{\tau}_1-\Delta)-C_1(t-\hat{\tau}_1+\Delta)]dt. \tag{3.11}$$

From Fig.3.1, the instantaneous delay estimate $\hat{\tau}_1^l$ of the PN code generator output, VCC, is related to e(t) by

$$\hat{\tau}_1^l = K_v T_c \int_{-\infty}^{t} e(\lambda)f(t-\lambda)d\lambda \tag{3.12}$$

where $f(t)$ is the loop filter transfer function in the time domain and K_v is the gain of the voltage controlled clock in Hz/V which drives the PN code generator. From the definition $\varepsilon_u T_c = \tau_u - \hat{\tau}_1$, the normalized code tracking jitter ε_1 for the desired user satisfies $|\varepsilon_1| \leq 1$ and is expressed by

$$\varepsilon_1 = \frac{\tau_1 - \hat{\tau}_1}{T_c}. \tag{3.13}$$

By using (3.3),(3.12), equation (3.13) can be rewritten

$$\frac{d\varepsilon_1}{dt} = \frac{d}{dt}(\frac{\tau_1}{T_c}) - K_v\Big[\frac{1}{2}\xi_1 D_1^P(0,\gamma_1)+N(t)\Big] * f(t) \tag{3.14}$$

where $*$ denotes the convolution operation.

3.2 Dynamic Partial Correlation (DPC)

Next, we will evaluate the PSD in (3.14) by its autocorrelation functions. Since all noise sources are pairwise uncorrelated with respect to one another, the autocorrelation of N(t) is represented separately and its PSD is

$$S_N(f) = \int_{-T_l}^{T_l} \mathcal{R}_N(m)e^{-j2\pi fm}dm \tag{3.15}$$

with

$$\begin{aligned}\mathcal{R}_N(m) &= E\{N(t)N(t+m)\} \\ &= \mathcal{R}_{I^P}(m) + \mathcal{R}_{I^l}(m) + \mathcal{R}_{I^h}(m) + \mathcal{R}_{n_e}(m). \end{aligned} \tag{3.16}$$

We have assumed that the phase difference $\theta_u = \phi_u - \hat{\phi}_1$ is uniformly distributed on the interval $[0, 2\pi]$, τ_u is uniformly distributed on the interval $[0, NT_c]$, and α_u is Rayleigh distributed. Also, the data symbols d_u^r are asumed to take on values +1 or -1 with equal probability.

3.2.1 Case for pilot interference $\mathcal{R}_{I^P}(m)$

Because the combination of data sequence and channelization code of pilot channel is all 1's, partial correlation between desired code and the other code for the pilot channel is not needed. Therefore, $\mathcal{R}_{I^P}(m)$ does not depend on m, i.e, the shifted versions by m are same since all PN codes are periodic with T_l. Φ_u^P is a special case of (2.19) with $\alpha = 0, \beta = T_l$, and $d(t)W(t) = 1$.

Let the phase difference be $\gamma = kT_c + \delta_\gamma$. $p_u(t)$ and $q_u(t)$ taking on values of ± 1, are the same as (2.20) and (2.21) except that the definition $p_u(l) = C_1(l)C_u(N - 1 - l - k)$ and $q_u^r(l) = C_1(l)C_u(N - l - k)$.

Therefore the crosscorrelation between two pilot PN codes in a region $[0, T_l]$ is defined as

$$\begin{aligned}\Phi_u^P(m,\gamma) &= \int_m^{T_l+m} C_u(t-\gamma)C_1(t)dt \\ &= \int_0^{T_l} C_u(t-\gamma)C_1(t)dt \\ &= \int_0^{T_l} p_u(t,\gamma)dt + \int_0^{T_l} q_u(t,\gamma)dt \\ &= \sum_{l=0}^{N-1} [\delta_\gamma p_u(l) + (T_c - \delta_\gamma)q_u(l)] \\ &= a_u(\gamma). \end{aligned} \tag{3.17}$$

Thus, the autocorrelation of $I^P(t)$ is

$$\begin{aligned}\mathcal{R}_{I^P}(m) &= \frac{1}{4}E\{\xi^2\}E\{e^{2(\phi_u-\hat{\phi_1})}\}\sum_{u=2}^{U}E\{[\Phi_u^p(0,\gamma_u^-)-\Phi_u^p(0,\gamma_u^+)]^2\} \\ &= \sum_{u=2}^{U}[a_u(\gamma_u^-)-a_u(\gamma_u^+)]^2 \end{aligned} \tag{3.18}$$

where we define $E\{e^{2(\phi_u-\hat{\phi_1})}\}=1$ and $E\{\xi_u^2\}=E\{(\alpha_u\hat{\alpha_1})^2\}\approx 4$ thus, we remove $(1/4)E\{\xi_u^2\}\ E\{e^{2(\phi_u-\hat{\phi_1})}\}$ in the next cases since it is one. The PDF and properties of ξ_u will be discussed in the numerical analysis.

The PSD of $\mathcal{R}_{I^P}$ is

$$S_{R_{I^P}}(f)=\sum_{u=2}^{U}[a_u(\gamma_u^-)-a_u(\gamma_u^+)]^2S_1(0,T_l,f). \tag{3.19}$$

3.2.2 Case for low-rate $\mathcal{R}_{I^l}(m)$

From now, for simplicity, let the DPC function $M_u^r(\alpha,\beta\,\gamma)=M_u^r(\alpha,\beta)$ since γ is a common factor and we define the operation $\otimes$ as

$$A^{\pm}\otimes B^{\pm}=A^+B^+-A^+B^--A^-B^++A^-B^-. \tag{3.20}$$

Mark $\pm$ means that the denoted terms are including $\pm\Delta$. Therefore the $+$ term and the $-$ term are distinghished from each other.

The autocorrelation function of the low-rate MAI is represented by the DPC terms as

$$\mathcal{R}_{I^l}(m)=\sum_{u}^{U_l}(G^l)^2\mathcal{R}_{D_u^l}(m) \tag{3.21}$$

where

$$\begin{aligned}\mathcal{R}_{D_u^l}(m) &= E\{\Phi_u^l(0,\gamma_u^{\pm})\otimes\Phi_u^l(m,\gamma_u^{\pm})\} \\ &= \begin{cases} J_{11}^{l\pm},\otimes M_u^l(m,\gamma_u^{\pm})+J_{12}^{l\pm}\otimes M_u^l(\gamma_u^{\pm},T_l+m) & for\ \ 0\le m<\gamma_u^{\pm} \\ J_{21}^{l\pm}\otimes M_u^l(m,T_l+\gamma_u^{\pm})+J_{22}^{l\pm}\otimes M_u^l(T_l+\gamma_u^{\pm},T_l+m) & for\ \ \gamma_u^{\pm}\le m\le T_l \end{cases} \end{aligned} \tag{3.22}$$

with 4 constant terms, Js, not depending on m given by

$$\begin{cases} J_{11}^{l\pm} = M_u^l(0, \gamma_u^{\pm}), \quad J_{12}^{l\pm} = M_u^l(\gamma_u^{\pm} T_l) \\ J_{21}^{l\pm} = M_u^l(0, T_l), \quad J_{22}^{l\pm} = M_u^l(T_l + \gamma_u^{\pm}, T_l) \end{cases} \tag{3.23}$$

In (3.22), the continuous partial crosscorrelation $\Phi_u^l(m, \gamma_u^{\pm})$ derived from (3.10) and (2.19) as

$$\begin{aligned} &\Phi_u^l(m, \gamma_u^{\pm}) \\ &= \int_m^{T_l+m} d_u^l(t-\tau_u) W^l(t-\tau_u) C_u(t-\tau_u) C_1(t-\hat{\tau}_1 \pm \Delta) dt \\ &= \begin{cases} d_u^l(-1) M_u^l(m, \gamma_u^{\pm}) + d_u^l(0) M_u^l(\gamma_u^{\pm}, T_l + m) & for \;\; 0 \le m < \gamma_u^{\pm} \\ d_u^l(0) M_u^l(m, T_l + \gamma_u^{\pm}) + d_u^l(1) M_u^l(T_l + \gamma_u^{\pm}, T_l + m) & for \;\; \gamma_u^{\pm} \le m \le T_l \end{cases} \end{aligned} \tag{3.24}$$

where we assume $E\{d_u^l(p) d_u^l(q)\} = 1$ for p=q and $E\{d_u^l(p) d_u^l(q)\} = 0$, otherwise, and the subscripts, -1,0, and 1 indicate the turn of entry. As shown in (3.22) and (3.24), data bits at that time are decided by the position of m. That is, if m is less than $\gamma_u^{\pm}$, then $d_u^l(-1)$ and $d_u^l(0)$ are used and if m is greater than $\gamma_u^{\pm}$, then $d_u^l(0)$ and $d_u^l(1)$ are used. To find these two regions of m is easy for the low-rate case since one low data bit matches to one PN code with length T_l. In the case of high-rate, the regions of m are increased relative to ratio Ω.

After changing all DPC functions M_u^l in (3.22), if a Fourier transform is taken by m, the PSD of $I^l(t)$ is

$$S_{I^l}(f) = \sum_{u=1}^{U_l} (G^l)^2 S_{D^l}(f) \tag{3.25}$$

with

$$S_{D^l}(f) = \begin{cases} K_{11}^{l\pm} S_m(0, \gamma_u^{\pm}, f) + K_{12}^{l\pm} S_1(0, \gamma_u^{\pm}, f) & for \;\; 0 \le m < \gamma_u^{\pm} \\ K_{21}^{l\pm} S_m(\gamma_u^{\pm}, T_l, f) + K_{22}^l(n) S_1(\gamma_u^{\pm}, T_l, f) & for \;\; \gamma_u^{\pm} \le m < T_l \end{cases} \tag{3.26}$$

where we introduce the following constant terms for the low-rate with $n = 1, 2$ as

$$\begin{cases} K_{n1}^{l\pm} = J_{n1}^{l\pm} \otimes \mathcal{F}^l(m, \gamma_u^{\pm}) + J_{n2}^{l\pm} \otimes \mathcal{G}^l(T_l + m, \gamma_u^{\pm}) \\ K_{n2}^{l\pm} = J_{n1}^{l\pm} \otimes [\mathcal{G}^l((n-1)T_l + \gamma_u^{\pm}, \gamma_u^{\pm})((n-1)T_l + \gamma_u^{\pm}) + \mathcal{H}^l(m, (n-1)T_l + \gamma_u^{\pm}, \gamma_u^{\pm})] \\ \qquad + J_{n2}^{l\pm} \otimes [\mathcal{F}^l((n-1)T_l + \gamma_u^{\pm}, \gamma_u^{\pm})((n-1)T_l + \gamma_u^{\pm}) \\ \qquad + \mathcal{G}^l(T_l + m, \gamma_u^{\pm}) T_l + \mathcal{H}^l((n-1)T_l + \gamma_u^{\pm}, T_l + m, \gamma_u^{\pm})] \end{cases}$$

(3.27)

3.2.3 Case for high-rate $\mathcal{R}_{I^h}(m)$

The autocorrelation function of the high-rate MAI is represented as

$$\mathcal{R}_{I^h}(m) = \sum_{u}^{U_h} (G^h)^2 \mathcal{R}_{D_u^h}(m) \tag{3.28}$$

where

$$\begin{aligned}
\mathcal{R}_{D_u^h}(m) &= E\{\Phi_u^h(0,\gamma_u^{\pm}) \otimes \Phi_u^h(m,\gamma_u^{\pm})\} \\
&= \begin{cases} J_{11}^{h\pm} \otimes M_u^h(m, \gamma_u^{\pm} - aT_h) + J_{12}^{h\pm} + J_{13}^{h\pm} \otimes M_u^h(\gamma_u^{\pm} + (\Omega - a - 1)T_h, m + T_l) \\ for \;\; 0 \le m < \gamma_u^{\pm} - aT_h \end{cases} \\
&= \begin{cases} J_{21}^{h\pm} \otimes M_u^h(m, \gamma_u^{\pm} + (b-a+1)T_h) + J_{22}^{h\pm} + J_{23}^{h\pm} \otimes M_u^h(\gamma_u^{\pm} + (\Omega - a + b)T_h, m + T_l) \\ for \;\; \gamma_u^{\pm} + (b-a)T_h \le m < \gamma_u^{\pm} + (b-a+1)T_h \end{cases} \\
&= \begin{cases} J_{31}^{h\pm} \otimes M_u^h(m, \gamma_u^{\pm}(\Omega - a) + T_h) + J_{32}^{h\pm} + J_{33}^{h\pm} \otimes M_u^h(\gamma_u^{\pm} + (2\Omega - a - 1)T_h, m + T_l) \\ for \;\; \gamma_u^{\pm} + (\Omega - a - 1)T_h \le m < T_l \end{cases}
\end{aligned} \tag{3.29}$$

As is mentioned in the low-rate case, while the number of region of m for high-rate is relative to the ratio Ω, the region is decided by γ_u where $0 \le \gamma_u^{\pm} \le NT_c = T_l = \Omega T_h$. Thus, the region varies according to γ_u and 'a' in (3.29) is a indicator with $\{0, 1, \cdot\cdot, \Omega - 1\}$ that decides the region. For example, if $\gamma_u^{\pm} \le T_h$ then 'a' is zero, if $T_h < \gamma_u^{\pm} \le 2T_h$ then 'a' is one, and so forth. Additionally we need 'b' to represent middle regions except for the first and last region. It is a integer with values $\{0, 1, \cdot\cdot, \Omega - 2\}$.

In (3.29) 9 constant terms, Js, not depending on m are the following with $n = 1, 2, 3$ and $N(1) = -a$, $N(2) = b - a + 1$, $N(3) = \Omega - a$,

$$\begin{cases} J_{n1}^{h\pm} = M_u^h(0, \gamma_u^\pm + N(n)T_h) \\ J_{n2}^{h\pm} = \sum_{i=0}^{\Omega-2} M_u^h(\gamma_u^\pm + (i+N(n))T_h, \gamma_u^\pm + (i-N(n)+1)T_h) \\ \qquad \otimes \sum_{i=0}^{\Omega-2} M_u^h(\gamma_u^\pm + (i+N(n))T_h, \gamma_u^\pm + (i-N(n)+1)T_h) \\ J_{n3}^{h\pm} = M_u^h(\gamma_u^\pm + (N(n) + \Omega - 1)T_h, T_l) \end{cases} \tag{3.30}$$

where the high-rate continuous partial crosscorrelation is :

$$\begin{aligned} &\Phi_u^h(m, \gamma_u^\pm) \\ &= \int_m^{T_l+m} d_u^h(t-\tau_u) W^h(t-\tau_u) C_u(t-\tau_u) C_1(t-\hat{\tau}_1 \pm \Delta) dt \end{aligned}$$

$$= \begin{cases} d_u^h(-a-1) M_u^h(m, \gamma_u^\pm - aT_h) \\ + \sum_{i=0}^{\Omega-2} d_u^h(i-a) M_u^h(\gamma_u^\pm + (i-a)T_h, \gamma_u^\pm + (i-a+1)T_h) \\ + d_u^h(\Omega - 1 - a) M_u^h(\xi_u + (\Omega - 1 - a)T_h, m + T_l) \\ for \;\; 0 \le m < \gamma_u^\pm - aT_h \end{cases}$$

$$\begin{cases} d_u^h(b-a) M_u^h(m, \gamma_u^\pm + (b-a+1)T_h) \\ + \sum_{i=0}^{\Omega-2} d_u^h(i-a+b+1) M_u^h(\gamma_u^\pm + (i-a+b+1)T_h, \gamma_u^\pm + (i-a+b+2)T_h) \\ + d_u^h(\Omega-a-b) M_u^h(\gamma_u^\pm + (\Omega-a+b)T_h, m+T_l) \\ for \;\; \gamma_u^\pm + (b-a)T_h \le m < \gamma_u^\pm + (b-a+1)T_h \end{cases}$$

$$\begin{cases} d_u^h(\Omega - 1 - a) M_u^h(m, \gamma_u^\pm + (\Omega - a)T_h) \\ + \sum_{i=0}^{\Omega-2} d_u^h(\Omega-a+i) M_u^h(\gamma_u^\pm + (\Omega-a+i)T_h, \gamma_u^\pm + (\Omega-a+i+1)T_h) \\ + d_u^h(2\Omega-a-1) M_u^h(\gamma_u^\pm + ((2\Omega-a-1)T_h, m+T_l) \\ for \;\; \gamma_u^\pm + (\Omega - a - 1)T_h \le m < T_l \end{cases} \tag{3.31}$$

Similar to the low-rate case, the PSD of the high-rate term can be represented as

$$S_{I^h}(f) = \sum_{u=1}^{U_h} (G^h)^2 S_{D^h}(f) \tag{3.32}$$

with

$$S_{D^h}(f) = \begin{cases} K_{11}^{h\pm} S_m(0, \gamma_u^{\pm} - aT_h, f) + K_{12}^{h\pm} S_1(0, \gamma_u^{\pm} - aT_h, f)], \\ \quad for \;\; 0 \le m < \gamma_u^{\pm} - aT_h \\ K_{21}^{h}(n) S_m(\gamma_u^{\pm} + (b-a)T_h, \gamma_u^{\pm} + (b-a+1)T_h +, f) \\ +K_{22}^{h} S_1(\gamma_u^{\pm} + (b-a)T_h, \gamma_u^{\pm} + (b-a+1)T_h +, f)], \\ \quad for \;\; \gamma_u^{\pm} + (b-a)T_h \le m < \gamma_u^{\pm} + (b-a+1)T_h \\ K_{31}^{h}(n) S_m(\gamma_u^{\pm} + (\Omega - a - 1)T_h, T_l, f) + K_{32}^{h}(n) S_1(\gamma_u^{\pm}, (\Omega - a - 1)T_h, T_l, f)], \\ \quad for \;\; \gamma_u^{\pm} + (\Omega - a - 1)T_h \le m < T_l \end{cases} \tag{3.33}$$

where the constant terms are the following with $n = 1, 2, 3$ and $N(1) = -a$, $N(2) = b - a + 1$,$N(3) = \Omega - a$ which is defined in (3.30),

$$\begin{cases} K_{n1}^{h\pm} = J_{n1}^{h\pm} \otimes \mathcal{F}^h(m, \gamma_u^{\pm}) + J_{n3}^{h\pm} \otimes \mathcal{G}^h(m + T_l, \gamma_u^{\pm})) \\ K_{n2}^{h\pm} = J_{n1}^{h\pm} \otimes [\mathcal{G}^h(\gamma_u^{\pm} + N(n)T_h, \gamma_u^{\pm})(\gamma_u^{\pm} + N(n)T_h) \\ \qquad +\mathcal{H}^h(m, \gamma_u^{\pm} + N(n)T_h, \gamma_u^{\pm})] + J_{n2}^{h\pm} \\ \qquad +J_{n3}^{h\pm} \otimes [\; \mathcal{F}^h(\gamma_u^{\pm} + (N(n) + \Omega - 1)T_h, \gamma_u^{\pm})(\gamma_u^{\pm} + (N(n) + \Omega - 1)T_h) \\ \qquad +\mathcal{G}^h(m + T_l, \gamma_u^{\pm})T_l + \mathcal{H}^h(\xi_u^{\pm} + (N(n) + \Omega - 1)T_h, m + T_l, \xi_u^{\pm}) \;] \end{cases} \tag{3.34}$$

3.2.4 Case for AWGN $\mathcal{R}_{n_e}(m)$

As we assumed, since $n(t)$ is an AWGN process with zero mean and PSD $N_0/2$,the autocorrelation of AWGN is represented by

$$\mathcal{R}_{n_e}(m) = \frac{1}{4} E\{\hat{\alpha}_1^2\} \int_0^{T_l} \int_m^{T_l+m} E\{[n(t)n(t+m)]\} E\{[C_1(t+m-\tau-\Delta) - C_1(t+m-\tau+\Delta)]$$

$$
\begin{aligned}
& \times[C_1(t-\tau-\Delta) - C_1(t-\tau+\Delta)]\}d(t+m)dt \\
= & \frac{N_0}{4}\int_0^{T_l}\int_0^{T_l}[C_1(t-\tau-\Delta)-C_1(t-\tau+\Delta)][C_1(t-\tau-\Delta)-C_1(t-\tau+\Delta)]\ \delta(m)dtdt \\
= & \frac{1}{2}N_0T_l[T_l - \Phi_1^P(0,2\Delta)]\ \delta(m) \\
\approx & \frac{1}{2}N_0T_l^2\delta(m) \qquad (3.35)
\end{aligned}
$$

where $E\{\hat{\alpha}_1^2\} = E\{\beta\} = 2$ and $\Phi_1^P(0,2\Delta) = \int_0^{T_l} C_1(t-\tau-\Delta)C_1(t-\tau+\Delta)$ is ignored. Since we assumed $\Delta = T_c/2$, the phase difference between $C_1(t-\tau-\Delta)$ and $C_1(t-\tau+\Delta)$ is T_c. See (3.17). Since $\gamma = T_c$, $\delta_\gamma = 0$. Thus $\Phi_1^P(0,2\Delta) = T_c\sum_0^{N-1} q_1(l)$ with $q_1(l) = C_1(l)C_1(N+l-1)$. If the Gold code is used with length $N = 2^n - 1$, then $T_c\sum_0^{N-1} C_1(l)C_1(N+l-1)$ has three values, $\{-T_c, -T_ct(n), T_c[t(n)-2]\}$, where $t(n) = 1 + 2^{0.5(n+1)}$ for n odd, $t(n) = 1 + 2^{0.5(n+2)}$ for n even. Because three values are much less than T_l or NT_c, $\Phi_1^P(0,2\Delta)$ can be ignored in (3.35). σ_r^2 is the second moment of the α defined by two complex gaussian random variables.

Hence, it's PSD is

$$S_{R_{ne}}(f) = \frac{1}{2}N_0T_l^2. \qquad (3.36)$$

3.3 System Analysis

The solution of nonlinear stochastic differential equations such as (3.14) for the steady-state probability density function (PDF) $p(\varepsilon)$ may be accomplished via the Fokker-Planck method [4], [11], [14], [17]. To illustrate the theory, we shall consider the case of a first-order loop (i.e., F(s) = 1) and also assume $d(\tau_1)/dt = 0$ and a negligible recovered carrier phase error = 0. Notice $D_1^P(0,\gamma_1)$ in (3.3) can be represented by $D_1^P(0,T_c\varepsilon_1)$ since $\gamma_1 = \tau_1 - \hat{\tau_1} \pm \Delta = T_c\varepsilon_1 \pm \Delta$. Let $\varepsilon_1 = \varepsilon$ for simplicity. The PDF $p(\varepsilon)$ satisfies the stationary equation:

$$\frac{d}{d\varepsilon}[A(\varepsilon)p(\varepsilon)] = \frac{1}{2}\frac{d^2}{d\varepsilon^2}[B(\varepsilon)p(\varepsilon)] \qquad (3.37)$$

where $A(\varepsilon)$ and $B(\varepsilon)$ can be found from (3.14) [4].

$$A(\varepsilon) = -K_v D_1^P(0, T_c\varepsilon) \tag{3.38}$$

$$B(\varepsilon) = \frac{1}{2}K_v^2 S_N(f) \tag{3.39}$$

where $S_N(f)$ is the PSD of the total noise defined in (3.4).

The solution to (4.28) takes the well-known form [11], [17] of

$$p(\varepsilon \mid \tau_1, \cdot\cdot, \tau_u) = \Lambda \frac{exp\left[\int_0^{\varepsilon} \frac{2A(\alpha)}{B(\alpha)} d\alpha\right]}{B(\varepsilon)} \tag{3.40}$$

where the normalization constant is

$$\Lambda = \frac{1}{\int_{-\frac{3}{2}}^{\frac{3}{2}} \frac{exp\left[\int_0^{\gamma} \frac{2A(\beta)}{B(\beta)} d\beta\right]}{B(\gamma)} d\gamma} \tag{3.41}$$

Finally, the PDF and the mean-squared tracking jitter variance over the code phases $\{\tau_u\}$ can be found as

$$p(\varepsilon) = \frac{1}{(T_l)^{U-1}} \int_0^{T_l} \cdot\cdot \int_0^{T_l} p(\varepsilon \mid \tau_1, \cdot\cdot, \tau_u) d\tau_1, \cdots, d\tau_u \tag{3.42}$$

$$\sigma_\varepsilon^2 = E^2\{\varepsilon\} = \int_{-\frac{3}{2}}^{\frac{3}{2}} \varepsilon^2 p(\varepsilon) d\varepsilon \tag{3.43}$$

3.4 Numerical Analysis

We now evaluate in detail the PDF of the steady-state tracking jitter of the delay-locked loop in a Multirate Multiple Access Interference(MMAI) environment. The transmitter has three distinct channels that can be seperated by channelization codes. Since the high rate data is set to be 4 times faster than the low one, W^l is both 4 times longer than W^h and orthogonal to the set $\{W^h\}$. Each transmitter for an individual user (or cell site) is spread by Gold codes with length 128.

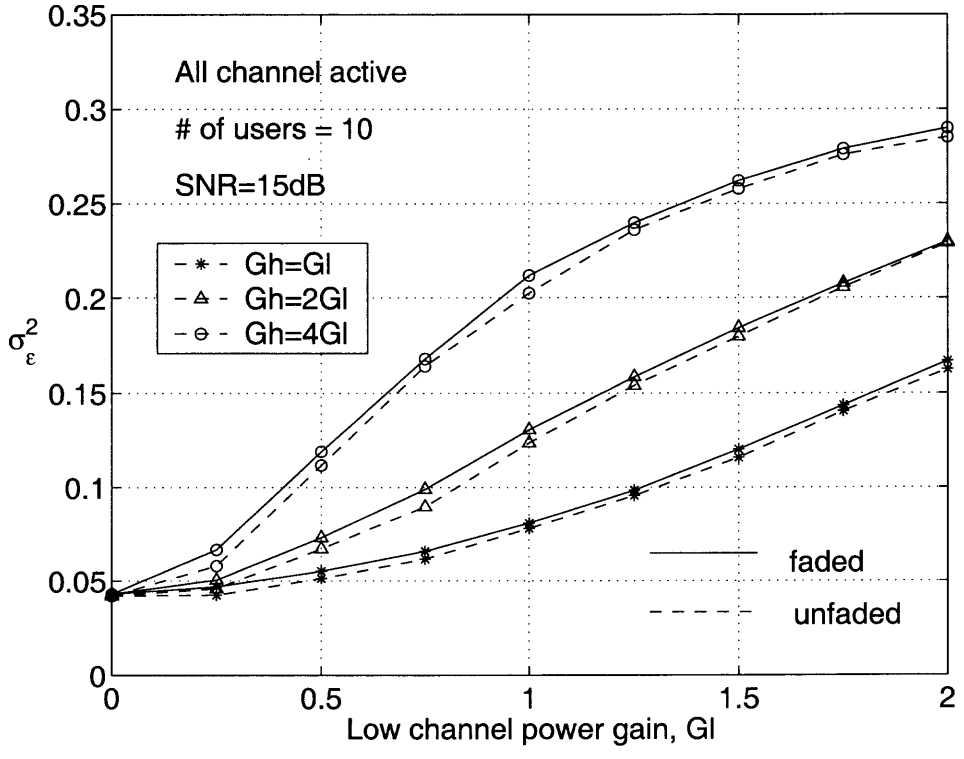

Figure 3.2 The variance of the tracking jitter as a function of the power gain.

Figure 3.2 shows the variance of the tracking jitter as a function of power gain of the data channels. Power gain of the pilot channel is set to 1 and all other power gains are normalized to it. Though the DLL tracks the PN code, actually it is the pilot channel that is tracked since the pilot channel does not have any signal except the PN waveform. Therefore, the two data channels affect the DLL performance

as interference. The variance of the tracking error for faded channel is higher than that for unfaded channel. This means that the error tracking ability of DLL for faded channel is degraded in contrast to that for the unfaded channel. The variance difference bewteen the faded and the unfaded channel is very close since the power gain of the data channel is much higher than that of pilot and thus the unfaded channel has the effect of much more active users.

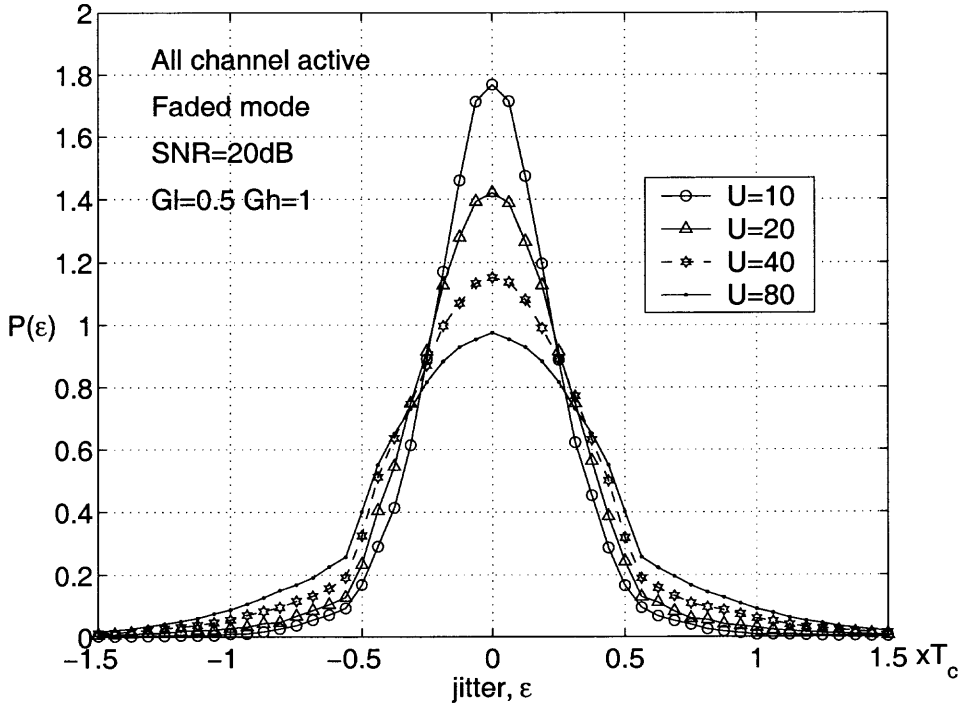

Figure 3.3 PDF of the tracking jitter when both data channels are active with pilot.

Seeing Figure 3.2 again, when the two data channels are not active i.e., $G_l = 0$ and $G_h = 0$, the variance is about 0.045. If we set G_l and G_h to 0.5 and 1 respectively, the amount of variance is increased about 0.025. It means that two data channels cause the performance to be decreased by 1.8dB. Thus, the choice of the power gains is important since a tradeoff exists between the noise effect of the data channel and power efficiency. Since the high-rate signal should be transmitted with a larger

power than the low-rate signal to maintain their performance generally in a practical system, we used a G_h that is two times G_l. The calculated PDF of the code phase jitter given by (3.42) is now compared for different situation.

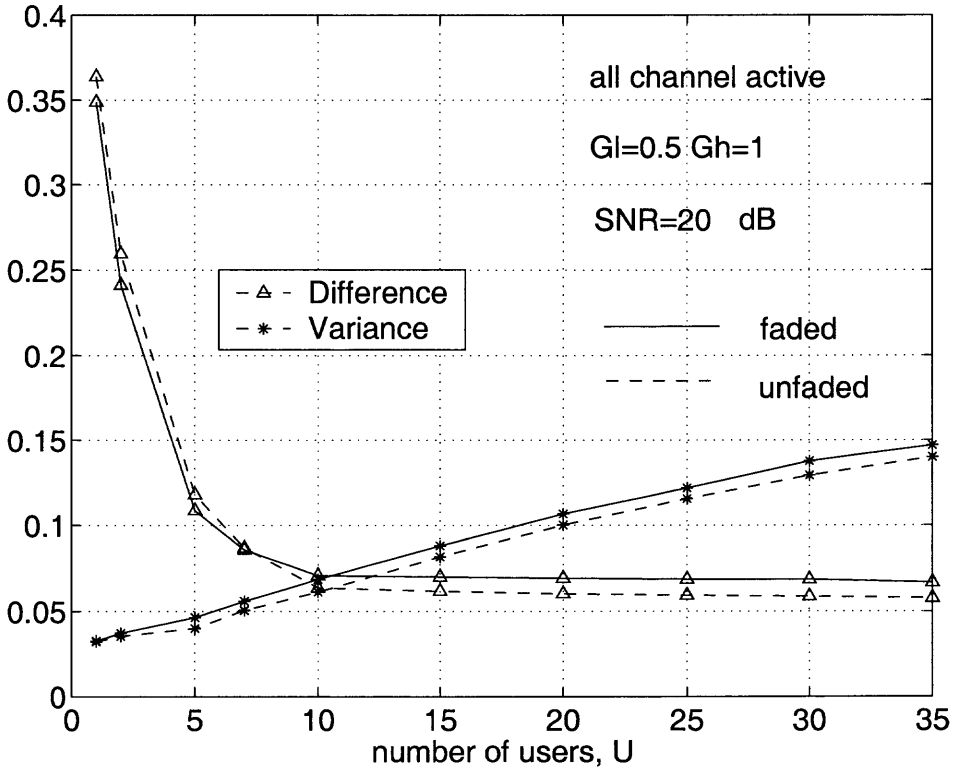

Figure 3.4 The difference between the PDFs of the tracking jitter and Gaussian

Figure 3.3 shows the PDFs for different number of users when all data channels are active. The peak height of the PDF is decreased exponentially as the number of active channels increases. It means that the capacity of a channel decreases rapidly and thus the performances between 40 and 80 channels are closer than 10 and 20 channels. The shape of the PDF looks Gaussian but is not. The absolute sum of the difference between PDFs of the tracking jitter and gaussian is shown with the variance in Figure 3.4. The difference decreases rapidly but it does not go to zero since we assumed the code phase delay was limited in T_c and the jitters happen either

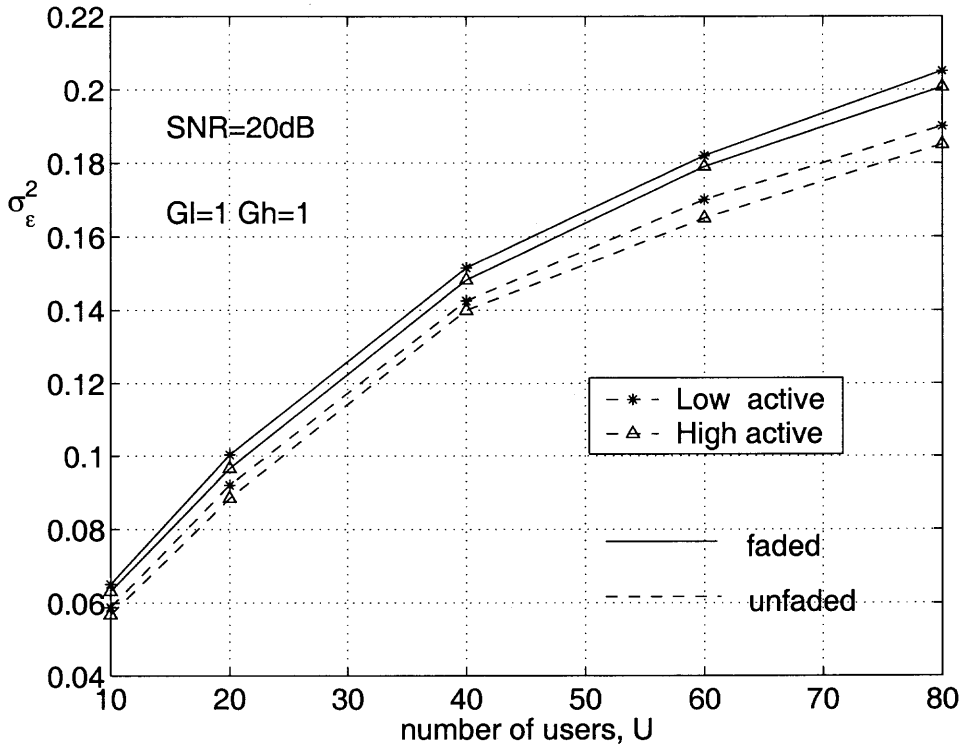

Figure 3.5 The variance comparison of the low and high rate interferences with same power gain

very rarely or not outside of $3T_c/2$. Consquently, the variance of tracking error of DLL increases as the number of users increases and thus, the channel capacity is decreased and the performance of demodulation is degraded.

Next we fixed power gains to 1 and we varied the number of active channels. Two cases are compared : when the high data channel is not active and when the low data channel is not active, we seek to determine which data channel effects the performance as a worse interference. Figure 3.5 shows the worse interference is a low data channel. The reason can be found in the channelization code since the two data channels use the same scrambling code. While the channelization code is short and

periodic for the high rate, the one for the low rate is long as much as NT_c. Thus, it makes the scrambling PN code to more distorted.

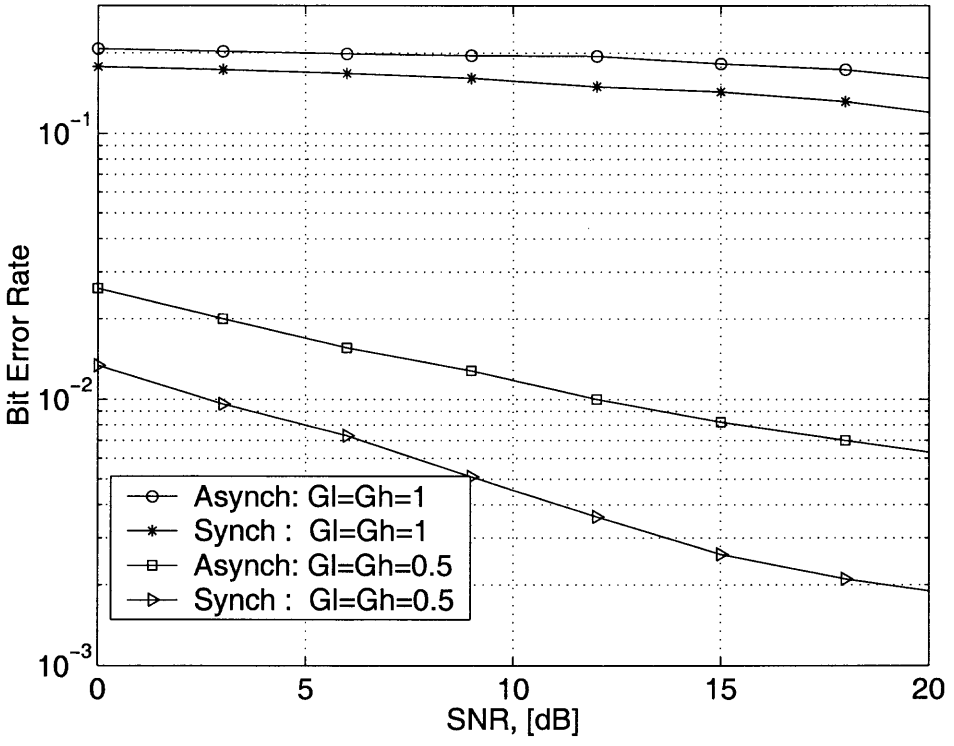

Figure 3.6 Bit error probability for chip synchronization in AWGN channel as a function of SNR

Figure 3.6 shows the bit error probability for chip synchronization in AWGN channel as a function of the SNR. As explained for Figure 3.2, when we demodulate only the desired user's pilot signal, the other users' pilot signals and corresponding multirate data signals interfere with the desired user's pilot signal. Therefore, the total of interfering users (or signals) is 3(U-1). For example, if the interfering users are 10, then the total interfering channels are 30. When the bit error probability is 10^{-2} for Gl=Gh=0.5, the required SNR is 3 and 12 dB, but it is much larger than that for Gl=Gh=1 in synchronous and asynchronous chip, respectively. This means that the more channels of multirate data signal for each user, the worse the channel

capacity, and thus the demodulation performance will be degraded quickly with the increase of the data channel.

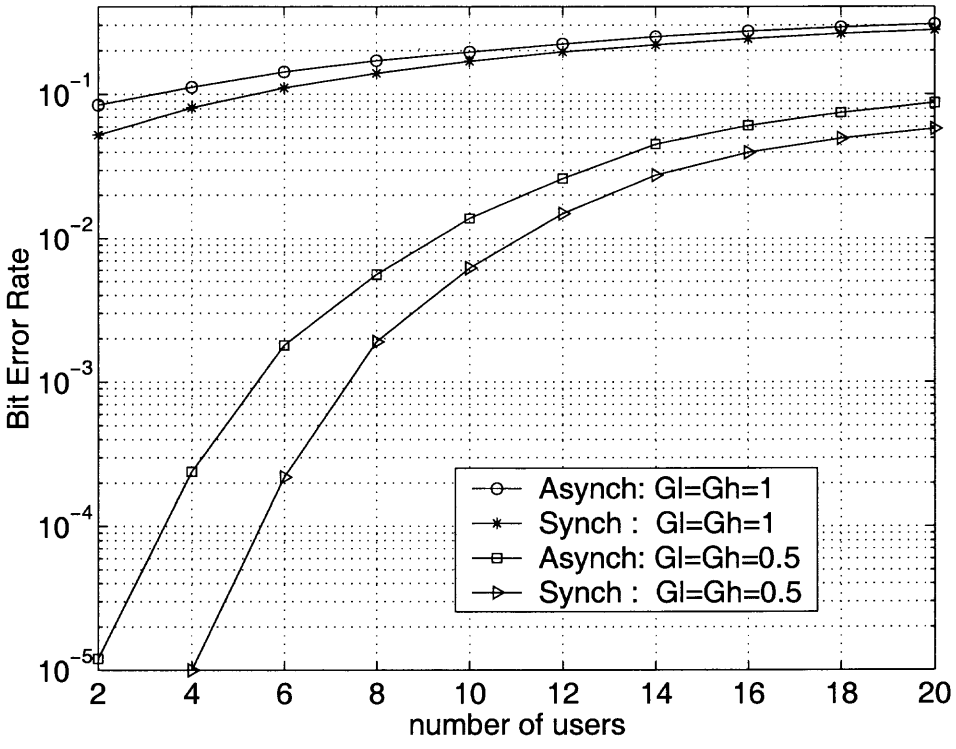

Figure 3.7 Bit error probability for chip synchronization in AWGN channel as a function of the number of users

Figure 3.7 shows the bit error probability for chip synchronization in AWGN channel as a function of the number of users. The bit error probability is degraded when the DLL does not track the code delay error exactly. For example, when the bit error probability is 10^{-2} for asynchronous case with Gl=Gh=0.5, the required number of users is 9 (or 27 interfering channels) more than 11 (or 33 interfering channels) that for synchronous case. This means that the chip delay jitter effects greatly the performance of receiver.

Figures 3.8 and 3.9 show the bit error probabilities for chip synchronization in Rayleigh fading channel as a function of the Average SNR per bit and the number

of users, respectively. The bit error probability decreases quickly when the power of data channel is small, but the probability decreases slowly when the power of data channel is big since the multiple access interference increases much more for the bigger power of data channel as seen in Figure 3.9.

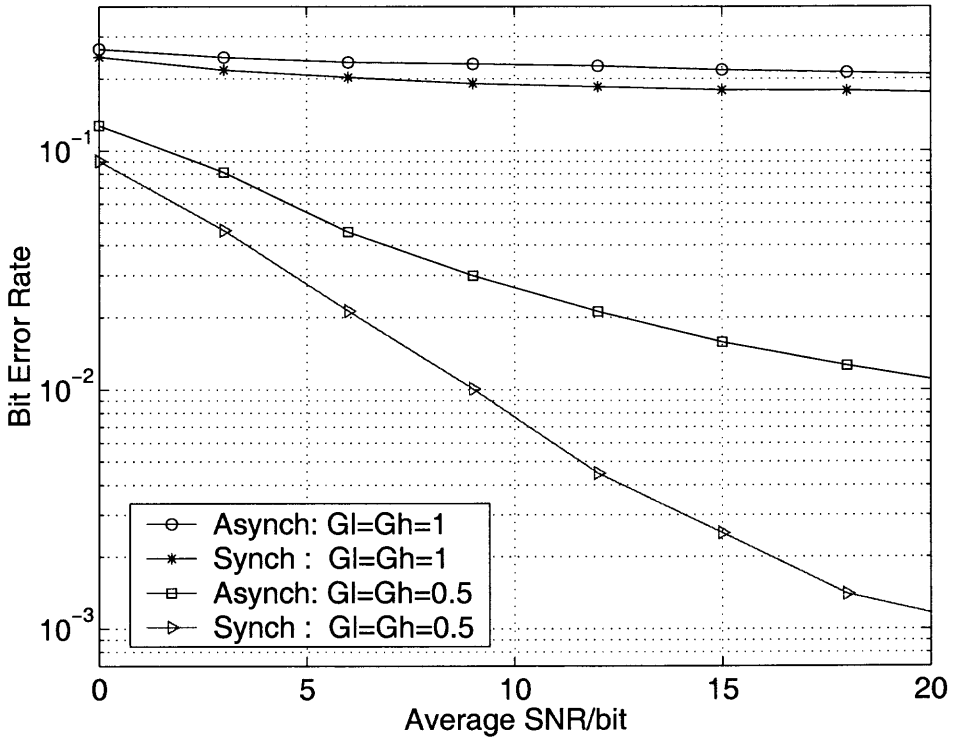

Figure 3.8 Bit error probability for chip synchronization in Rayleigh fading channel as a function of the Average SNR per bit

This chapter has focused on code tracking performance of coherent DLL in an asynchronous multirate CDMA environment with MMAI over additive white gaussian noise and Rayleigh fading channels. We proposed the DPC method to analyze the autocorrelation and PSD of the time function having MMAI crosscorrelation. The PDF of the code tracking jitter and its variance were derived in a first order loop and several results showed the effect of MMAI under various conditions. The bit error probability of the code tracking jitter shown through a comparison of

code synchronous case and asynchronous case as the functions of the average SNR per bit and the number of users over AWGN and Rayleigh fading channel.

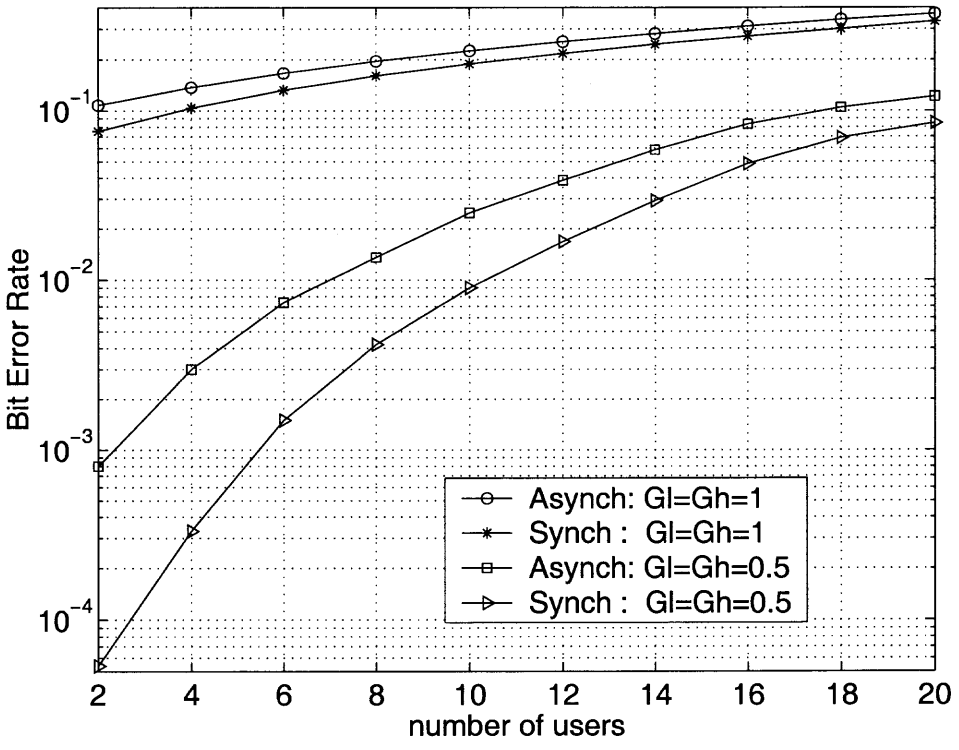

Figure 3.9 Bit error probability for chip synchronization in Rayleigh fading channel as a function of the number of users

CHAPTER 4

ONE-SHOT LINEAR DECORRELATING DETECTOR

We propose Hybrid Selection Diversity/Maximal Ratio Combining (Hybrid SD/MRC) one-shot window linear decorrelating detector (LDD) for asynchronous DS-CDMA systems. The selection diversity scheme at the input of the Hybrid SD/MRC LDD is based on choosing the branch with the maximum signal-to-noise ratio (SNR) of all filter outputs. The MR Combining scheme at the output of the Hybrid SD/MRC LDD adopts to maximize the output SNR and thus compensates for the enhanced output noise. The Hybrid SD/MRC one-shot LDD with PLL is introduced to track its phase error and to improve the demodulation performance. The probability density functions of the maximum SNR of the SD combiner , the near-far resistance (NFR) of one-shot LDD by Gaussian approximation, and the maximum SNR of the MR combiner for Hybrid SD/MRC LDD are evaluated, and the bit error probability is obtained from these pdfs. The performance of Hybrid SD/MRC one-shot LDD is assessed in a Rayleigh fading channel.

4.1 Introduction

Multiuser detection is used to improve performance by canceling the intra-cell interference and thus increasing the system capacity. The actual capacity increase depends on the efficiency of the algorithm, radio environment, and the system load. In addition to capacity improvement, multiuser detection alleviates the near-far problem typical to DS-CDMA mobile systems.

The idea of multiuser detection was first mentioned in 1979 by Schneider [35]. In 1983, Kohno et al. published a study on multiple access interference cancellation receivers [36]. In 1984, Verdu proposed and analyzed the optimal multiuser detector and the maximum likelihood sequence detector, which, unfortunately, is too

complex for practical implementation since its complexity grows exponentially as a function of the number of users [37]. Consequently, Verdu's work inspired a number of researchers to find suboptimal multiuser detectors, which could achieve a close to optimal performance with reasonable implementation complexity.

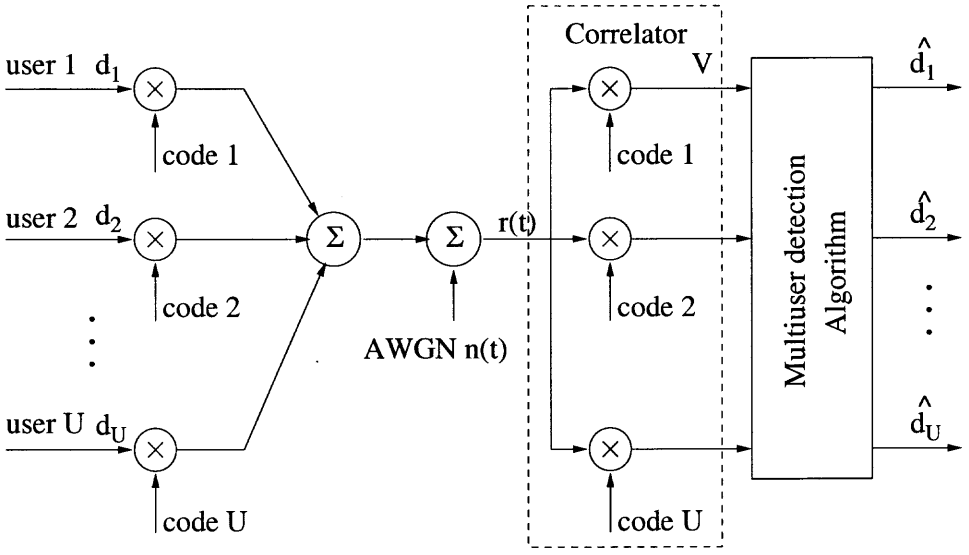

Figure 4.1 System model of multiuser detection

Fig.4.1 depicts a system for multiuser detection. Each user is transmitting data bits, which are spread by the spreading codes. The signals are transmitted over an additive white gaussian noise (AWGN) channel. In the receiver, the received signal is correlated with replicas of the user spreading codes. The correlator consists of a multiplier. A matched filter can also be used. Multiuser detection processes the signals from the correlators jointly to remove the unwanted multiple access interference from the desired signal. The output of a multiuser detection block are the estimated data bits.

A CDMA channel with U users sharing the same bandwidth is shown in Fig.4.1. The signaling interval of each user is T seconds, and the input alphabet is antipodal binary +1,-1. The objective is to detect those polarities, which contain the trans-

mitted information. During the n^{th} signaling interval, the input vector is $\mathbf{d}(n) = [d_1(n), d_2(n), \cdots, d_U(n)]^T$, where $d_u(n)$ is the input symbol of the u^{th} user. User u (u = 1,2, $\cdots$, U) is assigned a signature waveform (or code, or spreading chip sequence) $c_u(t)$ which is zero outside [0, T] and is normalized

$$\int_0^T c_u^2(t)dt = 1. \tag{4.1}$$

The baseband signal of the u^{th} user is

$$s_u(t) = \sum_{n=0}^{\infty} d_u(n)\alpha_u(n)c_u(t - nT - \tau_u), \tag{4.2}$$

where τ_u is the transmission delay, and $\alpha_u(n)$ is the channel attenuation. According to (4.2), each user's signal travels along a single path, so this model does not illustrate multipath propagation. For synchronous CDMA, the delay $\tau_u = 0$ for all users. For asynchronous CDMA, the delays can be different. The channel attenuation is

$$\alpha_u(n) = \sqrt{P_u(n)}\cos\phi_u(n) \tag{4.3}$$

where $\sqrt{P_u(n)}$ and $\phi_u(n)$ are the received power and phase of the u^{th} user, respectively. The received signal at baseband is the noisy sum of all the users' signals :

$$r(t) = \sum_{u=1}^{U} s_u(t) + n(t) \tag{4.4}$$

where n(t) is additive white gaussian noise (AWGN). The first step in the detection process is to pass the received signal r(t) through a matched filter bank (or a set of correlators). It consists of U filters matched to individual signature waveforms followed by samplers at instances nT + τ_u, n = 1,2, $\cdots$. The outputs of the matched filter bank form a set of sufficient statistics about the input sequence $d(n)$ given r(t). Thus, we will consider the equivalent discrete time channel model which arises at

the output of the matched filter bank. The output vector $\mathbf{v} = [v_1, v_2, \cdots, v_U]^T$ can be expressed as

$$\mathbf{v} = \mathbf{R}\boldsymbol{\alpha}\mathbf{d} + \mathbf{n}, \tag{4.5}$$

where $\mathbf{R}$ is cross-correlation matrix and α are U×U diagonal matrices, and $\mathbf{n}$ is a colored Gaussian noise vector. The components of the matrix $\mathbf{R}$ are given by cross-correlation between signature waveforms

$$\rho_{u,j} = \int_0^T c_u(t)c_j(t)dt \tag{4.6}$$

and $\alpha = [P_1 \cos\theta_1, P_2 \cos\theta_2, \cdots, P_U \cos\theta_U]$ is the attenuation vector of the received signal.

For example, in a two-user system, the matrix

$$\mathbf{R} = \begin{pmatrix} 1 & \rho_{1,2} \\ \rho_{2,1} & 1 \end{pmatrix} \tag{4.7}$$

where ρ is the cross-correlation between the signature waveforms of the users in Eq.(4.6).

Inspection of Eq.(4.5) immediately suggests a method to solve for $\mathbf{d}$, whose components d_u contain the bit information sought. If $\mathbf{n}$ was identically zero, we have a linear system of equations, $\mathbf{v} = \mathbf{RPd}$, the solution of which can be obtained by inverting $\mathbf{R}$. With a non-zero noise vector $\mathbf{n}$, the result is

$$\mathbf{y} = \mathbf{R}^{-1}\mathbf{v} = \boldsymbol{\alpha}\mathbf{d} + \mathbf{n_y} \tag{4.8}$$

where it is seen that the information vector $\mathbf{d}$ is recovered but contaminated by a new noise term. From Eq.(4.8), the signal of the u^{th} user is

$$y_u = \alpha_u d_u + n_{yu}. \tag{4.9}$$

The decision is $d_u = sgn(y_u)$.

Note that the decorrelating detector completely eliminates MAI. However, the power of the noise n_{yu} is $N_0(\mathbf{R}^{-1})_u$ which is greater than the noise power N_0 at the output of the matched filter. For an example, in Eq.(4.7), the noise power at the output of the decorrelating detector is $N_0/(1 - \rho_{1,2}\rho_{2,1})$ and is larger than 1 since $\rho_{1,2}\rho_{2,1}$ is always smaller than 1. Fig.4.2 shows an example of AWGN power increment of conventional LDD output. The value of the inverse matrix of user 1 increases as the number of users increases for a fixed signal-to-AWGN ratio of 10 dB.

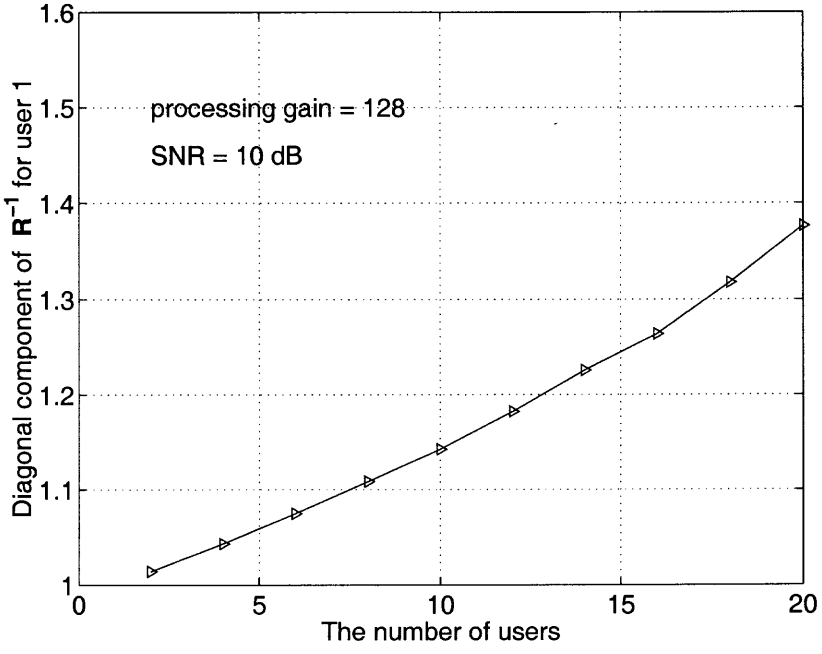

Figure 4.2 An example of noise power increment of LDD output

Despite this drawback, the decorrelating detector generally provides significant improvements over the conventional detector. A more significant disadvantage of the decorrelating detector is that the computations needed to invert the matrix $\mathbf{R}$ are difficult to perform in real time. For a synchronous system, the problem is somewhat simplified : we can decorrelate one bit at a time. In other words, we can apply the

inverse of a U×U correlation matrix. For an asynchronous system, however, **R** is of order NU, which is quite large for a typical message length N.

4.2 Hybrid SD/MRC One-shot LDD

As one of the main multiple-access techniques, code-division multiple access (CDMA) has been intensively investigated over the late decade. It has been found that the main obstacle to delivering CDMA's attractive promise in spectral efficiency is the near-far (NF) effect, especially in the direct sequence spread spectrum multiple access (DS/SSMA) systems [14], [38]. The NF effect exists when a weak received signal is interfered with by one or more strong signal such that the effective cross-correlations among the signals degrade the performance of the conventional CDMA receiver.

Multiuser detection is one of solutions to combat this problem. The interest in the problem of multiuser detection was motivated by the work of *Verdú* where he investigated the optimum maximum-likelihood multiuser receiver [30]. *Verdú*'s receiver is near-far resistant, but its complexity is exponential in the number of active users. Recently much attention has been given to suboptimal detectors. *Lupas* and *Verdú*'s proposed linear decorrelating detector has attracted wide attention [38]. Since the decorrelator is a sequence detector, the detection process cannot be started until the whole transmitted sequence is received at the receiver. In practice this is not feasible and would result in a very long delay. Therefore, several finite delay decorrelator schemes have been proposed. One of these schemes is the one-shot detection scheme [29]. Suboptimum decorrelating detectors, which are based on linear transformation of the sampled matched filter outputs, were considered in [38] for the synchronous channel. For the asynchronous case, *Verdú* proposed to use a one-shot linear decorrelating detector, in which 1+2(U-1) = 2U-1, (U is the number of users) filters are matched to the spreading code with one bit duration of a specific user [39].

Wireless communication systems are subject to severe multipath fading that can seriously degrade their performance. Thus, fading compensation is typically required to mitigate the effect of multipath. Diversity combining scheme, which combines multiple replicas of the received signal, is a classical and powerful technique to combat multipath impairment. Two of many diversity combining schemes : the maximum SNR selection combining and maximum ratio combining schemes have attracted wide attention for compensating the Rayleigh faded envelope of received signals [47],[48].

The maximum SNR selection diversity and maximal ratio combining schemes have been analyzed for the last fifty years. The probability density function (pdf) and symbol error probalibity of maximum-selection diversity reception schemes over a Rayleigh fading channel was obtained in [45],[46],[48]. The maximum SNR at the output of matched filter of the selection diversity combiner is random, and its pdf was already well evaluated by many researchers [44],[48]. The pdf and symbol error probalibity for conventional linear decorrelating detector was analyzed with Gaussian approximation in [51].

The power control problem in uplink of DS-CDMA systems arises because of the multiple access interference. Due to the propagation mechanism, the signal received by the base station from a user terminal close to the base station will be stronger than the signal received from another terminal located at the cell boundary. Hence, the distant users will be dominated by the close user. This is called the near-far effect. One solution to combat this near-far problem is multiuser detection where the receiver exploits the knowledge of the sprea spectrum signals of the interfering users to eliminate the near-far effect. The interest in the problem of multiuser detection was motivated by the work of Verdu [30]. Verdu proposed the asynchronous LDD with a packetized signal model [54], one of suboptimal detectors to combat the near-far problem.

In the asynchronous LDD, however, the detection should be delayed, at least, to the end of the packet. Of course, the shorter the packet is, the smaller the detection delay. However, the shorter packet means low channel efficiency since there should be a no-signal period between each packet transmission. Without this no-signal period, the asynchronous LDD proposed in [38] might be disturbed and all the interference can not be decorrelated.

Another asynchronous LDD scheme has also been proposed by Verdu [54], named as truncated window decorrelator or one-shot window decorrelator. Fig.4.3 (a) shows the bit period of the desired user and the truncated window for the decorrelator. There are three independent signal within the window for 2 users case :

$$c_{2L}(t) = \begin{cases} d_2(-1)c_2(t-\tau_2+T) & 0 < \tau_2 \\ 0 & otherwise \end{cases} \tag{4.10}$$

and

$$c_{2R}(t) = \begin{cases} 0 & 0 < \tau_2 \\ d_2(0)c_2(t-\tau_2) & otherwise. \end{cases} \tag{4.11}$$

In Fig.4.3 Verdu's one-shot window decorrelator has the size : $[2(U-1)+1]\times[2(U-1)+1]$. Verdu's decorrelator is to demodulate only the symbol of desired user while the number of the decorrelator's matrix operation is $(2U-1)^3$. To demodulate another user's symbol at the same time period, the matrix operation must be repeated with the same complexity as that in the previous. Thus, to detect simultaneously U-multiuser's symbols in one-shot window, the total number of the matrix operation is $U\times\ (2U-1)^3$.

On the other hands, In (b) of Fig.4.3, Hybrid SD/MRC one-shot LDD is to demodulate U-symbols of U-multiusers in one-shot window simultaneously while the decorrelator matrix size is 2U×2U. Thus, our decorrelator needs only one matrix operation and each user needs two pieces at the input of the decorrelator for asynchronous CDMA systems. The total number of the matrix operation with

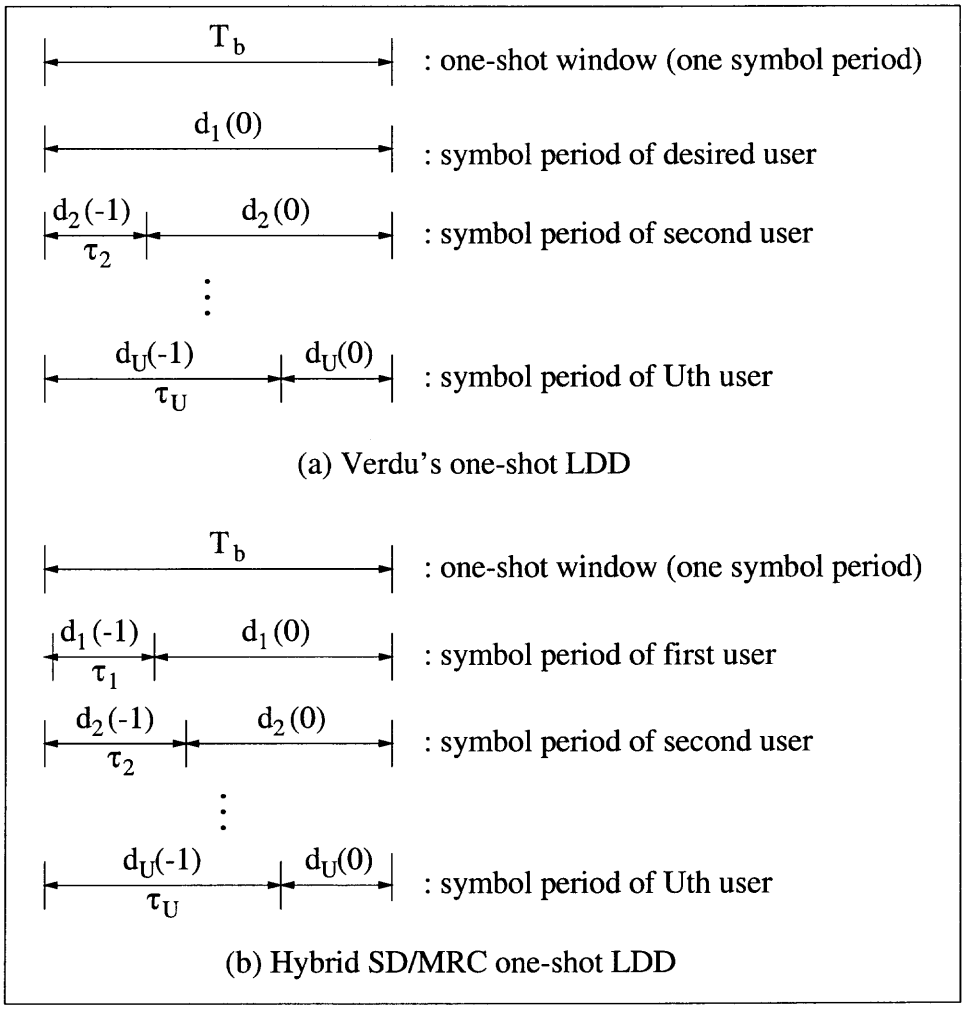

Figure 4.3 The comparison of Verdu's LDD and Hybrid SD/MRC LDD in asynchronous CDMA systems

post-decorrelation MR combining is $(2U)^3$ for combining of the left piece of the present window and the right piece of the next window.

In this paper, we consider the NFR which Verdu defined as the multiuser asymptotic efficiency [54] [29] [33] , and the compensation of the deep faded signal in multiple access communications over a Rayleigh fading channel, and thus present the Hybrid SD/MRC one-shot LDD which consists of the maximum SNR selection diversity scheme at the input of one-shot LDD and the maximal ratio combining scheme at the output of the LDD. The maximum SNR of the SD combiner output, each diagonal component of $\mathbf{R^{-1}}$ of LDD, and the maximum SNR of MR combiner are random variables, and thus each pdf of the random variables has been found by many researchers [47],[48],[50]. However, they did not treat the pdfs for the asynchronous one-shot LDD. Thus, we evaluated the joint pdf of the random variables, the BER, and assessed the performance of the LDD with the analytical and simulated results for the asynchronous one-shot LDD.

Fine synchronization of carrier phase error is also becoming increasingly important for the development of advanced receivers of DS-CDMA systems in which the NFR exists to overcome the reduction of system capacity. Thus, we adopt the conventional phase-locked loop (PLL) to track the carrier phase error, derive the steady-state pdf of the phase estimator error, and analyze the performance of the PLL in the Hybrid SD/MRC LDD. By applying a single-user phase synchronization scheme, phase locked loop (PLL), at each output of the LDD, it is shown that the Hybrid SD/MRC one-shot LDD can be used for the coherent detection of asynchronous CDMA without the preknowledge of user phase.

4.2.1 System Description

Consider an asynchronous CDMA system. Defining a rectangular pulse by $h_{T_\alpha}(t) = 1$ for $0 < t \leq T_\alpha$ and $h_{T_\alpha}(t) = 0$, otherwise, the spreading code waveform $c(t)$ and the

information wavefom d(t) can be expressed as

$$c(t) = \sum_{i=1}^{M} c(i) h_{T_c}(t - iT_c) \tag{4.12}$$

and

$$d(t) = \sum_{j=1}^{N} d(j) h_{T_b}(t - jT_b) \tag{4.13}$$

where consecutive signature and data bits $\{c(i)\}$ and $\{d(i)\}$ take on values of ± 1 with equal probabilities, and T_c and T_b are the chip duration of the spreading code and the data duration of the information, respectively.

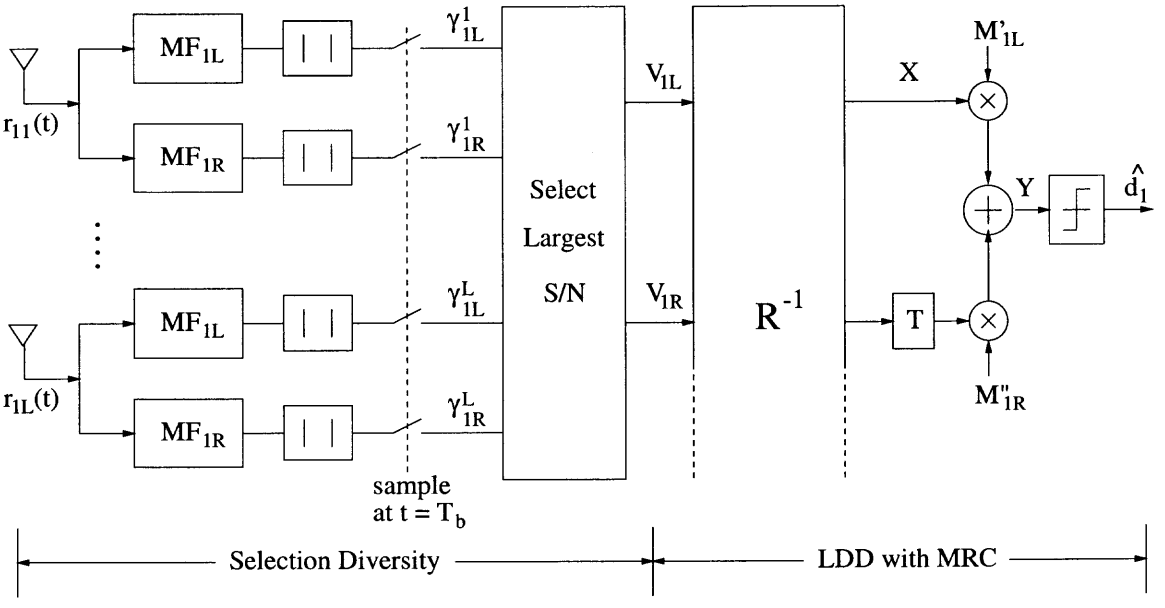

Figure 4.4 Hybrid SD/MRC one-shot LDD for first user

Consider there are L diversity channels, carrying the same information-bearing signal. Each channel is assumed to be slowly fading with Rayleigh distributed envelope statistics. The fading processes among the L diversity channels are assumed to be mutually statistically independent. The signal in each channel is corrupted by an additive zero-mean white gaussian noise. Thus, the equivalent low-pass received signals for the lth diversity channel of uth user can be expressed as

$$r_{ul}(t) = \sum_{n} \sqrt{2P_{ul}} d_u(n) c_u(t - nT_b - \tau_{ul}) \cos(\omega_c t + \phi_{ul}), \quad u = 1, 2, \cdots, U \quad (4.14)$$

where

- U : the number of total active users
- $d_u(n)$: the n^{th} data bit of the u^{th} user
- P_u : the received power of u^{th} user
- τ_u : the delay offset in each information bit
- ω_c : the carrier frequency
- ϕ_u : the initial carrier phase of u^{th} user
- $n(t)$: the AWGN with one side PSD N_0

and the u^{th} user's spreading code waveform $c_u(t) = c_{uL}(t) + c_{uR}(t)$ which satisfies :

$$c_{uL}(t) = \begin{cases} \frac{1}{\sqrt{E_{uL}}} c_u(t + T_b - \tau_u), & 0 < t \leq \tau_u \\ 0, & \text{otherwise} \end{cases} \quad (4.15)$$

and

$$c_{uR}(t) = \begin{cases} \frac{1}{\sqrt{E_{uR}}} c_u(t - \tau_u), & \tau_u < t \leq T_b \\ 0, & \text{otherwise.} \end{cases} \quad (4.16)$$

where $E_{uL} = \int_0^{\tau_u} c_u^2(t + T_b - \tau_u)dt$ and $E_{uR} = \int_{\tau_u}^{T} c_u^2(t - \tau_u)dt$, and L and R denote the left and right versions of the spreading waceform in one-shot window as shown in Fig.4.5, respectively.

Diversity reception schemes are used to reduce the effects of fading. The basic idea of a diversity reception is that if two or more independent samples of a signal are taken, then these samples will fade in an uncorrelated manner. This means that the probability of all the samples being simultaneously below a given level is much less

than the probability of any individual sample being below that level. The selection diversity combiner in Fig.4.4 is the simplest of all the diversity schemes. An ideal selection combiner chooses the signal with the highest instantaneous SNR, so the output SNR is equal to that of the best incoming signal.

In Fig.4.4, each user at the input of the SD combiner has two matched filters for correlating of the corresponding code. One filter is matched to the left part of its code in one-shot window, corresponding to the interval [0, τ_u] and other one is matched to the right part of the code, corresponding to the interval $[\tau_u, T_b]$. The SD combiner with each L diversity reception for each user has two outputs (v_{uL} and v_{uR}), each with maximum SNR.

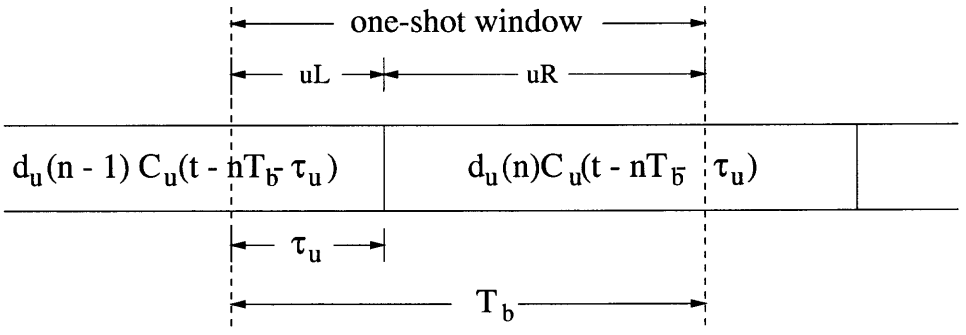

Figure 4.5 One-shot window for asynchronous CDMA

The idea of a one-shot LDD is to transform the detection of asynchronous CDMA into the detection of synchronous CDMA. Consider the one-shot window as shown in Fig.4.5. Here we take a one-shot window approach where in order to demodulate every bit we discard all information outside its interval. Defining $d_u(-1) = 0$, the received signal for uth user from Eq.(4.14) is rewritten as

$$\begin{aligned} r(t) &= \sum_{n=0}^{N} \sqrt{2P_{ul}(n)}\big[d_u(n-1)c_{uL}(t-nT_b) + d_u(n)c_{uR}(t-nT_b)\big] \\ &\quad \times \cos(\omega_c t + \phi_{ul}) + n(t). \end{aligned} \tag{4.17}$$

Assuming knowledge of the code delay waveform $\hat{c}_u(t - nT_b)$ and carrier delay phase $\hat{\phi}_u$ from the channel estimator, the SD combiner output can be expressed as

$$v_{ui}(n) = \int_{nT_b}^{(n+1)T_b} r(t)\hat{c}_{ui}(t - nT_b)\sqrt{2}\cos(\omega_c t + \hat{\phi}_u)dt, \quad i = L, R. \tag{4.18}$$

The output of the bank of matched filters in matrix notation is given by

$$\mathbf{v}(n) = \mathbf{RP}(n)\mathbf{d}(n) + \mathbf{n}(n) \tag{4.19}$$

where $\mathbf{P}(n) = diag[P_1(n), P_2(n), \cdots, P_u(n)]$, $\mathbf{d}(n) = [d_{1L}(n), d_{1R}(n), \cdots, d_{UL}(n), d_{UR}(n)]$ is a U-user's data vector, $\mathbf{n}(n) = [n_{1L}(n),\ n_{1R}(n),\ ...,\ n_{UL}(n),\ n_{UR}(n)]$ is a AWGN vector with $n_{ui}(n) = \int_{nT_b}^{(n+1)T_b} n(t)\hat{c}_{ui}(t)\sqrt{2}\cos(\omega_c t + \hat{\phi}_u)dt$, and letting $\rho_{uivj} = 2\int_0^{T_b} c_{ui}(t)\cos(\omega_c t + \phi_u) \cdot c_{vj}(t)\cos(\omega_c t + \phi_v)dt$, i,j = L, R, and u,v = 1,2,$\cdots$,U, the correlation matrix $\mathbf{R}$ with the relative phase delay θ_u (= ϕ_u - ϕ_v) between users can be expressed as

$$\mathbf{R} = \begin{bmatrix} \rho_{1L1L} & \rho_{1R1L} & \rho_{1L2L} & \cdots & \rho_{1LUR} \\ \rho_{1L1R} & \rho_{1R1R} & \rho_{1R2L} & \cdots & \rho_{1RUR} \\ \rho_{2L1L} & \rho_{2L1R} & \rho_{2L2L} & \cdots & \rho_{2LUR} \\ \vdots & \vdots & \vdots & \ddots & \vdots \\ \rho_{UR1L} & \rho_{UR1R} & \rho_{UR2L} & \cdots & \rho_{URUR} \end{bmatrix}_{:2UX2U} \tag{4.20}$$

The linear decorrelating detector output gives

$$\begin{aligned} \mathbf{x}(n) &= \mathbf{R}^{-1}\mathbf{v}(n) \\ &= \mathbf{P}(n)\mathbf{d}(n) + \mathbf{R}^{-1}\mathbf{n}_{\mathbf{x}}(n) \end{aligned} \tag{4.21}$$

where the decorrelating detector applies the inverse of the correlation matrix, $\mathbf{R}^{-1}$, to the conventional detector output in order to decouple the data.

Selection diversity is easy to implement, but it is not an optimal diversity scheme because it does not use all of the possible branches simultaneously. Maximal Ratio combining uses each of the LDD output pieces in a co-phased and weighted manner such that the highest achievable SNR is available at the receiver at all times

[48]. In Fig.4.4, the output of the LDD for first user has just two branches with each other's data bit.

The MR combining scheme weights each branch output proportional to the SNR for each branch to maximize the output SNR of the combiner. And, of course this combining is not for the multipath fading but for the compensation of the different noise enhancement by the inverse matrix decorrelating. Therefore, assuming perfect fine synchronization of the carrier phase error, the soft estimate of LDD with MR Combining scheme, $y_u(n)$, can be found by the sum of LDD output x_u as follows:

$$\begin{aligned} y_u(n) &= x_{uL}(n)M'_{uL} + x_{uR}(n-1)M''_{uR} \\ &= \sqrt{P_u}\sqrt{E_{uL}}d_u(n)M'_{uL} + \sqrt{P_u}\sqrt{E_{uR}}d_u(n)M''_{uR} + n_{xuL}(n)M'_{uL} + n_{xuR}(n)M''_{uR} \end{aligned} \tag{4.22}$$

where M'_{uL} and M''_{uR} are weighting coefficients to be determined to minimize the output SNR at $y_u(n)$ and the signs $'$ and $''$ denote the present matrix output and next matrix output of the LDD, respectively. Note that after decorrelation, there are only signal and enhanced background noise due to removing of interferences. The input SNR (signal-to-background noise ratio) at v_{1L} and v_{1R} are exactly the same. However, the output SNR at x_{1L} and x_{1R} are different from each other since each output branch for the desired user (user 1) experiences different noise enhancement by the inverse matrix filtering. The output SNR at each branch is enhanced by a factor of λ_{1L} and λ_{1R}, respectively, where $\lambda_{1L} = (\mathbf{R}^{-1})_{1L,1L}$ and $\lambda_{1R} = (\mathbf{R}^{-1})_{1R,1R}$. Since the input SNR is exactly the same, the factors λ_{1L} and λ_{1R} are proportional to the output SNR of each branch. And, thus, we can use these to post-decorrelation MR combining weights, i.e.,

$$M'_{uL} = \frac{\sqrt{E_{uL}}}{\lambda_{uL}}, \quad \text{and} \quad M''_{uR} = \frac{\sqrt{E_{uR}}}{\lambda_{uR}}. \tag{4.23}$$

Then, Eq.(4.22) can be rewritten as

$$y_u(n) = \sqrt{P_u}\left(\frac{E_{uL}}{\lambda_{uL}} + \frac{E_{uR}}{\lambda_{uR}}\right) \cdot d_u(n) + n_{yuL}(n) + n_{yuR}(n). \tag{4.24}$$

Thus, we see that the decorrelating detector completely eliminates the multiple access interference (MAI) and the Maximum Ratio Combining scheme does maximize the output SNR.

4.2.2 Carrier Phase Error Tracking by PLL

Tracking synchronization is becoming increasingly important for the development of advanced receivers for wideband DS-CDMA systems in which multiuser interference cancellation is employed to overcome the reduction of system capacity due to this fundamental source of interference. Carrier phase synchronization of wireless communication system is an already well-developed technique after the considerable research efforts provided in the past [12].

Fig.4.6 shows a block diagram of the LDD with a PLL to track the phase delay error θ_u. Assuming the phase delay error at all the diversity branches of the same user is the same, the information data recovered by the demodulator multiplies the soft estimate output of Eq.(4.22) to remove the data information component

$$\begin{aligned} \Psi(\theta_u) &= y_u \hat{d}_u(n-1) \\ &= \sqrt{P_u}\cos\theta_u + N(n) \end{aligned} \tag{4.25}$$

where $N(n) = n_{uR}(n-1) + n_{uL}(n)$.

The phase error estimate in Eq.(4.25) is fed into a loop filter F(S), followed by a VCC, K_p/S, where K_p is the overall closed-loop gain. The VCC is used to adjust the carrier phase. F(S) is the transfer function of the loop filter where F(S) = 1 for a first-order PLL, and K_p/S is the transfer function of the VCC. The instantaneous phase estimate $\hat{\phi}_u$ for the local oscillator is then related to the phase discriminator output $\Psi(\theta_u)$ as

$$\hat{\phi_u} = \frac{K_p F(S)}{S} \Psi(\theta_u) \tag{4.26}$$

where S is the Heaviside operator S = d/dt. Therefore the change rate of the phase estimator error can be expressed by

$$\frac{d\theta_u}{dt} = \frac{d\phi_u}{dt} - K_p \left[\sqrt{P_u} d_u(n) \hat{d}_u(n) \sin\theta_u + N(t) \right] * f(t) \tag{4.27}$$

where $d\phi_u/dt$ is the rate of change of the u^{th} user's initial phase, f(t) is the transfer function of the loop filter in the time domain, N(t) = $n_{yu'}(n)$ + $n_{yu''}(n)$, and * denotes the convolution operation.

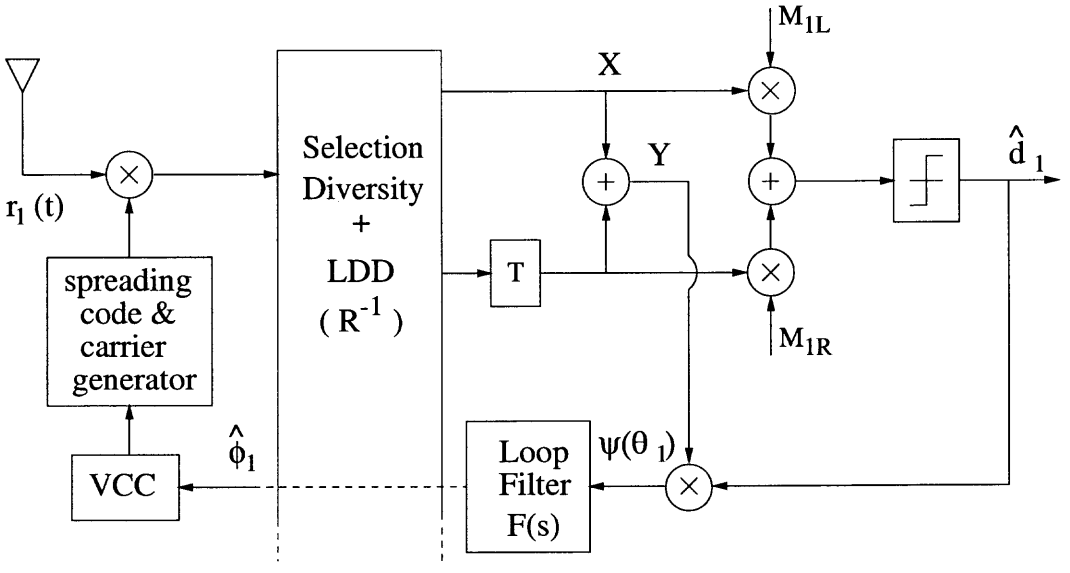

Figure 4.6 Hybrid SD/MRC One-shot LDD with PLL for first user

The solution of a nonlinear stochastic differential equation such as (4.27) for the steady-state probability density function (PDF), $p(\theta)$, may be accomplished via the Fokker-Planck method [4], [11], [14], [17]. From here on, we will use $\theta = \theta_u$ for convenience and simplicity. To illustrate the theory, we shall consider the case of

a first-order loop (i.e., F(s) = 1) and also assume $d(\phi_1)/dt = 0$. The PDF, $p(\theta)$, satisfies the stationary equation :

$$\frac{d}{d\theta}[A(\theta)p(\theta)] = \frac{1}{2}\frac{d^2}{d\theta^2}[B(\theta)p(\theta)] \tag{4.28}$$

where

$$A(\theta) = -K_p T_b \sqrt{P_u} d_u(n)\hat{d}_u(n)\sin\theta \tag{4.29}$$

$$B(\theta) = \frac{1}{2}K_p^2 S_N \tag{4.30}$$

with the power spectrum density of the noise term, S_N.

From (4.28), using the well-known method [1],[4], [22] we get the PDF of the phase estimator error as

$$p(\theta) = \frac{exp(\nu\cos\theta)}{2\pi I_0(\nu)} \tag{4.31}$$

where $I_0(\cdot)$ is the modified Bessel function of 0th-order. For ν, it can be shown by using the aymptotic formula $I_0(\nu) \approx exp(\nu)/\sqrt{2\pi\nu}$ that $p(\theta)$ tends to a Gaussian density function with zero mean and variance $\sigma^2_{\hat{\phi}}$. Parameter ν represents the loop signal-to-noise ratio(SNR).

4.2.3 Bit Error Probability

4.2.3.1 pdf of Maximum SNR of SD Combiner The bit error probability will be obtained in a traditional way with the branch of the diversity reception, l = 1,2,$\cdots$,L, by averaging the results for a slow Rayleigh fading channel over the distribution of the maximal instantaneous SNR. The pdf of the maximal instantaneous SNR over L independent identically distributed (*iid*) diversity paths is well known [47]. In practice, the system cannot perform on an instantaneous basis; so, to be successful, it is essential that the internal time constants of a selection diversity are substantially shorter than the reciprocal of the signal fading rate.

Consider L independent Rayleigh fading channels available at a receiver. We assume that the instantaneous amplitude received by each diversity branch is statistically independent of other branches but has equal average signal power $\overline{\alpha_l^2}$. The probability density function of the signal envelope, on branch l, is given by

$$f_{\alpha_l}(\alpha_l) = \frac{\alpha_l}{\overline{\alpha_l^2}} exp\Big(- \frac{\alpha_l^2}{2\overline{\alpha_l^2}}\Big). \tag{4.32}$$

Letting $\gamma_l = \alpha_l^2/2N_{0l}$ and $\gamma_0 = \overline{\alpha_l^2}/N_{0l}$ with the noise power in lth branch, N_{0l}, the probability density function for γ_l is given by

$$f_{\gamma_l}(\gamma_l) = \frac{1}{\gamma_0} exp\Big(- \frac{\gamma_l}{\gamma_0}\Big). \tag{4.33}$$

The probability that all L independent diversity branches receive signals which are simultaneously less than some specific SNR threshold γ is

$$Pr[\gamma_1, \cdots, \gamma_L \leq \gamma] = \int_0^{\gamma_{SD}} f_{\gamma_l}(\gamma_l) d\gamma_l = \Big(1 - exp\Big(- \frac{\gamma}{\gamma_0}\Big)\Big)^L \tag{4.34}$$

Therefore, the probability that at least one branch will exceed the threshold SNR value of γ is given by

$$Pr[\gamma_l > \gamma] = 1 - \Big(1 - exp\Big(- \frac{\gamma}{\gamma_0}\Big)\Big)^L. \tag{4.35}$$

To determine the average SNR of the received signal when diversity is used, it is first necessary to find the pdf of the fading signal. For selection diversity, the average SNR is found by differentiating Eq.(4.34). Therefore, letting γ_{SD} be the maximum SNR, its pdf $f_{\gamma_{SD}}(\gamma_{SD})$ is

$$f_{\gamma_{SD}}(\gamma_{SD}) = L\Big(1 - exp\Big(- \frac{\gamma_{SD}}{\gamma_0}\Big)\Big)^{L-1} \cdot \frac{1}{\gamma_0} exp\Big(- \frac{\gamma_{SD}}{\gamma_0}\Big), \quad \gamma_{SD} \geq 0. \tag{4.36}$$

4.2.3.2 pdf of NFR of One-shot LDD We found the pdf of the output SNR of the selection combiner at the input of the linear decorrelating detector. To obtain the bit error probability of the receiver, it is necessary to evaluate the pdf of NFR of the linear decorrelaing detector.

In the cross-correlation matrix of Eq.(4.20), each element except the diagonal element of the matrix is a cross-correlated term due to multiple access interference. *Lehnert* and *Pursley* introduced the Gaussian approximation to analyze the performance of the conventional detector for time varying CDMA signal [49] and *Yoon* and *Hong* used it for discrete time random signature sequences [50]. We will use the Gaussian aproximation to analyze the statistical characteristics for the off-diagonal components in the inverse matrix of $\mathbf{R}$.

Consider the detection of first user and the delay of the uth user with respect to the first user, $\tau_u = D_u + \delta_u$ for $D_u = 0,1,2,\cdots,(N-1)T_c$ and $0 \leq \delta_u < 1$. The pdf of ρ_{1LuL} and ρ_{1RuR} conditioned on D_u and δ_u can be expressed as

$$\rho_{1\Omega u\Omega}(D_u, \delta_u)\ \mathcal{N}(0, \sigma^2_{1\Omega u\Omega}(D_u, \delta_u)), \quad \Omega = L, R \tag{4.37}$$

where the variances are given by

$$\sigma^2_{1LuL}(D_u, \delta_u) = \frac{(D_u+1)(1-\delta_u)^2 + D_u\delta_u^2}{2N^2} \tag{4.38}$$

$$\sigma^2_{1RuR}(D_u, \delta_u) = \frac{(N-(D_u+1))(1-\delta_u)^2 + (N-D_u)\delta_u^2}{2N^2} \tag{4.39}$$

and, N is the processing gain (PG) and random variable $\rho_{1LuL} + \rho_{1RuR}$ has an unconditional distribution $\mathcal{N}(0, \mathrm{N}/3)$ [51].

Considering the diagonal element of $\mathbf{R^{-1}}$ corresponding to the left or right version of uth user in one-shot LDD, $\mathbf{R^{-1}_{u\Omega}}$, for Ω = L, R, in random CDMA system, the diagonal elements are random. Using the well-known method [52], [53], the

probability that the mth bit of uth user with the left or right version of one-shot window is misdetected is given by

$$P_u(m) = Q\Big(\frac{\sqrt{E_{u\Omega}(m)}}{\sigma_n \cdot \sqrt{(\mathbf{R}^{-1})_{mu\Omega}}}\Big) \tag{4.40}$$

where Q($\cdot$) is the Q-function : $Q(a) = 1/2\pi \int_a^\infty e^{t^2/2}dt$, uth diagonal element of $\mathbf{R^{-1}}$ and $W = 1/\sqrt{(\mathbf{R^{-1}})_{mu\Omega}}$ is the near-far resistance of LDD.

The NFR W is a random variable in a random-CDMA and thus we will evaluate the pdf of the NFR to get the bit error probability of LDD. The pdf of the off-diagonal element of asynchronous linear decorrelating detector for random CDMA has been analyzed by approximation in [51] but is covered briefly here for clarity. Their approach was based on the random signature sequences for one packet, set all the off-diagonal components in the cross-correlation matrix to zero except for one row and one column corresponding to the cross-correlation of the desired user's signature waveform with those of all other interfering users and showed the validity of the following approximation :

$$W^2 \approx 1 - \sum_{j=1,j\neq u}^{U} [\rho_{jLuL}^2 + \rho_{jRuR}^2] = 1 - \sum_{j=1,j\neq u}^{U} \Phi_j = 1 - \Phi \tag{4.41}$$

where the processing gain is assumed to be large enough such that $\Phi < 1$.

The approximation in Eq.(4.41) can be used in the one-shot LDD for random signature sequences since each cross-correlation term for one packet is the same as that for one bit. Therefore, we can get the approximate pdf of the near-far resistance for asynchronous LDD as [51]

$$f_W(w) = 2w \cdot f_\Phi(1 - w^2) \tag{4.42}$$

where

$$f_\Phi(\phi) = \chi^2_{2(U-1)}(\phi, \frac{1}{6N}) \tag{4.43}$$

and the chi-square distribution function with M degree of freedom :

$$\chi^2_{2(U-1)}(a,\sigma^2) = \mid \frac{1}{\sigma^2} \mid \cdot \frac{\left(\frac{a}{\sigma^2}\right)^{\frac{M-2}{2}} \cdot exp\left(-\frac{a/\sigma^2}{2}\right)}{2^{M/2} \cdot \Gamma[M/2]} \tag{4.44}$$

with gamma function $\Gamma[a] = \int_0^\infty t^{a-1}e^{-t}dt$.

4.2.3.3 Output SNR of MR Combiner In the previous subsection, we found the pdf of the maximum SNR of SD combiner and the pdf of NFR of LDD. The LDD output has only two branches with the corresponding partial energy for each user, the left version of the present one-shot window and the right version of the next one-shot window are weighted summed, and thus the demodulation output with the full energy of one-shot duration is found. prior to finding the hard decision of demoduation, we minimized SNR reduction due to the enhancement of LDD output noise by using the maximal ratio combining scheme.

The output of the MR combiner for uth user in Fig.4.4 is

$$\begin{aligned} Y_u &= X'_{uL}M'_{uL} + X''_{uR}M''_{uR} \\ &= \sqrt{P_u}\sqrt{E_{uL}}d_u(n)\frac{\sqrt{E_{uL}}}{\lambda_{uL}} + \sqrt{P_u}\sqrt{E_{uR}}d_u(n)\frac{\sqrt{E_{uR}}}{\lambda_{uR}} \\ &\quad + n'_{xuL}(n)\frac{\sqrt{E_{uL}}}{\lambda_{uL}} + n''_{xuR}(n)\frac{\sqrt{E_{uR}}}{\lambda_{uR}} \\ &= \left[\sqrt{E_{uL}}\frac{\sqrt{P_uE_{uL}}}{\lambda_{uL}} + \sqrt{E_{uR}}\frac{\sqrt{P_uE_{uR}}}{\lambda_{uR}}\right]d_u(n) + n_{yu}(n) \end{aligned} \tag{4.45}$$

where M'_{uL} and M''_{uR} were defined in Eq.(4.22), and $n_{yu}(n) = n'_{yuL}(n) + n''_{yuR}(n)$ has the variance :

$$var[n_{yu}] = \sigma^2\lambda_{uL} \cdot \frac{E_{uL}}{\lambda^2_{uL}} + \sigma^2\lambda_{uR} \cdot \frac{E_{uR}}{\lambda^2_{uR}} = \sigma^2\left[\frac{E_{uL}}{\lambda_{uL}} + \frac{E_{uR}}{\lambda_{uR}}\right]. \tag{4.46}$$

In Eq.(4.46), the $\lambda_{u\Omega}$ is a random variable and independent identically distributed [38],[51], and thus the SNR of MRC output can be expressed as

$$\gamma_{MR} = E\left\{ \frac{\left(\sqrt{E_{uL}} \cdot \frac{\sqrt{P_u E_{uL}}}{\lambda_{uL}} + \sqrt{E_{uR}} \cdot \frac{\sqrt{P_u E_{uR}}}{\lambda_{uR}} \right)^2}{\sigma^2 \cdot \left(\frac{E_{uL}}{\lambda_{uL}} + \frac{E_{uR}}{\lambda_{uR}} \right)} \right\}. \tag{4.47}$$

The partial energy terms E_{uL} and E_{uR} in Eq.(4.47) are not statisically independent for each other as defined in Eq.(4.17) and thus the normalized partial energy is E_{uR} = 1 - E_{uL}. It is difficult to evaluate the SNR with the mean of the partial energy. Therefore, we approximate $E[E_{u\Omega}]$ to 0.5 by normalization since the time delay τ_u is uniformly distributed in [0, T_b] and thus the mean value of the partial energy of left version is the same as that of right version in one-shot window.The SNR can be expressed as

$$\begin{aligned}
\gamma_{MR} &= E\left\{ \frac{\left(\sqrt{P_u} \cdot \frac{E_{uL}}{\lambda_{uL}} + \sqrt{P_u} \cdot \frac{E_{uR}}{\lambda_{uR}} \right)^2}{\sigma^2 \cdot \left(\frac{E_{uL}}{\lambda_{uL}} + \frac{E_{uR}}{\lambda_{uR}} \right)} \right\} \\
&= \frac{P_u}{\sigma^2} \cdot E\left\{ \frac{E_{uL}}{\lambda_{uL}} + \frac{E_{uR}}{\lambda_{uR}} \right\} \\
&= \frac{P_u}{\sigma^2} \cdot E\left\{ \frac{0.5}{\lambda_{uL}} + \frac{0.5}{\lambda_{uR}} \right\} \\
&= \frac{P_u}{\sigma^2} \cdot E\left\{ \frac{1}{\lambda} \right\}
\end{aligned} \tag{4.48}$$

where according to the assumption above $E\{E_{uL}\} = E\{E_{uR}\} = 0.5$, $E\{\lambda\} = E\{\lambda_{uL}\} = E\{\lambda_{uR}\}$ since λ_{uL} and λ_{uR} are independent identically distributed, and the expected value $E\{\frac{1}{\lambda}\} = \int f_W(w) w dw$ from Eq.(4.42).

The pdfs of maximum SNR of SD combiner, NFR of one-shot LDD and the maximum SNR of the MR combining output are known, and thus the average bit error probability can be expressed as

$$P_e(\gamma_{SD}, w) = \int_{\gamma_{SD}} \int_w Q\left(\sqrt{\gamma_{SD}} \cdot w \right) f_{\gamma_{SD}}(\gamma_{SD}) f_W(w) dw d\gamma_{SD} \tag{4.49}$$

where $f_{\gamma_{SD}}(\gamma_{SD})$ and $f_W(w)$ were evaluated in Eq.(4.36) and Eq.(4.42), respectively, and the Q-function was defined in the previous page.

4.2.4 Numerical Analysis

Using the results of the previous sections, a numerical evaluation of the performance of linear decorrelating detector with Selection Diversity and MR Combining schemes is given in this section. The code sequences used in the analysis use only code length N = 128 of 511 chip Gold codes to keep the property of random-CDMA code. The PLL performance in a conventional LDD is analyzed using the pdf in AWGN and Rayleigh fading channel environments. The performance of LDD with maximum SNR selection diversity and MR Combining scheme is shown through bit-error rate (BER) in AWGN and Rayleigh fading channel environments. All simulations used the Matlab tool.

Fading is caused by interference between two or more versions of the transmitted signal which arrive at the receiver at slightly different times. Rayleigh fading channel is the most severe mobile radio channel. Since third generation wideband CDMA uses fast closed loop power control, the near-far effect is mitigated by equalizing the user powers and signal-to-AWGN+MAI ratio(SNIR) performance is improved by compensating for the channel fading[16]. However, our simulation considers the uncompensated Rayleigh fading channel. Therefore, we analyze the performances of the Hybrid SD/MRC LDD in Rayleigh fading with the assumption of a power controlled environment.

Fig.4.7 shows the bit error probability for Maximal Ratio Combining (MRC) scheme to maximize the output SNR of LDD without SD scheme since we fixed AWGN term and thus the term is not random at the output of the SD combiner. The MRC scheme provides better improvement in bit error performance for moderate to high average SNR in AWGN channel. For example, when $P_e = 10^{-5}$, the required

average SNR per bit for MRC LDD is around 11dB, which is less than that required of CLDD. This shows that the MRC scheme improves the demodulation performance by the maximization of SNR at the LDD output.

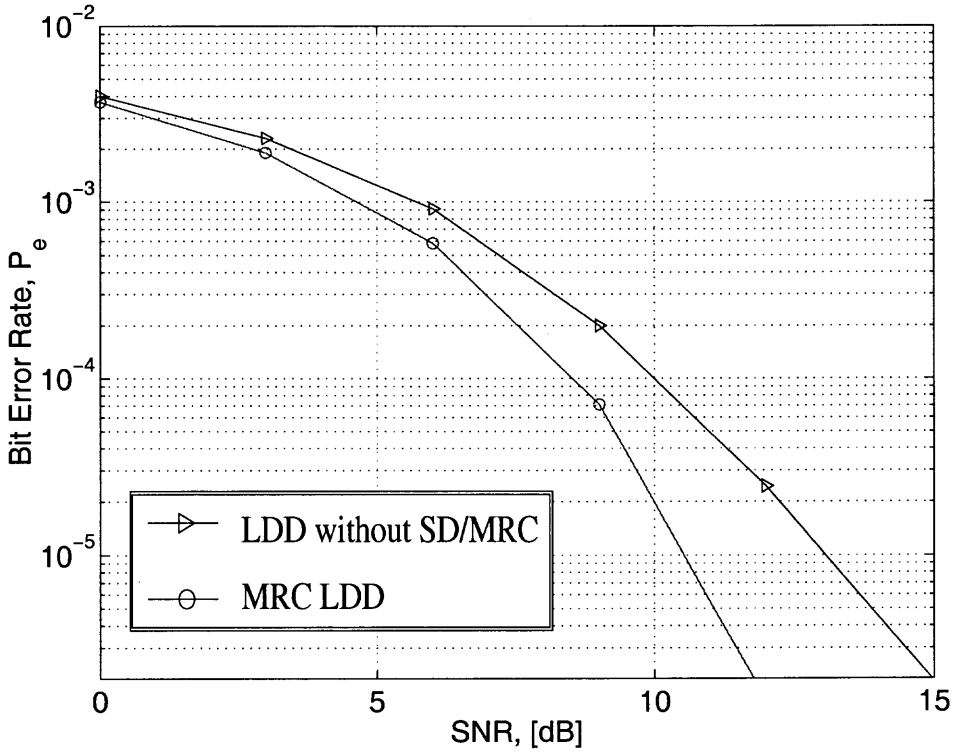

Figure 4.7 BER of LDD without SD/MRC and Hybrid SD/MRC LDD (L = 1) in AWGN channel

Fig.4.8 illustrates the concept of SD scheme in bit error probability. We compute the bit error probability for Hybrid SD/MRC LDD by using Eq.(4.49) for L = 2,4,8, and 16. When $P_e = 10^{-2}$, the LDD without SD/MRC needs the average SNR per bit, around 12 dB, while the required SNR of SD/MRC LDD receiver is just 8 dB at L = 2 and 6.5 dB at L = 4. The SD receiver can improve much better the performance of demodulation as the number of branches increases.

Fig.4.9 shows the bit error probability of LDD without SD/MRC, MRC LDD, and SD/MRC LDD with L=2,4 in Rayleigh fading channel. The instantaneous

maximum SNR SD scheme can compensate the performance degradation due to the deep faded signal and thus, provide much better performance than the LDD without SD/MRC. For example, when $P_e = 10^{-2}$, the required average SNR per bit for SD/MRC with L=2 is around 9 dB less than that for MRC LDD with L=1, while another 2.5 dB can be saved by an L=4 diversity scheme. This clearly demonstrates that the transmitter signal power may be reduced when selection diversity and maximal ratio combining schemes are adopted.

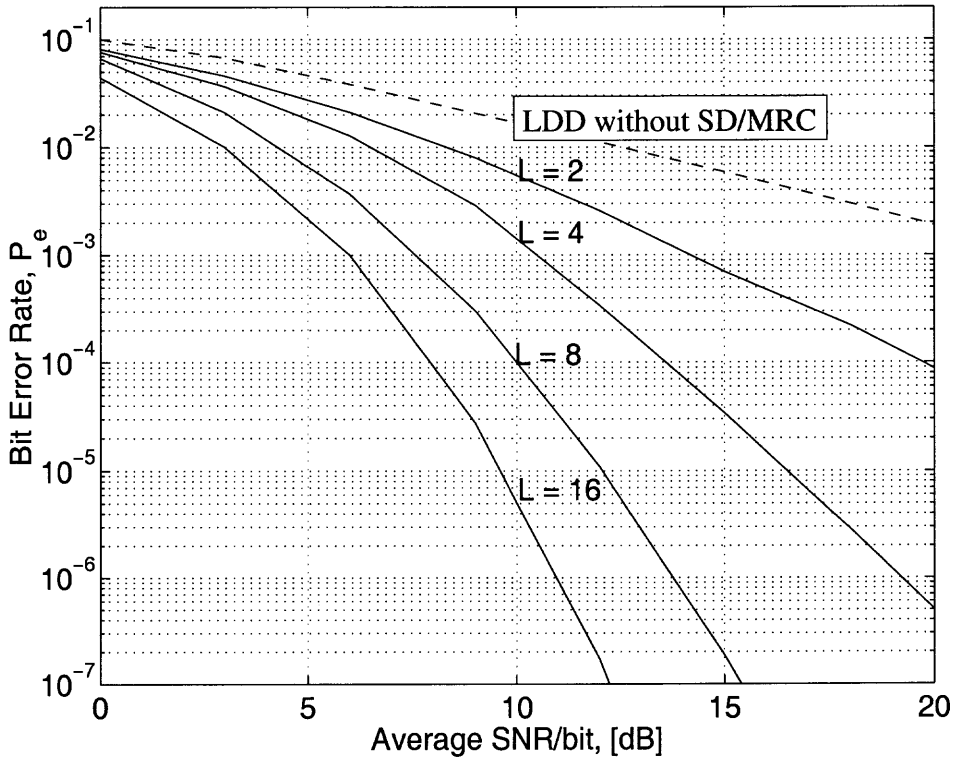

Figure 4.8 Analytical BER at L = 2, 4, 8, and 16 in Rayleigh fading channel

To verify the analysis derived in the previous section, the analytical BER is compared with the simulated results for asynchronous CDMA as a function of the number of users in Rayleigh fading channel. In this simulation, we used the base-band BPSK signal at the signal-to-AWGN ratio 10 dB. The BER is slicely degraded

as the number of users increases due to the enhancement of output noise term of the LDD.

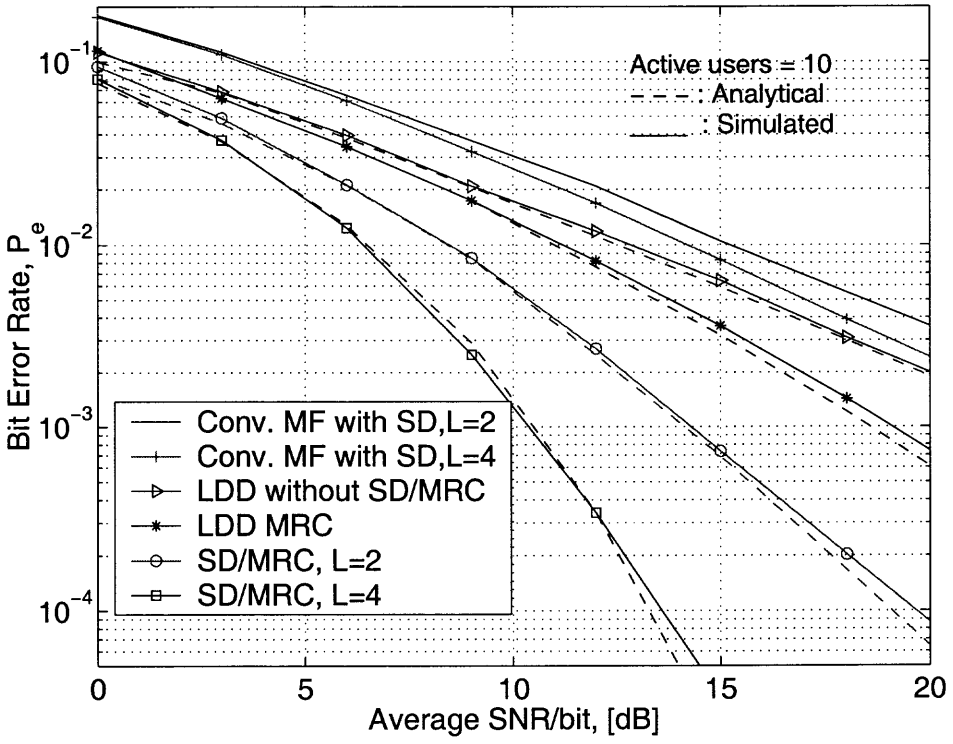

Figure 4.9 BER of Conventional matched filter (Conv. MF) with SD (L=2, L=4), LDD without SD/MRC, LDD with MRC scheme, and Hybrid SD/MRC LDD with L = 2,4 in Rayleigh fading channel

Fig.4.11 depicts the comparison of the simulated pdf and the analytical value as descrived by Eq.(4.42). For simplicity of simulation, we use the synchronous chip duration and thus, we changed the variance to 1/2N. The inversed value of diagonal component value of $\mathbf{R^{-1}}$ increase as a function of the number of users increases and the BER performance of the LDD is degraded with the increase of the number of users. For example, the mean value and peak height of the pdf are about 9.3 and 0.2 for 10 active users while the mean and peak height are about 0.85 and 0.06 for 20 active users.

Fig.4.12 illustrates the behavior of the phase estimator error pdf, p(θ), in AWGN and Rayleigh fading channels when the signal-to-AWGN power ratio is fixed at 10 dB. The height of the pdf was normalized with the reference of only one user's height. The peak height of the PDF clearly increases in AWGN channel. However, the peak decreases in Rayleigh fading channels. This means the tracking ability of the phase-locked loop is degraded as the channel environment is poor.

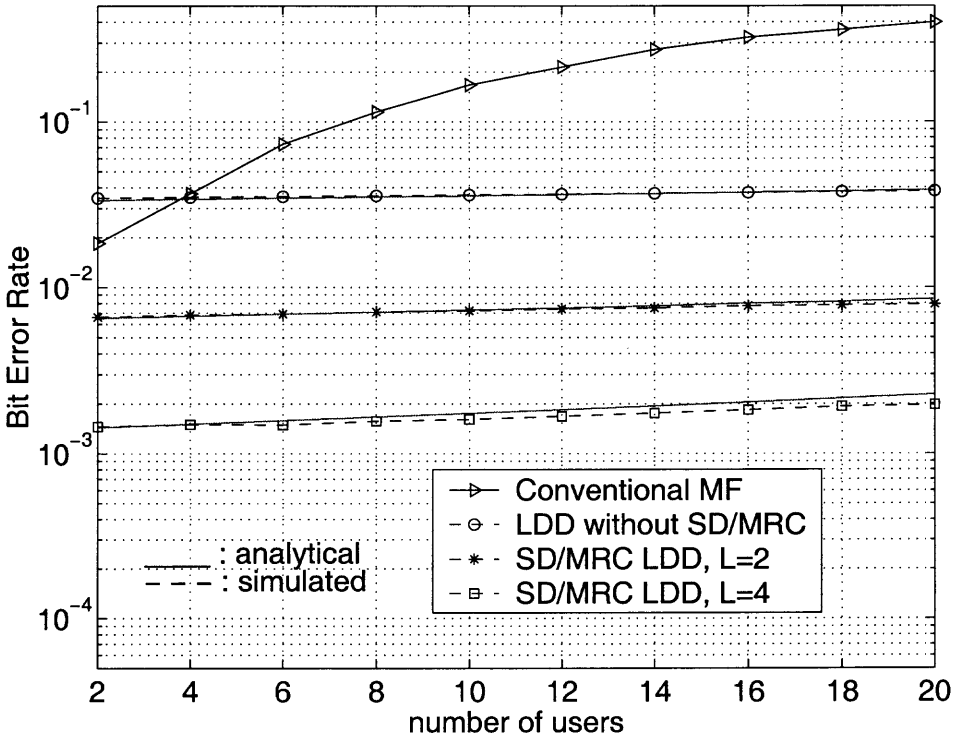

Figure 4.10 bit error probability with comparison of analytical and simulated results as a function of the number of users in Rayleigh fading channel environment

.

Fig.4.13 shows the bit error probability between the LDD with PLL and without PLL as a function of the average SNR per bit in AWGN and Rayleigh fading channels. The phase tracking error in a real system is very small after aquisition, but we used the range of the error, ± 10 degree, to investigate plainly the behavior of the error tracking of PLL. The carrier phase error causes the degardation of demodulation

performance in multiuser detection. For example, when the bit error probability is $P_e = 10^{-2}$ for the conventional LDD without PLL in Rayleigh fading channel, the required average SNR per bit is about 1 dB larger than that with PLL, while another 3 dB can be saved by SD/MRC LDD receiver. In AWGN, the required SNR per bit of the LDD without SD/MRC and SD/MRC LDDs can be also saved by PLL. This means that fine synchronization of carrier phase error can mitigate the degradation of performance of the receiver.

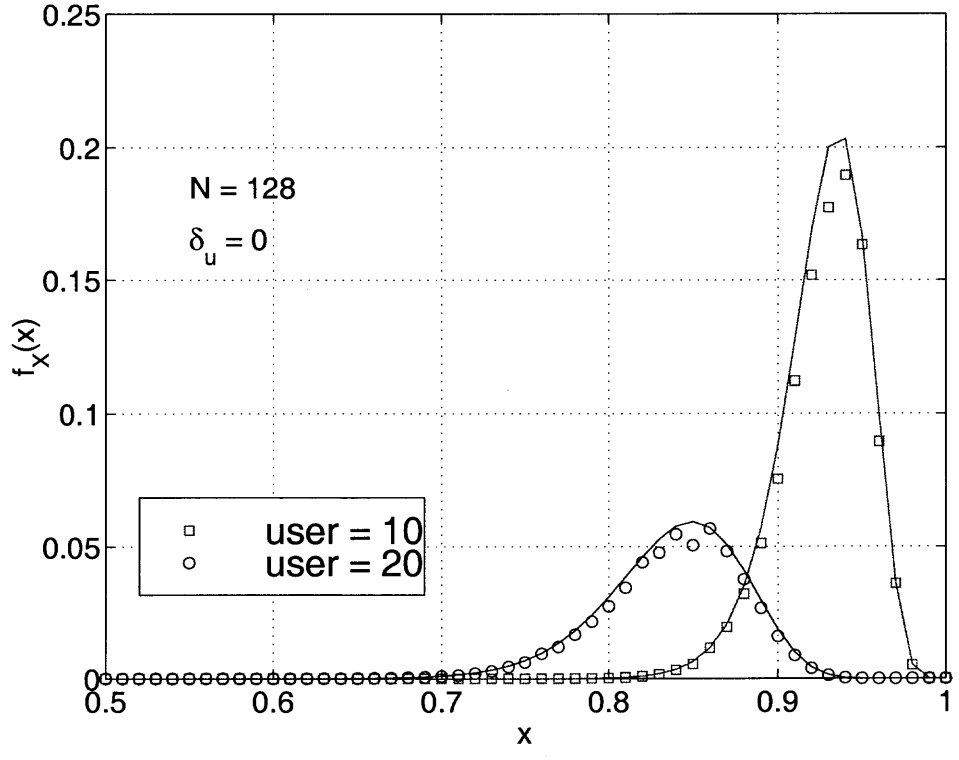

Figure 4.11 pdf of the inversed value of diagonal component of $\mathbf{R}^{-1}$ for first user's left version (N = 128, and $\delta_u = 0$)

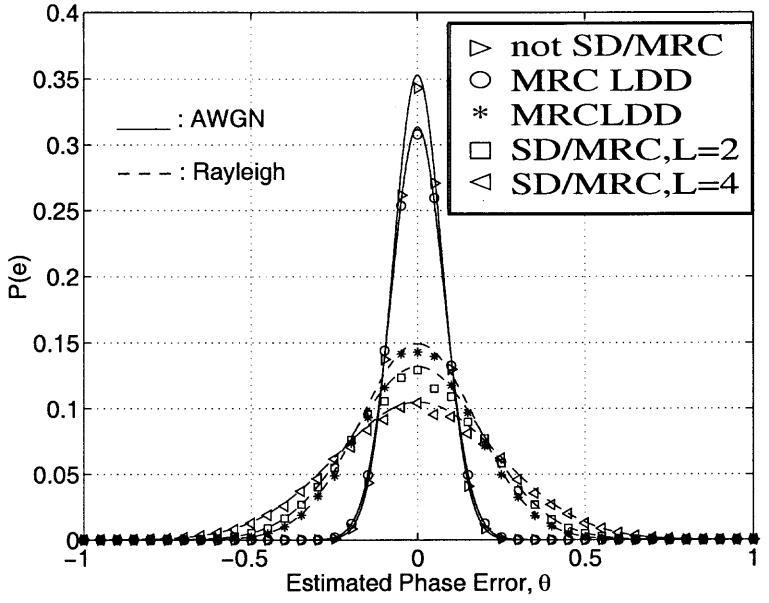

Figure 4.12 pdf of the phase estimator error in AWGN and Rayleigh fading channels

.

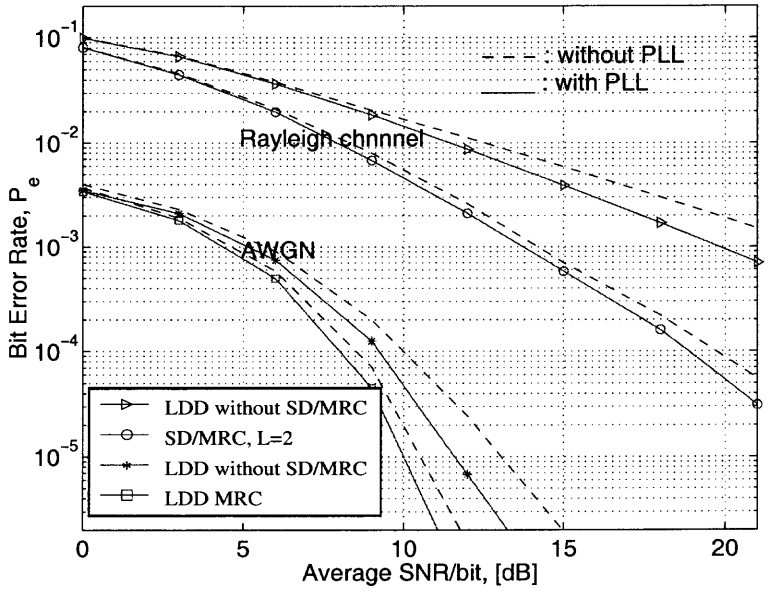

Figure 4.13 Comparison of BER between LDD with PLL and LDD without PLL in AWGN and Rayleigh fading channels

.

CHAPTER 5
CONCLUSION

This dissertation first analyze the phase-estimator error performance of a PLL in an asynchronous multirate DS-CDMA system with MMAI and AWGN. We constructed an integrated PLL and DLL receiver to synchronize the phase delay and the code delay simultaneously. In particular, we proposed the DPC method to evaluate the autocorrelation and its PSD of the crosscorrelation terms in a multirate signal environment.

A further focus is on code tracking performance of a coherent DLL in an asynchronous multirate CDMA environment with MMAI and AWGN. We proposed the DPC method to analyze the autocorrelation and PSD of the time function having MMAI crosscorrelation. The PDF of the code tracking jitter and its variance was derived for a first order loop and several results showed the effect of MMAI under various conditions. Though numerical results may be different in real systems, we chose parameters similar to those in a commercial system. Therefore, we expect that our results will facilliate the evaluation of third generation mobile communication systems

A main issue in multiuser detection is to decouple the MAI of the received signal of a DS-CDMA system. Among many linear multiuser detectors which decouple the multiple access interference from each of the interfering users, one-shot window linear decorrelating detector (LDD) based on a one bit period to reduce the complexity of the LDD has attracted wide attention as an implementation scheme. Therefore, we proposed Hybrid Selection Diversity/Maximal Ratio Combining (Hybrid SD/MRC) one-shot window linear decorrelating detector (LDD) for asynchronous DS-CDMA systems. The selection diversity scheme at the input of the Hybrid SD/MRC LDD is based on choosing the branch with the maximum signal-to-noise ratio (SNR) of all filter outputs. The MR Combining scheme at the output of the Hybrid SD/MRC

LDD adopts to maximize the output SNR and thus compensates for the enhanced output noise. The Hybrid SD/MRC one-shot LDD with PLL is introduced to track its phase error and to improve the demodulation performance. The probability density functions of the maximum SNR of the SD combiner , the near-far resistance (NFR) of one-shot LDD by Gaussian approximation, and the maximum SNR of the MR combiner for Hybrid SD/MRC LDD are evaluated, and the bit error probability was obtained from these pdfs. The performance of Hybrid SD/MRC one-shot LDD was assessed in a Rayleigh fading channel.

REFERENCES

1. Jacob Klapper, and John T. Frankle, *Phase-Locked and Frequency Feedback Systems,* New York: Academic Press, 1972.

2. Floyd M. Gardner, *Phaselock Techniques,* New York: John Wiley and Sons, 1979.

3. Andrew J. Viterbi, *CDMA : Principles of Spread Spectrum Communication,* Massachusetts: Addison-Wesley Publishing, 1995.

4. Andrew J. Viterbi, *Principles of Coherent Communications,* New York: McGraw-Hill, chpt.4, 1966.

5. Fumiyuki Adachi, Mamoru Sawahashi, and Hirohito Suda "Wideband DS-CDMA for Next-Generation Mobile Communications Systems," IEEE *Commun. Mag.,* vol. 36, pp.56-69, Sept. 1998.

6. Roger L. Peterson, Rodger E. Ziemer, David E. Borth, *Introduction to Spread Spectrum Communications,* Prentice Hall 1995.

7. Esmael H. Dinan and Bijan Jabbari, *Speading codes for Direct Sequence CDMA and Wideband CDMA Cellular Networks,* IEEE *Commun. Mag.,* vol. 36, pp.48-54, Sept. 1998.

8. F. Adachi, M. Sawahashi, and K. Okawa, "Tree-Structured Generation of Orthogonal Spreading Codes with Different Length for Forward Link of DS-CDMA Mobile Radio," Elect. Lett., vol. 33, pp.27-28, Jan. 1997.

9. Clarke, R.H., *"A Statistical Theory of Mobile-radio Reception," Bell Systems Technical Journal,* vol. 47, pp.957-1000, 1968.

10. D.R. Anderson and P.A. Wintz "Analysis of a spread-spectrum multiple-access system with a hard-limiter," IEEE *Trans. Commun. Technology,* vol. COM-17, pp.285-290, Apr. 1969.

11. Wei Huang, Ivan Andonovic, and Masao Nakagawa, "Code Tracking performance of DS-CDMA schemes in the Presence of multisuer interference and additive gaussian noise," IEEE *ISSSTA'98,* Sun City, South Africa, vol.3/3, pp.843-847, Sept, 1998.

12. Michael B. Pursley, "Performance Evaluation for Phase-Coded Spread-Spectrum Multiple-Access Communications-Part I: System Analysis", IEEE *Trans. Commun.*, vol. COM-25, pp.795-799, Aug. 1977.

13. Urbashi Mitra, "Comparison of Maximum-Likelihood-Based Detection fot Two Multirate Access Schemes for CDMA Signals," IEEE *Trans. Commun.*, vol. 47, pp.64-77, Jan. 1999.

14. Jack K. Holmes, *Coherent Spread Spectrum Systems,* New York, John Wiley and Sons, 1982.

15. J.J. Spilker, Jr., "Delay lock tracking of binary signals," IEEE *Trans. Space Electron. Telemetry,* vol. SET-9, pp.1-9, Mar. 1963.

16. Tero Ojanpera, and Ramjee Prasad, *Wideband CDMA for Third Generation Mobile Communications,* Boston: Artech House Publishers, 1998.

17. Marvin K. Simon, "Noncoherent pseudonoise code tracking performance of spread spectrum receivers," IEEE *Trans. Commun.*, vol. COM-25, pp.327-345, March 1977.

18. Andreas Polydoros and Charles L. Weber, "Analysis and Optimization of Correlative Code-Tracking Loop in Spread-Spectrum Systems" IEEE *Trans. Commun.*, vol. COM-33, pp.30-43, Jan. 1985.

19. James Caffery, Jr. and Gordon L. Stüber "Performance of Non-coherent DLL in Multiple Access Interference," IEEE *ISSSTA'98*, Sun City, South Africa, vol.3/3, pp.823-827, Sept, 1998.

20. Riccardo De Gaudenzi and Marco Luise "Decision-Directed Coherent Delay-Lock Tracking Loop for DS-Spread-Spectrum Signals," IEEE *Trans. Commun.*, vol.39, pp.758-765, May 1991.

21. Heinrich Meyr, "Delay-Lock Tracking of Stochastic Signals," IEEE *Trans. Commun.*, vol. COM-24, pp.331-339, March 1976.

22. Wei Huang, Ivan Andonovic, and Masao Nakagawa, " PLL Performance of DS-CDMA Systems in the Preence of Phase Noise, Multiuser Interference, and Additive Gaussian Noise", IEEE *Trans. Commun.*, vol. 46, pp.1507-1515, Nov. 1998.

23. Chang Y. Yoon, William C. Lindsey, " Phase-Locked Loop Performance in the Presence of CW Interference and Additive Noise", IEEE *Trans. Commun.*, vol. COM-30, pp.2305-2311, Oct. 1982.

24. Fulvio Gini, Georgios B. Giannakis, "Frequency Offset and Symbol Timing Recovery in Flat-fading Channel: A Cyclostationary Approach", IEEE *Trans. Commun.*, vol. 46, pp.400-411, March 1998.

25. Aaron Weinberg, Bede Liu "Discrete Time Analyses of Nonuniform Sampling First- and Second-Order Digital Phase Lock Loops ", IEEE *Trans. Commun.*, vol. COM-22, pp.123-137, Feb. 1974.

26. John E. Ohlson, "Phase-Locked Loop Operation in the Presence of Impulsive and Gaussian Noise ", IEEE *Trans. Commun.*, vol. COM-21, pp.991-996, Sep. 1973.

27. Martin T. Hill, Antonio Cantoni, "A Frequency Steered Phase-Locked Loop ", IEEE *Trans. Commun.*, vol. 45, pp.737-743, June 1997.

28. R. Lupas, S. Verdu, "Linear Multiuser Detectors for Synchronous Code-Division Multiple Access Channels", IEEE *Trans. Info. Theory*, vol. IT-35, pp.123-136, Jan. 1989.

29. R. Lupas, S. Verdu, "Near-Far Resistance of Multiuser Detectors in Asynchronous Channels", IEEE *Trans. Commun.*, vol. COM-38, pp.496-508, Apr. 1990.

30. S. Verdu, "Minimum Probability of Error for Asynchronous Gaussian Multiple-Access Channels", IEEE *Trans. Info. Theory*, vol. IT-32, pp.85-96, Jan. 1986.

31. Z. Xie, R.T. Short, C.K. Ruthforth, "A Family of Suboptimum Detectors for Coherent Multiuser Communication", IEEE *JSAC*, vol. 8, pp.683-690, May 1990.

32. U. Madhow, M.L. Honig, "MMSA Interference Suppression for Direct-Sequence Spread-Spectrum CDMA", IEEE *Trans. Commun.*, vol. COM-42, pp.3178-3188, Dec. 1994.

33. R. Lupas, "Near-far resistance linear multiuser detection", *Ph.D. thesis*, Dept. Elec. Eng., Princeton Univ., 1989.

34. T. Ottoson and A. Svensson "Multi-rate Schemes in DS/CDMA Systems," IEEE *VTC'95*, Chicago, pp. 1006-1010, July, 1995.

35. Schneider, K.S., *Optimum detection of code division multiplexed signals,* IEEE *Trans. Aeros. Electron. Syst.*, vol. AES-15, No.1, pp.181-185, Jan. 1979.

36. Kohno, R., H. Imai, and M. Hatori, *Cancellation technique of co-channel interference in asynchronous spread-spectrum multiple access systems,* IEICE *Trans. Commun.*, vol. 65-A, pp.416-423, May 1983.

37. Verdu, S., *Optimum Multiuser Signal Detection,* Ph.D. Thesis, University of Illinois, Urbana-Champaign, 1984.

38. Lipas, R., and Verdu, S., *Near-far resistance of multiuser detectors in asynchronous code-division multiple access communications,* IEICE *Trans. Commun.*, COM-38, pp.496-508, Apr. 1990.

39. Peng, M., Y.J. Guo, S.K. Barton, *One-shot Linear Decorrelating Detector for Asynchronous CDMA, Proceedings of Globecom'96.*, pp.1301-1305, 1996.

40. Bernard Sklar, *Rayleigh Fading Channels in Mobile Digital Communication Systems, Part I : Characterization, IEEE Communications Magazine,* pp.90-109, July 1997.

41. Shimon Moshavi, *Multi-User Detection for DS-CDMA Communications, IEEE Communications Magazine*, pp.124-136, Oct. 1996.

42. Alexandra Duel-Hallen, Jack Holtzman, and Zoran Zvonar, *Multiuser Detection for CDMA Systems, IEEE Personal Communications*, pp.46-58, Apr. 1995.

43. Zoran Zvonar and David Brady, *Multiuser Detection in Single-Path Fading Channels, IEEE Trans. on Commun.*, pp.1729-1739, Feb./Mar./Apr. 1994.

44. L. R. Khan, *Radio Squarer, Proc. of IRE*, 42 Nov. 1954.

45. Michel D. Yacoub, *Foundations of Mobile Radio Engineering,* Boca Raton: CRC Press, 1993.

46. Vijay K. Garg and Joseph E. Wilkes, *Wireless and Personal Communications Systems,* ATT Bell Lab.: Prentice Hall, 1996.

47. Elisabeth A. Neasmith and Norman C. Beaulieu, *New Results on Selection Diversity, IEEE Trans. commun.*, Vol.46, pp.695-704, May 1998.

48. Gwo-Tsuey Chyi, John G. Proakis, and Catherine M. Keller, *On the Symbol Error Probabiliy of Maximum-Selection Diversity Reception Schemes Over a Rayleigh Fading Channel, IEEE Trans. commun.*, Vol.37, pp.79-83, Nov. 1989.

49. J. S. Lehnert and M. B. Pursley, *Error Probabiliy for Binary Direc-Sequence Spread Spectrum Communications with Random Signature Sequences, IEEE Trans. commun.*, Vol.COM-35, pp.87-98, Nov. 1987.

50. S. H. Yoon and K. S. hong, *Bit Error Probability of Linear Decorrelating Detector for random Signature Sequences, Proc. of Vehicular Technology Conference (Fall).*, Amsterdam, The netherlands Sep. 1999.

51. S. H. Yoon and Yeheskel Bar-Ness, *An Approximate Analysis of Asynchronous Linear Decorrelating Detector for Dynamic CDMA System, Proc. of ISSSTA2000*, New Jersey, USA Sep. 2000.

52. Theodore S. Rappaport, *Wireless Communications: Principles and Practice,* New Jersey: Prentice Hall, 1996.

53. F. Zheng and S. K. Barton, *Near-Far Resistant Detection of CDMA Signals via Isolation Bit Insertion, IEEE Trans. commun.*, Vol.COM-43, pp.1313-1317, Feb./March/April. 1987.

54. S. Verdu, *Multiuser Detection, Cambridge University Press*, 1998.